NON-PERTURBATIVE APPROACHES TO STRONGLY CORRELATED ELECTRON SYSTEMS

BY

KA WAI LO

DISSERTATION

Submitted in partial fulfillment of the requirements
for the degree of Doctor of Philosophy in Physics
in the Graduate College of the
University of Illinois at Urbana-Champaign, 2013

Urbana, Illinois

Doctoral Committee:

Assistant Professor Shinsei Ryu, Chair
Professor Philip Phillips, Director of Research
Professor S. Lance Cooper
Professor Rob Leigh

Abstract

Strong electron correlation phenomena are ubiquitous, such as unconventional superconductivity and the metal-insulator transitions. Having a proper understanding of strongly correlated electron systems requires a non-perturbative analysis because Fermi liquid theory inevitably breaks down due to the strong correlation. In this thesis, we will study two non-perturbative approaches to tackle strongly correlated electronic system: 1.) multi-dimensional bosonization and 2.) the AdS/CFT correspondence. Multidimensional bosonization is the generalization of bosonization to spatial dimensions larger than one. The bosonized theory is an effective field theory in terms of the bosonic particle-hole fluctuations in different patches of the Fermi surface. The bosonized theory is quadratic and hence can be solved non-perturbatively. The AdS/CFT correspondence is a conjecture that $d-$dimensional field theory is dual to a $d+1$ dimensional quantum gravitational theory. Problems in strongly coupled field theory then have an equivalent description using weakly interacting gravitational theory, allowing a non-perturbative analysis.

Chapter 1 will serve as an introduction. We will review several experiments which show a breakdown of Fermi liquid theory. Formalisms for multidimensional bosonization and the AdS/CFT correspondence will then be reviewed. In chapter 2, the two-orbital Hubbard model with degenerate d_{xz} and d_{yz} orbitals are investigated. We apply multidimensional bosonization to solve this problem exactly and discover a $z = 3$ overdamped collective modes that emerges at the orbital-ordering quantum critical point. These modes modify the single-particle density of states and lead to non-Fermi liquid behavior which can provide a possible explanation for the recently observed zero-bias enhancement in the point contact spectroscopy signal on iron pnictides. Chapters 3, 4 and 5 discuss the applications of the AdS/CFT correspondence to model various condensed matter systems. In chapter 3, We consider an interaction term between a bulk spinor field and a gauge field in the Reissner-Nordström AdS background. When the Pauli interaction term is large enough, a dynamical gap is generated and spectral weight transfer is observed in the spectral density, mimicking the behavior of the Hubbard model. We further consider the finite temperature case and discover that the ratio between the dynamical gap and the critical temperature has the same order as that of VO_2. The Pauli coupling is also studied in the superconducting background. Chapter 4 consider the propagation

of a neutral scalar field in the geometry called the electron star. The electron star has Lifshitz scaling with finite dynamical critical exponent at the interior, which is suitable for the modeling of quantum criticality and quantum phase transition with a neutral order parameter, for example for antiferromagnetism. We find that the quantum phase transition has the Berezinski-Kosterlitz-Thouless characteristic and the dynamical critical exponent can change across the quantum critical point. In chapter 5, we construct a gravity dual of the nematic phase by studying the condensation of a spin-two field in the Schwarzschild-AdS background. The condensation of a spin-two field can distort the rotational symmetry of the Fermi surface as long as the spin-two field is coupled to a probe spinor field in the bulk gravity dual.

Acknowledgments

First of all, I would like to thank my advisor Philip Phillips, without him this thesis would be impossible. Philip is one of the most interesting and creative guys that I have ever met. He always has interesting ideas and his deep understanding on physics always inspires me a lot. From him, I learnt how to integrate different seemingly unrelated physics together. He is also very open-minded and willing to try various new approaches when facing difficult problems. I am sure this attitude would be beneficial to me no matter what I would do in the future.

I need to thank all my collaborators, Mohammad Edalati, Prof Rob Leigh and especially Wei-Cheng Lee and Seungmin Hong. Wei-Cheng has always been very patient to listen to me and explained the physics to me when I had any difficulty in the research. It was a very enjoyable experience for me to collaborate with him. I thank Seungmin for helping me a lot in developing the code for transport calculation and I enjoyed numerous discussions with him both academically and non-academically. I would also like to thank all the other group members Wei-Cheng Lv, Tony Hegg, Brandon Langley, Garrett Vanacore and Zhidong Leong and my thesis committee members, Prof Rob Leigh, Prof Shinsei Ryu, and Prof Lance Cooper.

Lastly, I would like to give my sincere gratitude to my family for their continuos support and love. It has been my pleasure to meet and know many wonderful friends during my graduate study, Edwin Leung, Tak-Kei Lui, Billy Lo, Kwok-Yan Chan, Jacky Lie, Tommy So, Raymond Wong, Joseph Ching, Pak-On Chan, Boyce Tsang, Ricky Chue and Kin Lam. In particular, I am grateful to Boyce Tsang for teaching me playing guitar and all my roommates Tak-Kei Lui, Billy Lo, Kwok-Yan Chan and Kin Lam for giving me a home-like environment.

The works in this thesis are supported by National Science Foundation under Grants No. DMR-0940992 and DMR-1104909 and the Center for Emergent Superconductivity, a DOE Energy Frontier Research Center, Award Number DE- AC0298CH1088.

Table of Contents

List of Figures

List of Abbreviations

AdS	Anti de Sitter.
BF	Breitenlohner–Freedman
BGP	Buchbinder, Gitman and Pershin
BKT	Berezinski-Kosterlitz-Thouless
CFT	Conformal Field Theory.
FOOQCP	Ferro-Orbital Ordering Quantum Critical Point
OOQCP	Orbital Ordering Quantum Critical Point
PCS	Point Contact Spectroscopy
RN-AdS	Reissner-Nordström AdSd+1
RPA	Random Phase Approximation
WKB	WentzelKramersBrillouin

Chapter 1

Introduction

Understanding strongly correlated electron system remains one of the hardest problems in condensed matter physics. Many phenomena are now known to originate from strong electron correlations, for example unconventional superconductivity, metal-insulator transition, heavy fermion behavior, non-Fermi liquid behavior, quantum phase transitions and quantum criticality. Unfortunately, conventional theory in solid state physics based on the Fermi liquid theory is insufficient to explain these phenomena and there is still no consensus on the mechanism of these phenonmena. The major difficulty to obtain a satisfactory theoretical description of them lies in the nature of the strong correlations. It is well known that even for the simplest model for strongly correlated systems, the Hubbard model, no exact solution is known except for the one-dimensional case. Perturbative analysis in strongly correlated systems is often singular or leads to an uncontrollable expansion. More importantly, the ground states of strongly correlated systems cannot be perturbatively connected to those of the free system. In other words, the quasi-particle picture from traditional Fermi liquid theory is no longer applicable in strong correlation problems. In order to obtain new insights to these systems, a non-perturbative analysis is necessary, which is the subject of this thesis.

In this thesis, we will investigate the uses of two non-perturbative calculation methods on different strongly correlated systems, namely multidimensional bosonization and the Anti de-Sitter/conformal field theory (AdS/CFT) correspondence (also known as gauge/gravity duality or holography). Before introducing these two non-perturbative calculation schemes, we will first briefly review the traditional Fermi liquid theory and experimental evidence for its breakdown.

1.1 Break down of Fermi quasi-particle picture

1.1.1 Fermi liquid theory

Fermi liquid theory is a phenomenological model for interacting electronic systems [1, 2]. Thanks to the renormalization group analysis, its applicability has been proven in many systems, for example the normal state of metals and liquid Helium [3]. The key result of Fermi liquid theory is that there exist quasi-particle

excitations which are adiabatically connected to the non-interacting fermions and the energy functional of Fermi liquids can be expressed as the momentum distribution function of these quasi-particles. The single particle Green function for Fermi liquid takes the form

$$G(\omega, \vec{k}) = \frac{Z}{\omega + \mu - \epsilon_{\vec{k}} + i\gamma}, \tag{1.1}$$

where Z is the quasi-particle residue with $0 < Z \leq 1$, $\epsilon_{\vec{k}}$ is the excitation energy of a single particle and γ is the damping factor. The equation $\epsilon_{\vec{k}} = 0$ defines the Fermi surface where the excitation energy is zero and the excitations are gapless. The existence of a Fermi surface is necessary for the renormalization group analysis as all the short-range repulsion are renormalized towards the Fermi surface upon integration. The analytical structure of the single-particle Green function for Fermi liquids remains unchanged under renormalization and is the same as that of the Green function for non-interacting fermions, *i.e.* , a single pole, which is a reflection of the one-to-one correspondence between the Fermi liquid quasi-particle and a non-interacting fermion. While Fermi liquid theory has been a great success in describing many solid state systems, not all single-particle Green functions have single-pole singularities and fall within the Fermi-liquid picture. The most well known example is the Luttinger liquid in one-dimension [4, 5], which has an essential power-law singularity instead of a single pole. The Marginal Fermi liquid, which is a phenomenological model for the normal phase of the cuprates, has a logarithmically vanishing quasi-particle residue at the Fermi surface [6]. Another possibility is that the divergent self-energy due to strong correlations which leads to a zero in the single-particle Green function [7]. In all these systems, the Fermi liquid picture breaks down. Indeed, plenty of experiments in strongly correlated electron systems have demonstrated phenomena that are not explainable within the the traditional Fermi liquid theory. We will now review some of them below.

1.1.2 Experimental evidences for the breakdown of Fermi liquid picture

Spectral weight transfer

Redistribution of spectral weight over large energy scales has been observed in many Mott systems [8–10]. For example, the left panel of figure 1.1 shows the real part of the optical conductivity for VO_2 in the insulating and metallic states. Optical conductivity experiment measures the electrical conductivity in the presence of an alternating electric field. As the temperature decreases from 360K to 295K, VO_2 changes from a conducting state to an insulating state. Associated with the metal-insulator transition is a redistribution of spectral weight from the vicinity of the chemical potential to high energy states over 6eV away, as shown in Figure 1.1. The energy scale associated with spectral weight transfer vastly exceeds any

energy scale associated with orderings, but is consistent with the energy scale for the Coulomb repulsion, U. Hence spectral weight transfer is a consequence of strong correlation. Indeed, it was suggested that spectral weight transfer would mediate new low energy degrees of freedom which are orthogonal to the bare electron, resulting in the breakdown of Fermi liquid theory [11].

The breakdown of Fermi liquid theory in Mott system can be more clearly seen by the Oxygen 1s x-ray absorption experiment on $La_{2-x}Sr_xCuO_4$[8], which is shown in the right panel of Figure 1.1. The x-ray absorption experiment probes the available states of $La_{2-x}Sr_xCuO_4$ by exciting an electron from core Oxygen 1s orbitals to the unoccupied 2p orbitals and measures the fluorescence yield when the excited electron relaxes back to the valence states as a function of energy. The intensity of the peak at 530 eV is transferred to 528 eV as the doping level x increases. This can be understood using the Hubbard model. The higher-energy and lower-energy peaks in the absorption spectrum correspond to the valence state in the upper Hubbard band and lower Hubbard band respectively. The atomic limit of the Hubbard model predicts that the numbers of valence states in the lower Hubbard band and upper Hubbard band are $2x$ and and $1-x$ respectively. However, the x-ray absorption experiment reveals that the increases in the electron addition spectrum in the lower-energy peak exceeds $2x$ and decreases of the high-energy peak is faster than $1-x$, deviate from the values predicted by the atomic limit of the Hubbard model. The differences are due to dynamical corrections, and the existence of dynamical spectral weight transfer has a profound implication. The total spectral weight in the lower Hubbard band is $1+x+\alpha$, where α is the dynamical correction and is always positive [12]. Since the number of ways of adding electrons to lower Hubbard band is always $1+x$, this implies that electrons alone cannot exhaust the low energy degree of freedom. There exists new low energy degrees of freedom which are dynamically generated and are not adiabatically connected to the bare electron, a clear indication of the breakdown of Fermi liquid theory [13].

Spectral weight transfer will be studied in chapter 3, where AdS/CFT correspondence will be used to model Mott systems.

Transport anisotropy

Transport anisotropies have been discovered in many multi-orbital systems, for example in iron pnictides [14, 15], strontinum ruthenates [16] and manganites [17]. The left panel of figure 1.2 shows that the resistivities anisotropy measurement of three 122 iron pnitcides, $BaFe_2As_2$, $CaFe_2As_2$ and $SrFe_2As_2$. Above the temperature of the structural phase transition, the resistance along the a-axis (direction of antiferromagnetic chains) is approximately equal to the resistances along the b-axis (direction of ferromagnetic chains) for all three materials. Below structural phase transition temperature, the resistivities along the b-axis becomes

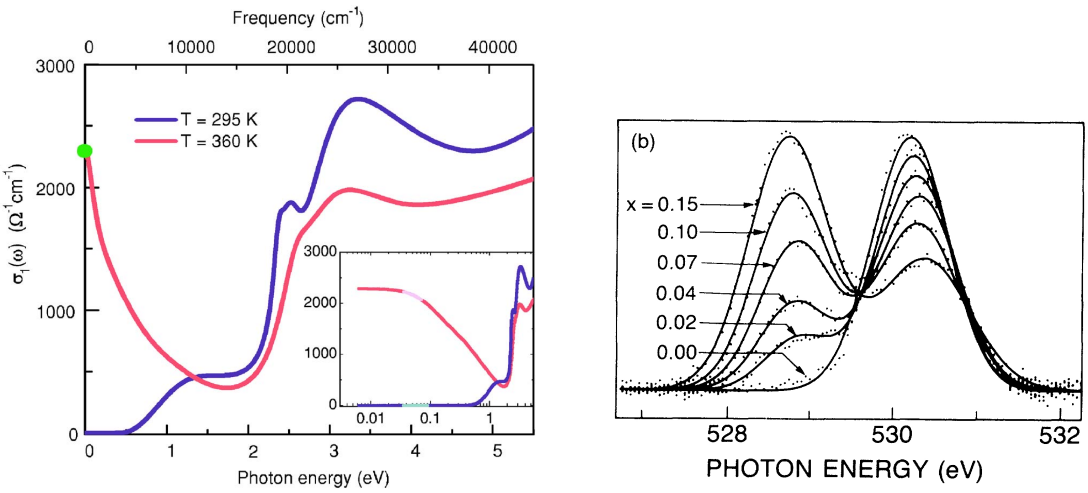

Figure 1.1: (Left) Real part of optical conductivity measurement for VO_2 in the insulating state (purple, 295K) and metallic state (pink, 360K). The inset shows the same plot in logarithmic scale. Figure taken from [9]. (Right) Gaussian fit to Oxygen 1s x-ray absorption spectrum of $La_{2-x}Sr_xCuO_4$ at 528eV and 530eV with background subtracted. From Ref. [8].

larger than along the a-axis, and anisotropies emerge.

Similarly, the right panel of Figure 1.2 shows that the in-plane magnetoresistivity for strontinum ruthenates $Sr_3Ru_2O_7$ when a magnetic field is applied 77° away from the a-b plane. The in-plane magnetic field is applied along the a-axis. When the applied magnetic field is around 7.8T (close to the magnetic-field-tuned quantum critical point [18]), the resistivity anomaly (an sudden increases in the magnetoresistivity) is absent for measurements along b-axis (black curve) but persists for measurements along a-axis (red curve). This resistivity anisotropy demonstrates that anomalous scattering exist for current parallel to the in-plane magnetic field but absent when current is perpendicular to the in-plane magnetic field. More surprisingly, neutron single-crystal diffraction shows that the underlying lattice remains C_4 symmetric even when the transport anisotropy exists.[16][1] This pinpoints that the transport anisotropy in $Sr_3Ru_2O_7$ is not driven by any structural phase transition, but rather is due to electron correlation.

The breaking of $x - y$ symmetry as shown by transport anisotropy demonstrates that these systems cannot be described by Fermi liquid theory. Indeed, they should be described by the so-called nematic liquid [20]. The nematic phase transition is an example of the Pomeranchuk instability of a Fermi liquid where the rotational symmetry of the Fermi surface is spontaneously broken and the nematic phase is characterized by a neutral tensor order parameter. The nematic transition is described in Chapters 2, 4 and 5. In Chapter 2, we would study the orbital order quantum phase transition and show that it is equivalent to the nematic

[1]There is a more recent experiment in the in-plane thermal expansion measurements claiming that there is a tiny lattice distortion which breaks the C_4 symmetry in $Sr_3Ru_2O_7$ [19]. However, such a tiny lattice distortion alone is not sufficient to explain the observed transport anisotropy.

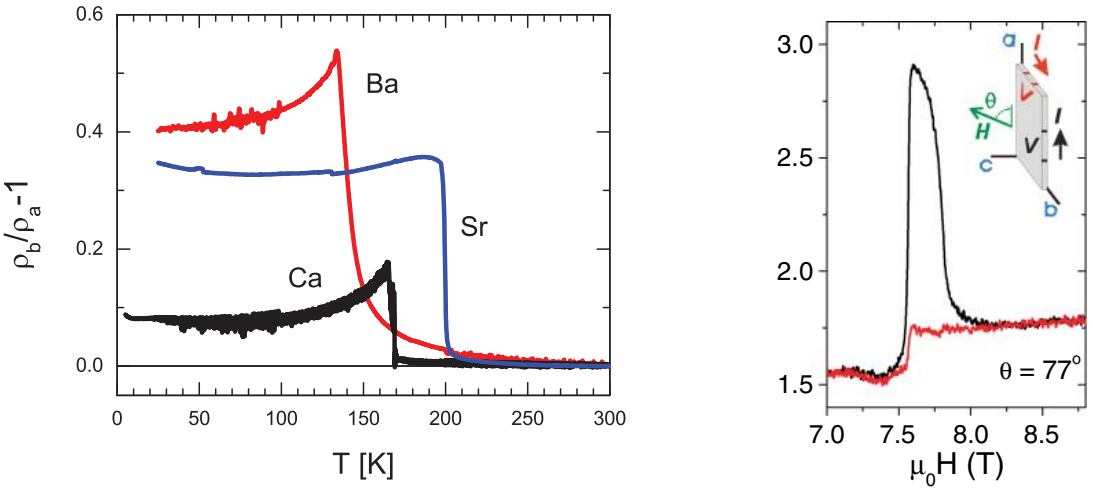

Figure 1.2: (left) Ratio of resistance as a function of temperature for three Fe_2As_2 compounds. Below temperatures for structural phase transition, all three compounds exhibit resistivity anisotropy. Figure taken from Ref.[14].(Right) In-plane magnetoresistivity for $Sr_3Ru_2O_7$. The black and red curve correspond to ρ_{aa} and ρ_{bb} respectively. From Ref. [16]

transition through multidimensional bosonization. In Chapters 4 and 5, we would discuss how to model a quantum phase transition with a neutral order parameter and broken rotational symmetry using AdS/CFT correspondence, respectively.

Zero bias enhancement in point contact spectroscopy

Another experiment that can be used to show the deviation from Fermi liquid behavior is point contact spectroscopy (PCS). In the (ballistic limit of) PCS, electrical current (or its derivatives) through a contact with size much smaller than the mean free path of a charge carrier is measured. PCS has been used as an energy-resolved spectroscopy for quasi-particle scattering inside normal metals [21]. It can also be used to probe strong electron correlation, where onset of a Kondo lattice can be detected as a Fano line shape in the PCS [22]. Recently, a zero bias enhancement in PCS has been detected in iron pnictide [23, 24] and was argued to be an indication of non Fermi liquid behavior [25].

Fig 1.3 shows the measurement of differential conductance as a function of applied bias voltage for different temperature in $BaFe_2As_2$. At temperatures above the structural phase transition (177K, black curve), the measured differential conductance is roughly constant at small applied voltage; it can be explained within the Fermi liquid theory as the conductance for a weakly interacting system is given by [26]

$$\frac{dI}{dV} \propto \int dk |\nu_k| \mathrm{Im} G(k, eV). \tag{1.2}$$

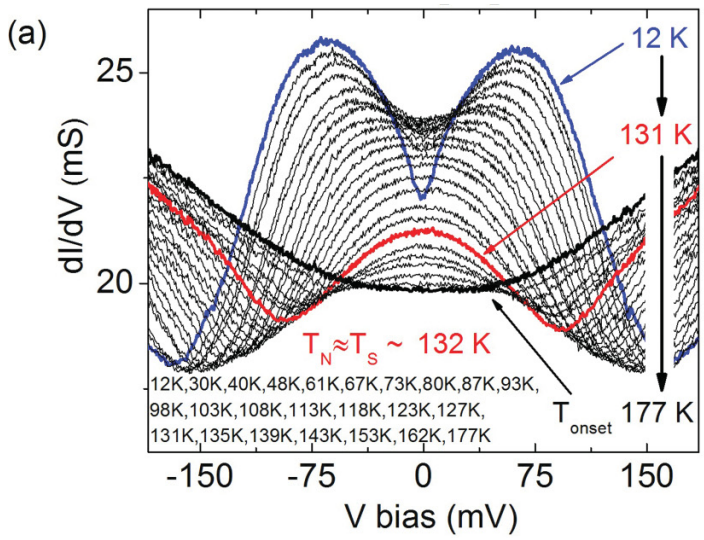

Figure 1.3: Point contact measurement of differential conductance for $BaFe_2As_2$ versus applied voltage for different temperature. The black curve (177K) shows the measurement at the tetragonal phase. The red curve (132K) shows the measurement at the structural phase transition. From Ref.[24].

By using $\mathrm{Im}G(k,\omega) = \delta(\omega - \epsilon_k)$ for weakly interacting system, the integral can be done easily and the differential conductance is roughly constant for small applied voltage. Hence, the black curve in Figure 1.3 matches with the prediction from Fermi liquid theory.

However, an enhancement in the differential conductance at small voltages is observed as temperatures decrease to the critical value for the structural phase transition $T_N \approx 132K$ (red curve in figure 1.3). This zero bias enhancement cannot be explained by Fermi liquid theory and is clear evidence for the breakdown of Fermi liquid and the emergence of non Fermi liquid behavior. As the differential conductance at small voltage is a rough measurement of the single-particle density of state, it also indicates an increase in single particle density of state and is consistent with that of nematic fluid[27]. The zero bias enhancement in PCS and emergence of nematic fluid is related to the work in Chapter 2.

Indeed, there are plenty of other experiments that demonstrate non-Fermi liquid behavior and breakdowns of the Fermi quasi-particle picture in various systems [28–31]. Since the quasi-particle picture can no longer be applied in strongly correlated systems, it is desirable to have a non-perturbative analysis for these systems. In below, we will review two non-perturbative techniques to solve models describing strongly correlated electronic systems.

1.2 Bosonization

Bosonization is the technique to rewrite the interacting (quartic) fermionic system into a quadratic bosonic system. It is done by identifying the low energy excitations that are bosonic in nature and obtaining an

effective field theory in terms of these bosons. As the resulting bosonic theory is quadratic, it can be solved exactly by simply doing a Gaussian integral. Hence, bosonization is a great tool for studying strongly correlated electron systems, especially in one-dimensional system [32].

1.2.1 Bosonization in one dimension

Bosonization in one dimension has been a great success. It was first shown by Tomonaga that elementary excitations in interacting one-dimensional fermionic systems behave like bosons [33]. In 1963, Luttinger proposed a one-dimensional interacting fermionic model that can be solved exactly by bosonization [5]. However, the solution by Luttinger is not correct and the correct treatment was later given by Mattis and Lieb [34]. They correctly determined that the electron density commutator is non-vanishing and given by

$$[\rho_{r,\sigma}(p), \rho_{r',\sigma'}(-p')] = -\delta_{r,r'}\delta_{\sigma,\sigma'}\delta_{p,p'}\frac{rpL}{2\pi}, \tag{1.3}$$

where $r = \pm 1$. This algebra is known as the U(1) Kac-Moody algebra. From the electron density commutator, they were able to solve the model exactly and obtain the energy spectrum. A remarkable result of the Luttinger model is the spin-charge separation where electrons are split into charge collective degrees of freedom (holon) and spin collective degrees of freedom (spinon) which propagate independently. The low energy excitations for interacting systems, holons and spinon, cannot be perturbatively connected to the excitations for non-interacting systems and clearly demonstrate the violation of Fermi liquid theory. Haldane showed that the properties of the Luttinger model are actually general features of interacting electrons in one-dimensional conducting systems and called them Luttinger liquids [35]. One important difference between Fermi and Luttinger liquids is the difference in the momentum distribution function. For Fermi liquids, there is a finite jump at the Fermi momentum for the momentum distribution function and that finite jump defines the quasi-particle residue in the Green function. In Luttinger liquids, though the Fermi surface can be defined by the momentum where derivatives of the momentum distribution function become singular, there is no finite jump at the Fermi momentum. Instead, the momentum distribution of the Luttinger liquid vanishes algebraically close to the Fermi surface and hence the quasi-particle residue is zero. As a result, the fermionic quasi-particle picture cannot be applied to Luttinger liquids and the low-energy excitations are the bosonic holon and spinon instead.

1.2.2 Bosonization in higher dimensions

Since bosonization in one-dimension has been a great triumph in demonstrating the breakdown of Fermi liquid theory non-perturbatively and it is an ideal tool to study quantum phase transitions in one-dimension [36]. In fact, bosonization in higher dimension can be done in a similar way to the one-dimensional problem by defining the density fluctuation operator that satisfies the high dimensional generalization of the U(1) Kac-Moody algebra. However, this is possible only if we have carefully divided the Fermi surface into different patches and certain geometrical restrictions should be imposed on the patches as we discuss below. Though it does not lead to an intrinsic breakdown of a Fermi liquid and the emergence of Luttinger liquids as in the one-dimensional case, it still offers a great opportunity for us to study quantum criticality in a non-perturbative way. In particular, non-Fermi liquid behavior has been shown to obtain at the nematic transition of a Fermi liquid using multidimensional bosonization [27]. We will now briefly review the calculation scheme for bosonization in two dimensions. Our presentation follows that in [37, 38].

The first attempt to generalize bosonization to higher dimensions is due to Luther [39]. His idea was to treat the particle-hole excitation pair at each radial $\vec{k}$ direction as an individual one-dimensional problem. However, a major drawback of this construction is that the interaction between different radial sectors is not allowed unless scattering between them is taken into account. To overcome this difficulty, Haldane suggested that the Fermi surface should be divided into small patches with finite width instead [40]. In this construction, particle-hole excitations are not restricted to be normal to the Fermi surface and motion parallel to the Fermi surface can be considered without considering scattering processes between difference patches. By working with patches, it is assumed that the degrees of freedom outside the patches have been integrated out, and it is the remaining effective field theory that must be bosonized. Figure 1.4 shows an illustration of dividing a two dimensional Fermi surface into twelve patches with width Λ and thickness λ.

We can then introduce the density fluctuation operator in each patch S,

$$\delta n_{S,\sigma\vec{q}} = \sum_{\vec{k},\sigma} \theta(S,\vec{k})\theta(S,\vec{k}+\vec{q})(c^{\dagger}_{\vec{k},\sigma} c_{\vec{k}+\vec{q},\sigma} - \delta_{\vec{q},0} n_{\vec{k},\sigma}), \tag{1.4}$$

where the Heaviside step function restricts the creation of a particle-hole pair to be within the patches. The density fluctuation operator satisfies the following commutation relation with correction terms,

$$[\delta n_{S,\sigma\vec{q}}, \delta n_{T,\sigma\vec{q}'}] = \delta_{S,T}\delta_{\vec{q}+\vec{q}',0}\vec{q}\cdot\vec{v}_S\delta(\mu-\epsilon_S) + \ldots, \tag{1.5}$$

where $\vec{v}_S$ and ϵ_S are the Fermi velocity and energy of patches S, respectively, and the correction terms

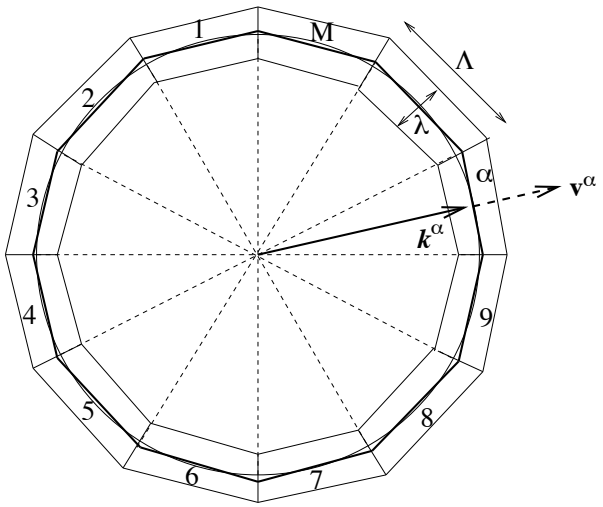

Figure 1.4: Figure illustrating the idea of dividing two dimensional Fermi surface into patches labeled by α by $\alpha = 1, 2, \cdots, M$ with width Λ and thickness λ. Figure taken from [41].

vanish if $q << \lambda << \Lambda$. Physical speaking, the condition $q << \lambda << \Lambda$ minimizes the momentum transfer scattering process between different patches. Hence, the density fluctuation operator satisfies bosonic commutation relations (multiplied by constant factor) if $\lambda/\Lambda \to 0$ in the long-wavelength limit.

The kinetic energy part of the Hamiltonian takes the form of $H_t = \sum_{\sigma,\vec{k}} \epsilon_{\vec{k}} c^\dagger_{\sigma,\vec{k}} c_{\sigma,\vec{k}}$. In order to bosonize our Hamiltonian, we need to linearize the dispersion relation, for momentum $\vec{k}$ within the patches S, $\epsilon_{\vec{k}} = \vec{v}_S \cdot (\vec{k} - \vec{k}_S)$. As the Fermi velocity with in each patch is replaced by $\vec{v}_S$, this requires the Fermi velocities do not vary much within the patch, which in turn requires the patch to be quasi-flat. Hence, we also require $\Lambda << k_F$ in order to minimize the curvature of the Fermi surface within each patch. Rewriting the summation over momentum as a summation over different patches, we find that the the kinetic part of the Hamiltonian and the density fluctuation operator then satisfy a simple commutation relation,

$$[H_t, \delta n_{S,\sigma\vec{q}}] = -\vec{q} \cdot \vec{v}_S \delta n_{S,\sigma\vec{q}} \delta(\mu - \epsilon_S) \frac{1}{N(0)}, \tag{1.6}$$

where the factor $\delta(\mu - \epsilon_S)/N(0)$ restricts the momentum vector for the center of each patch $\vec{k}_S$ to lie on the Fermi surface and $N(0) = \sum_S \delta(\mu - \epsilon_S)$ is the density of state at the Fermi surface.

From the commutation relation in (1.5), we obtain the following commutation relation,

$$[\sum_{\vec{q}'} \sum_{S,\sigma} \delta n_{S,\sigma}(-\vec{q}') \delta n_{S,\sigma}(\vec{q}'), \delta n_{S,\sigma}(\vec{q})] = -2\vec{q} \cdot \vec{v}_S \delta n_{S,\sigma\vec{q}} \delta(\mu - \epsilon_{\vec{k}_S}). \tag{1.7}$$

Comparing (1.6) and (1.7), the kinetic energy part of the Hamiltonian can be bosonized as

$$H_t = \sum_{\vec{q}} \sum_{S,\sigma} \frac{N}{2N(0)} \delta n_{S,\sigma}(-\vec{q}) \delta n_{S,\sigma}(\vec{q}). \tag{1.8}$$

Note that the kinetic part of the Hamiltonian can be written in a free boson representation only if the dispersion relation around Fermi surface has been linearized, otherwise, non-linearity in the dispersion relation will enter as correction terms to the free boson representation [41].

Similarly, a quartic interaction term in the Hamiltonian can also be bosonized by grouping pairs of fermionic creation and annihilation operators into the density fluctuation operator (1.4). For example, the on-site Hubbard interaction can be bosonized as

$$\begin{aligned} U \sum_i n_{i\uparrow} n_{i\downarrow} &= U \sum_{\vec{q}} n_{\vec{q}\uparrow} n_{-\vec{q}\downarrow} \\ &= U \sum_{\vec{q}} \sum_{S,\vec{k}} c^\dagger_{\vec{k}+\vec{q}\uparrow} c_{\vec{k}\uparrow} \theta(S,\vec{k}) \theta(S,\vec{k}+\vec{q}) \sum_{T,\vec{k}'} c^\dagger_{\vec{k}'-\vec{q}\downarrow} c_{\vec{k}'\downarrow} \theta(T,\vec{k}) \theta(T,\vec{k}'-\vec{q}) \\ &= U \sum_{\vec{q}} \sum_{ST} \delta n_{S\uparrow}(\vec{q}) \delta n_{T\downarrow}(-\vec{q}), \end{aligned} \tag{1.9}$$

where constants have been dropped in the last step. Therefore, the fermionic Hamiltonian with quartic interactions can be transformed into a quadratic bosonic Hamiltonian and hence can be solved non-perturbatively.

As a check on the correctness, we note that the properties of a Fermi liquid have been reproduced by the technique of multi-dimensional bosonization [37]. It has also been used to study the breakdown of Fermi liquid theory and nematic transitions in a continuum model non-perturbatively [27]. The quasi-particle residue was calculated to be zero at the nematic critical point and hence the nematic liquid is an example of a non-Fermi liquid. In the next Chapter, we will apply this technique to a two-orbital Hubbard model to investigate the orbital ordering quantum phase transition and the emergence of non-Fermi liquid behavior at the orbital ordering quantum critical point (OOQCP).

1.3 AdS/CFT correspondence

Another approach used to solve strongly correlated electronic systems is the AdS/CFT correspondence proposed by Maldacena in 1997 [42]. It is a conjecture that the large N limits ('t Hooft limit, where the rank of the gauge group $N \to \infty$ and the 't Hooft coupling λ_{YM} is fixed. The 't Hooft coupling is defined $\lambda_{YM} = g^2_{YM} N$, where g_{YM} is the gauge coupling constant [43].) of certain $d-$dimensional conformal field theories have an equivalent description using supergravity on the product of $d+1-$dimensional AdS space

and other compact manifolds. The duality was first studied between the Type IIB string theory on $AdS_5 \times S^5$ space and $\mathcal{N} = 4$ $d = 4$ $U(N)$ super Yang-Mills gauge theory and later generalized to many other systems, including those without conformal symmetry [44].

In the 't Hooft limit, the amplitude of a Feynman diagram expansion in a gauge theory can be written as $\sum_{g\geq 0} N^{2-2g} f_g(\lambda_{\rm YM})$, where g is the genus number of the surface. This expansion has the same structure as the loop expansion of string theory $\sum_{g\geq 0} {g_s}^{2g-2} Z_g$, where g_s is the string coupling constant [45]. By comparing the two expansions, it is suggestive that $N = 1/g_s$. Hence, the large N limit in the CFT corresponds to the classical string limit, $g_s \to 0$. Maldacena also conjectured the parameters in Type IIB string theory and the supersymmetric Yang-Mills theory are related as $4\pi g_s = g^2_{\rm YM}$ and $L^4/l_s^4 = \lambda_{\rm YM}$, where L is the AdS radius and l_s is the string length [42]. These relations are important as they tell us that the AdS/CFT correspondence has the property of *strong-weak coupling duality*, where the strong coupling limit of one theory is mapped to the weak coupling limit of the dual theory. When $\lambda_{\rm YM} \gg 1$, the gauge theory is strongly coupled and we can no longer perform a perturbative expansion. Luckily, the limit $\lambda_{\rm YM} \gg 1$ translates to $L \gg l_s$ in string theory from Maldacena's conjecture. In this limit, the AdS radius is much larger than the string length, a low-energy approximation to string theory is allowed, and string theory can be approximated by classical gravity [45]. This provides a non-perturbative description of strongly correlated gauge theories using classical gravity which are much easier to solve in general. It is this weak-strong coupling duality that makes the AdS/CFT correspondence a useful tool to study strongly coupled systems.

Certain condensed matter systems have conformal symmetry, for example Luttinger liquids and or the quantum critical point of the Bose-Hubbard model at the Mott lobe. It is natural to use the AdS/CFT correspondence to model them. However, most condensed matter system do not possess conformal symmetry due to the existence of certain energy scales such as the chemical potential or temperature. Nevertheless, the AdS/CFT correspondence can still be useful in these cases as we will see below. The AdS/CFT correspondence has now been used to model many condensed matter systems, for example holographic superconductors [46, 47], non-Fermi liquids [48] , and strange metals [49]. For reviews of applications of the AdS/CFT correspondence in condensed matter physics, please refer to [50, 51].

1.3.1 CFT and AdS

Let us first be precise about what CFT and AdS mean. Conformal field theory is the field theory with conformal symmetry. Under the conformal transformation, the space-time metric preserve its form up to a scale factor, *i.e.* $g_{\mu\nu}(x) \to \Omega^2(x) g_{\mu\nu}(x)$. The conformal group includes Lorentz rotations, translation dilatations and the special conformal transformation. The generators of the conformal group satisfy the

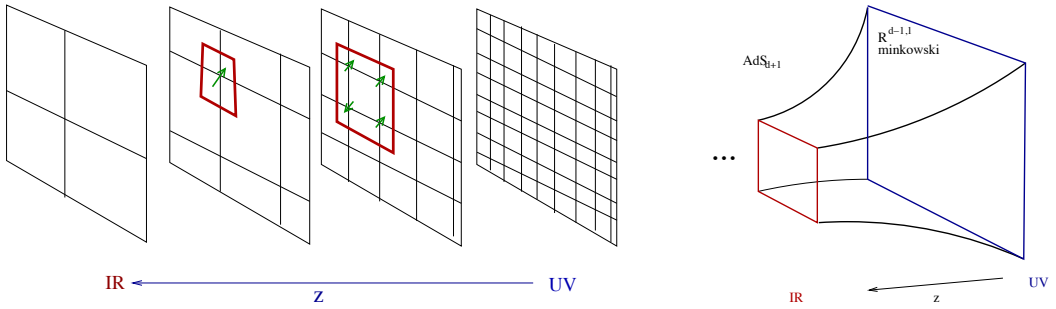

Figure 1.5: (Left) The dual field theory undergoes block-spin transformation with different length scales z. (Right) The correspondence gravity is AdS space. The dimension z governs the length scale in the Minkowski space. Changing the z coordinate can be viewed as changing the resolution of the dual field theory. Figure taken from [52].

conformal algebra, and the conformal algebra is isomorphic to the algebra of $SO(d,2)$ in Minkowski space and $SO(d+1,1)$ in Euclidean space.

The conformal dimension Δ of a field defines how it scales under spatial dilatation. If we scale the coordinate by a factor of λ, the field that transforms as $\phi'(x) = \lambda^{\Delta}\phi(\lambda x)$ is said to have conformal dimension Δ. Due to conformal symmetry, two-point correlation functions for a scalar field with scaling dimension Δ is restricted to be

$$\langle \mathcal{O}(0)\mathcal{O}(x)\rangle \propto \frac{1}{|x|^{2\Delta}} \tag{1.10}$$

Conformal symmetry also determines many other properties of the CFT, such as its equation of state, the scaling dimension of the energy-momentum tensor and any conserved current of global symmetry.

To describe the CFT using a gravity dual, we would require the isometry group of the geometry to be the same as the $d-$dimensional conformal group, which is $SO(d+1,1)$ in Euclidean signature. It turns out that such a spacetime is called Anti de-Sitter space and it is the maximally symmetric vacuum solution to the Einstein's equation with negative cosmological constant.

Its space-time metric is given by

$$ds^2 = \frac{L^2}{z^2}\left(dz^2 + g_{\mu\nu}dx^\mu dx^\nu\right) \tag{1.11}$$

with AdS radius L. It can be considered as a set of Minkoswki spaces with prefactor $(L/z)^2$. Hence, the coordinate z describes the length resolution scale of the dual field theory. In other words, the extra dimension on the gravity side is mapped to the energy scale of the field theory. Figure 1.5 illustrates the idea of viewing AdS space as Minkoswki space with a different length scale z.

In this picture, the boundary and the interior of the AdS space corresponds to the UV and IR limits of the dual field theory respectively. In the field theory, conformal symmetry can be broken upon renormalization group; hence only the UV limit of the dual field theory is required to have conformal symmetry. On the gravity side, it means the gravity dual need not be pure AdS space. The only requirement is the spacetime be asymptotically AdS. Indeed, this is precisely how we do model finite temperature and finite density matter phase using the AdS/CFT correspondence. Temperature and chemical potential can be introduced to the field theory by adding a black hole and a gauge field to the gravity side as we will see below. The presence of black hole and gauge field will break the conformal symmetry only in the interior of the geometry, and the boundary will remain AdS. In the field theory, it means that we would have a UV conformal symmetric fixed point that flows to an IR fixed point with broken conformal symmetry upon renormalization.

For example, under the renormalization group, quantum critical systems usually flow to an IR fixed point with emergent scaling symmetry. One possibility is the Lifshitz scaling symmetry with finite dynamical critical exponent z. A system with dynamical critical exponent z remains unchanged when the spatial coordinate is scaled by a factor of λ and the time coordinate scale by the factor of λ^z. The gravity duals of these systems would then have the Lifshitz scaling in the interior of the geometry but remain AdS at the asymptotic boundary [53, 54]. This allows us to use the AdS/CFT to model wide classes of condensed matter systems.

1.3.2 Short summary of AdS/CFT correspondence

In this subsection, I will present a very brief summary on the AdS/CFT correspondence (for details, see [45, 52]. In particular, I will mainly focus on the simplest example – pure AdS space which is dual to vacuum CFT, to illustrate how to do calculations using the AdS/CFT correspondence. The AdS/CFT correspondence will then be applied on other gravity duals to model more sophisticated condensed matter systems in later chapters.

The AdS/CFT correspondence relates the (source of) operator in the CFT to the boundary value of the bulk field in the asymptotic AdS boundary. For example, let us consider the simplest case of a vacuum CFT which is dual to pure AdS space. Let $\mathcal{O}$ denote a bosonic operator in the CFT and ϕ_0 be its source. It is dual to a bulk scalar field ϕ with the boundary condition $\phi(z=0)=\phi_0$ on the asymptotic boundary. The basic conjecture of the AdS/CFT correspondence is

$$Z_{\rm CFT}[\phi_0] = Z_{\rm quantum-gravity}\left[\phi(\vec{x}, z=0)=\phi_0(\vec{x})\right]. \tag{1.12}$$

It states that the partition function of the CFT is the same as the partition function of the quantum gravity theory with the boundary condition $\phi(z=0)=\phi_0$. From eq (1.12), we can compute the correlation function in the CFT from the gravity dual. We can also derive the so-called dictionaries of the AdS/CFT, for example the relation between the mass of the bulk field in gravity and the conformal dimension of the operator in the CFT.

The left-hand side of (1.12) is given by

$$Z_{\rm CFT}[\phi_0]=\left\langle \exp\left(-\int d^dx\phi_0(\vec{x})\mathcal{O}(\vec{x})\right)\right\rangle_{\rm CFT}. \tag{1.13}$$

Note that due to the conformal invariance of $Z_{\rm CFT}[\phi_0]$, if the conformal dimension of $\mathcal{O}$ is Δ, then the conformal dimension of ϕ_0 must be $d-\Delta$. The correlation function for the CFT can be computed by taking derivatives of the partition function with respect to the source fields

$$\langle \mathcal{O}(x_1)\mathcal{O}(x_2)\cdots\rangle=\left.\frac{\partial^n \ln Z_{\rm CFT}[\phi]}{\partial\phi_0(x_1)\partial\phi_0(x_2)\cdots}\right|_{\phi=0} \tag{1.14}$$

By using (1.12) to replace $Z_{\rm CFT}$ by $Z_{\rm quantum-gravity}$ in (1.14), we can compute the correlation function of the CFT by taking derivatives of $Z_{\rm quantum-gravity}$ instead. However, $Z_{\rm quantum-gravity}$ is, in general, very hard to know. Fortunately, the strong-coupling limit of the gauge theory is mapped to the classical gravity limit of the dual theory in the AdS/CFT correspondence as we discussed above. In the limit where the dual field theory is strongly correlated, we can do the saddle-point approximation to the gravitational partition function

$$Z_{\rm quantum-gravity}\left[\phi(\vec{x},z)|_{z=0}=\phi_0(\vec{x})\right]\approx\exp\left(-S_{\rm gravity}[\phi_{\rm cl}]\right) \tag{1.15}$$

where $S_{\rm gravity}$ is the low energy effective action of the classical Einstein gravity and $\phi_{\rm cl}$ is the field that extremizes the classical Einstein gravity action with the boundary condition $\phi(z=0)=\phi_0$.

The classical Einstein gravitational action including the contribution from the bulk scalar field can be

written as

$$S_{\text{gravity}} = \int d^{d+1}x\sqrt{g}\left(\mathcal{L}_{\text{Einstein}} + \mathcal{L}_{\text{scalar}}\right) \tag{1.16}$$

$$\mathcal{L}_{\text{Einstein}} = \frac{1}{2\kappa^2}\left(R + \frac{d(d-1)}{L^2}\right) \tag{1.17}$$

$$\mathcal{L}_{\text{scalar}} = \frac{1}{2\kappa^2\lambda}\phi\left(-D_\mu D^\mu + m^2\right)\phi \tag{1.18}$$

where R is the Ricci scalar, κ^2 is Newton's constant and λ determines the coupling strength between the scalar field and geometry. The AdS metric is the solution to Einstein's equations without the scalar field. In general, the presence of any bulk field may alter the background geometry, and the new background metric should be determined by solving the Einstein equations and the equation of motion for the bulk field simultaneously. However, we can consider the case where the coupling parameter between the scalar field and the background geometry λ tends to infinity. In this limit, the backreaction of the scalar field to the background can be neglected and the background geometry is unaltered.

From eq (1.18), the equation of motion for scalar field can be deduced and ϕ_{cl} in eq (1.15) is the solution with the boundary condition $\phi = \phi_0$. Since the metric is translationally invariant except the z direction, we can assume ϕ behaves as a plane-wave except along the z direction, *i.e.* $\phi(z, \vec{x}) \sim f(z)e^{ik_\mu x^\mu}$. By assuming the z dependence of ϕ is z^δ and using the $z \to 0$ limit of the AdS metric, we find that there are two solutions for δ [52],

$$\delta_\pm = \frac{d}{2} \pm \sqrt{\left(\frac{d}{2}\right)^2 + m^2L^2}. \tag{1.19}$$

Hence, close to the asymptotic boundary $z \to 0$, the field goes as

$$\phi(z \to z_0) \to A(1 + \cdots)z^{\delta_-} + B(1 + \cdots)z^{\delta_+}, \tag{1.20}$$

The leading term on the boundary is Az^{δ_-}. In order to have a finite value for the source, we would define the renormalized source field as $\phi_0^{\text{Ren}} = \phi(z = \epsilon)\epsilon^{-\delta_-} = A$. The renormalized source field has conformal dimension δ_-.

Since the conformal dimension of the source and response fields must add up to d (from eq (1.13)), the conformal dimension of (renormalized) operator, Δ, is then given by $d - \delta_-$. We have derived how the

conformal dimension of the operator in the CFT relates to the mass of the bulk field in the dual theory,

$$\Delta = \frac{d}{2} + \sqrt{\left(\frac{d}{2}\right)^2 + m^2 L^2}. \tag{1.21}$$

Furthermore, by drawing an analogy to the Lagrangian mechanics and considering the radial coordinate z as the time coordinate, it can be shown that the response of the operator is proportional to the subleading term B in (1.20) [52]. The Green function $G(k, \omega)$ of $\mathcal{O}$ in the field theory is then proportional to B/A. (The choice of A as the source field and B as the response is known as the 'standard quantization'. For suitable range of mass, we may take an alternative quantization scheme and interchange the role of A and B [55].) Taking the Fourier transform, we reduce the spatial correlator to the form of eq(1.10), reproducing the calculation on the CFT side. This demonstrates an example of the *field-operator correspondence*, where properties of operators in the field theory can be obtained by calculating the asymptotic properties of the corresponding fields in the dual gravity.

The finite temperature phase of the field theory can be described by adding a black hole to the dual gravity and the temperature is given by $T = \kappa/2\pi$, where κ is the surface gravity. The metric where a black hole is added to the AdS space is called the Schwarzschild-AdS metric. To compute the temperature of the black hole, we can perform an analytic continuation to imaginary time and define a new near horizon radial coordinate $\bar{z}$, where $\bar{z}^2 \propto (z - z_h)$ and z_h is the radial coordinate of the horizon. The time and new radial coordinates of the near horizon metric will then behave as polar coordinates and the imaginary time coordinate have period $2\pi/\kappa$. As the periodicity of the imaginary time is equal to the inverse temperature, the temperature of a black hole is given by $\kappa/2\pi$ [56]. Due to the temperature of the black hole, a finite energy scale is introduced and the conformal symmetry is then broken in the interior of the geometry as we discussed previously.

We can also apply the field-operator correspondence to other fields. For example, we can consider fields with additional symmetry. A bulk $U(1)$ gauge field in gravity is dual to an operator with global $U(1)$ symmetry in the field theory. To describe realistic condensed matter systems, we can introduce a finite charge density to the field theory by adding a bulk Maxwell field on the gravity side. Similarly to the case of a bosonic operator, the response and source of the $U(1)$ charge operator in the dual field theory can be read off from the asymptotic behavior of the bulk Maxwell field. For an asymptotic AdS metric,

$$A_t = \mu + z^{d-2}\rho + \cdots, \tag{1.22}$$

provides the relation between the chemical potential and the charge density of the field theory and the

asymptotic behavior of the time component of the bulk $U(1)$ gauge field on the gravity side. If we consider the backreaction of the Maxwell field to the background metric, the metric will be modified to the so-called Reissner-Nodström AdS metic. This metric has interesting properties, namely when the temperature is zero, the near horizon geometry behaves as $AdS_2 \times R^{d-1}$. This implies that the IR limit of the corresponding field theory has an emergent conformal symmetry which is different from UV conformal symmetry. This also leads to differences in the Breitenlohner–Freedman (BF) bound for the near horizon geometry and boundary geometry, where the BF bound is the range of mass squares below which a bulk scalar field becomes unstable [57]. The difference of the BF bound in the interior and asymptotic boundary allows a new kind of instability in the black hole where the black hole develops scalar hair and corresponds to the a condensation of bosonic operator in the field theory [46, 58]. If the scalar hair is charged, the dual field theory will develop superconductivity [46]. (For a charged scalar field, Schwarzschild-AdS black hole metric is sufficient for the development of scalar hair as the effective mass can also be modified by the charge. A neutral scalar hair cannot arise in Schwarzschild-AdS black hole unless an additional coupling term is considered, such as a Weyl coupling to the metric [59].)

We can also consider fields with different statistics. A spinor field in the bulk gravity is dual to a fermionic operator in the dual field theory. It has been shown that the fermionic correlator that is dual to a spin $1/2$ field in the Reissner-Nodström AdS metric can take the form of a Fermi liquid, marginal Fermi liquid and or non-Fermi liquid depending on the conformal dimension of the IR field theory [60]. This is a very promising result as the marginal Fermi liquid can be used to describe the T-linear resistivity observed in the strange metal phase of the cuprates [6]. Due to the strongly correlated nature of the cuprates, no systematic method has been known to produce the marginal Fermi liquid before. Hence, the AdS/CFT correspondence may provide us new insight to understand the unsolved problem of high temperature superconductivity. In Chapter 3, we will consider an additional bulk dipole coupling p between the spinor field and the gauge field in RN-AdS. Interestingly, when the dipole interaction is large enough, a gap is opened in the spectral function which resembles the behavior of the Hubbard model.

The RN-AdS black hole metric has a drawback in that its entropy is non-zero even at zero temperature and the dynamical critical exponent is infinity due to the presence of a black hole. Hartnoll finds that when backreaction of the fermion is taken into account, a new geometry called the electron star is formed [54]. The electron star has an emergent IR Lifshitz scaling with finite dynamical critical exponent and zero entropy at zero temperature. This gravitational system is very suitable to study the problem of quantum criticality as many quantum critical systems have finite dynamical critical exponents. While the interior geometry has Lifshitz scaling, the asymptotic boundary remains AdS-like. Hence, the BF bounds are not the same

at the interior and asymptotic boundary regions, and neutral bosonic operators in the dual field theory can spontaneously condense. This system will be studied in Chapter 4 and can be useful to study quantum phases with neutral order parameters such as a magnetic phase, in particular antiferromagnetism.

We can even consider fields with higher spin, For example, a spin-two field in the bulk gravity is dual to a tensor operator in the field theory. However, for a spin-two field to propagate with the correct number of propagating degrees of freedom, the background metric is highly constrained [61]. One possible geometry is Schwarzschild-AdS without the backreaction of any field. In Chapter 5, we will study the spin-two field with Weyl coupling in the Schwarzschild-AdS which is dual to a nematic phase in the field theory. By introducing probe fermionic fields coupled to the spin-two field, the rotational symmetry of the Fermi surface can be spontaneously broken if the spin-two field is condensed, thereby leading to the Pomeranchuk instability.

Chapter 2

Non-Fermi liquid in the orbital ordering quantum critical point

The critical behaviour of a two-orbital model with degenerate d_{xz} and d_{yz} orbitals is investigated by multi-dimensional bosonization. This kind of model can describe the breaking of rotational symmetry in the $x-y$ plane of numerous materials. We find that the corresponding bosonic theory has an overdamped collective mode with dynamical exponent $z = 3$, which appears to be a general feature of a two-orbital model and becomes the dominant fluctuation in the vicinity of the orbital-ordering quantum critical point. Since the very existence of this $z = 3$ overdamped collective mode induces non-Fermi liquid behaviour near the quantum critical point, we conclude that a two-orbital model generally has a sizable area in the phase diagram showing non-Fermi liquid behaviour. Furthermore, we show that the bosonic theory resembles the continuous model near the d-wave Pomeranchuk instability, suggesting that orbital order in a two-orbital model is identical to nematic order in a continuous model. Our results can be applied to systems with degenerate d_{xz} and d_{yz} orbitals such as iron-based superconductors and bilayer strontium ruthenates $Sr_3Ru_2O_7$.

2.1 Introduction

A key puzzle with the iron-pnictide superconductors is one of size: the 0.3% change in the lattice constant at the structural transition is not commensurate with the subsequent massive reorganization in the electronic system as evidenced incommensurate changes are also seen in the Hall and Seebeck coefficients as well as an enhanced tunneling signal at zero-bias in point-contact spectroscopy[24] but most notably by a transport anisotropy that can exceed a factor of two. As such transport anisotropy is difficult to square with standard Fermi liquid behaviour, its mere existence is of great importance as it suggests that non-Fermi liquid behaviour underlies the physics of the pnictides. Since the hunt for non-Fermi liquids is at a nascent stage, a concrete model which is capable of explaining the observed transport anomalies is a pressing problem. In this Chapter, we propose a concrete model for non-Fermi liquid behaviour in the pnictides which is also capable of capturing the origin of the structural transition.

While on theoretical grounds such physics might be accountable for in the spin sector alone, the pnictides

contain an additional orbital degree of freedom which, when present, has been used successfully to explain the discrepancy between the electron transport and the tiny lattice distortion in systems such as the manganites and the ruthenates[62–65]. The reason is that orbital degrees of freedom are part of the spatial symmetry, not an internal symmetry possessed by the spin sector. Relying on the spin to generate transport anomalies would rest then on the magnitude of the spin-orbit effect on the Fe atom, which is however not sufficient to give rise to such transport anisotropies. The same is true in the ruthenates and the manganites. Further, as is well known from the manganites, coupling fluctuating spins with the lattice can only yield modest changes in the transport properties [66].

We now know from the crucial work of Kugel and Khomskii in the context of multi-orbital Mott systems, that orbital degrees can acquire dynamics and hence can order in a manner identical to $SU(2)$ spins. Orbital ordering, or equivalently orbital polarization, although driven by a small lattice distortion, can yield sizable transport effects in the electronic sector. Based on the success of the orbital ordering program in multi-orbital systems such as the manganites and the ruthenates, one of us[67, 68] as well as others[69–72] has advocated that similar physics applies to the pnictides, though not Mott insulators exhibit many of the characteristics of bad metals. In the pnictides, as a result of the C_4 symmetry in the high-temperature phase, the d_{xz} and d_{yz} orbitals are degenerate. Unequal occupancy of the former two lowers the lattice symmetry to C_2 and sizable rearrangements obtain in the electronic sector consistent with experiment. For example, two of us have shown[25] using the random-phase approximation that orbital fluctuations between the d_{xz} and d_{yz} orbitals in a five-band model[73] for the pnictides can lead to a break-down of perturbation theory and drive an instability to a non-Fermi liquid state.

In this Chapter, we approach the problem of the emergence of non-Fermi liquid states of matter using multidimensional bosonization[38, 40, 74, 75]. Since we are after universal physics, rather than starting from the complexity of a five-band model, we focus just on a two-band model with degenerate d_{xz} and d_{yz} orbitals to see if orbital fluctuations can give rise to non-Fermi liquid behaviour. We establish that as approaching the ferro orbital ordering quantum critical point (FOOQCP), a branch of $z = 3$ overdamped collective modes emerges at low energies and small momenta. When these collective modes dominate over the low energy physics at the FOOQCP, electrons are scattered off them strongly, which leads to non-Fermi liquid behaviour. This type of non-Fermi liquid behaviour has been well-studied in Hertz-Millis theory[76, 77], and it is the existence of this mode that is the finger print[20, 25, 27, 78, 79] of non-Fermi liquid behaviour associated with the d-wave Pomeranchuk instability in continuum and square lattice models. (Due to the existence of $z = 3$ overdamped mode, the self-energy of quasi-particle is modified to $\mathrm{Im}\Sigma \sim \omega^{2/3}$, contrasts to the case of Fermi liquid with $\mathrm{Im}\Sigma \sim \omega^2$.) We show that the emergence of a $z = 3$ overdamped mode in our system can

be obtained analytically and further confirmed by diagonalization of our bosonized Hamiltonian. It should be stressed that the system being studied in this Chapter is different from [80] because the dispersions for d_{xz} and d_{yz} orbitals do not intersect when interactions are present in our setup.

2.2 Model Hamiltonian

We wish to describe a two-orbital interacting system. Hence, our starting Hamiltonian contains a kinetic term of the form,

$$H_t = \sum_{\vec{k}\sigma} \psi^\dagger_{\vec{k}\sigma}[(\epsilon_{+,\vec{k}} - \mu) + \epsilon_{-,\vec{k}}\tau_3 + \epsilon_{xy,\vec{k}}\tau_1]\psi_{\vec{k}\sigma}, \tag{2.1}$$

defined on a square lattice with degenerate d_{xz} and d_{yz} orbitals per site. $\psi^\dagger_{\vec{k}\sigma} = (d^\dagger_{xz,\sigma}(\vec{k}), d^\dagger_{yz,\sigma}(\vec{k}))$ and $d^\dagger_{a,\sigma}(\vec{k})$ creates an electron on the orbital a with momentum $\vec{k}$ and spin σ. τ_i are Pauli matrices. $\epsilon_{+,-,xy}(\vec{k})$ can be obtained by including various hopping parameters which vary from material to material, their explicit expressions are given by

$$\begin{aligned}
\epsilon_{\pm,\vec{k}} &= \frac{\epsilon_{x,\vec{k}} + \epsilon_{y,\vec{k}}}{2} \\
\epsilon_{x,\vec{k}} &= -2t_1 \cos k_x - 2t_2 \cos k_y - 4t_3 \cos k_x \cos k_y \\
\epsilon_{y,\vec{k}} &= -2t_2 \cos k_x - 2t_1 \cos k_y - 4t_3 \cos k_x \cos k_y \\
\epsilon_{xy,\vec{k}} &= -4t_4 \sin k_x \sin k_y
\end{aligned} \tag{2.2}$$

The definitions of hopping amplitudes t_1, t_2, t_3 and t_4 are the same as that in [81]. It should be stressed that with numerical values of hopping amplitudes different from [81], the two-orbital model is capable to describe systems other than iron pnictides phenomenologically.

Since we are interested in an orbital ordering instability in the charge channel, only effective inter- and intra-orbital Coulomb interactions are considered here [82]. As a result, the minimal interacting Hamiltonian H_I is

$$H_I = \sum_{ia} U n_{ia\uparrow} n_{ia\downarrow} + \sum_{i,b>a} \left(U' - \frac{J}{2}\right) n_a n_b, \tag{2.3}$$

where U and U' are the intra- and inter-orbital interactions, and J is Hund's coupling.

Previously, we used RPA to show that non-Landau damping exists in a 5-band model [25]. To set the stage for the bosonization calculation, we discuss briefly the results of an RPA analysis on the two-band model considered here. We find that the self-energy of the quasiparticle on the Fermi surface shows a non-

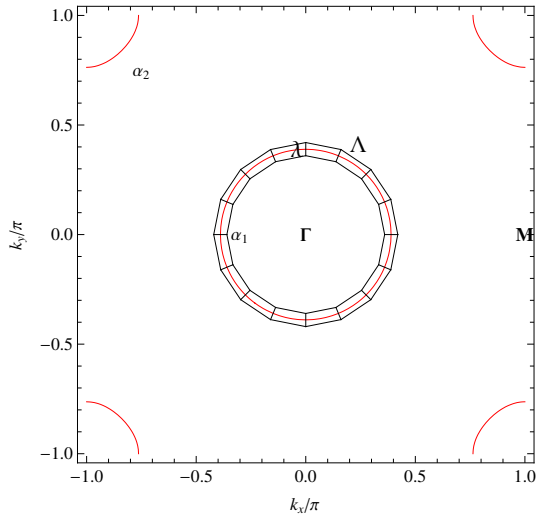

Figure 2.1: Illustration of the Fermi surface patches used in the multidimensional bosonization. The tight-binding hopping parameters are $t_1 = -1$, $t_2 = 0.5$, $t_3 = -0.6$, $t_4 = -0.5$, and the chemical potential is $\mu = 0.5$. There is two disconnected hole pockets, denoted respectively by α_1 and α_2, and no electron hole pocket.

Fermi liquid behaviour (i.e. $\mathrm{Im}\Sigma(\vec{k}_F, \omega) \sim \omega^\lambda$ with $\lambda < 1$) in the critical region near the orbital ordering quantum critical point (OOQCP). The consistency of this result with our previous 5-band model implies that it is the fluctuations associated with the d_{xz} and d_{yz} orbitals that leads to the non-Fermi liquid behaviour. Moreover, the simplicity of the present two-orbital model allows us to do further analysis on the overdamped $z = 3$ mode using a non-perturbative approach, the details of which we now present.

2.3 Multidimensional Bosonization

Multi-dimensional bosonization is ideally suited to this two-band problem because the d_{xz} and d_{yz} bands are quasi-1d. Following the standard procedure[27, 38, 40, 74, 75], we rewrite the tight-binding Hamiltonian in the eigen-band index in order to correctly identify the Fermi surfaces and the interactions between quasi-particles on the Fermi surfaces. Following the same convention used in [83], we introduce a unitary matrix $U_{a\nu,\vec{k}}$ such that the creation operators in the band index can be expressed as $\gamma^\dagger_{\nu\sigma\vec{k}} = \psi^\dagger_{a\sigma\vec{k}} U_{a\nu,\vec{k}}$, where ν denotes α (hole) or β (electron) Fermi surface. Using the recipe outlined by Haldane, we coarse-grain the Fermi surfaces into N equally sized patches of width Λ and thickness λ, as shown in Fig. 2.1. We enforce the limit of $\lambda \ll \Lambda \ll k_F$ so that the deviation from the multidimensional bosonization due to the processes of momentum-transfer between patches and the effect of curvature within each patch can be significantly reduced[40].

In the limit of low energy and long wavelength, the energy dispersion can be linearized near the Fermi surface, effectively reducing the kinetic term to $H_t = \sum_{\vec{k}} \vec{v}_{\vec{k},\nu} \cdot (\vec{k} - \vec{k_F}) \gamma^\dagger_{\nu\sigma,\vec{k}} \gamma_{\nu\sigma,\vec{k}}$. It has been shown[27, 38,

40, 74, 75] that this Hamiltonian can be entirely described by the density fluctuation operator defined as

$$\delta n_{S,\nu\vec{q}} = \sum_{\vec{k},\sigma} (\gamma^{\dagger}_{\vec{k},\nu\sigma}\gamma_{\vec{k}+\vec{q},\nu\sigma} - \delta_{\vec{q},0} n_{\vec{k},\nu\sigma}), \tag{2.4}$$

where the summation over momentum is restricted to be within patch S. Making use of the special commutation relation between these density fluctuation operators[37], we rewrite the kinetic term as

$$H_t = \sum_{S,\nu,\vec{q}} \frac{1}{2N_\nu(0)} \delta n_{S,\nu\sigma,-\vec{q}} \delta n_{S,\nu\sigma,\vec{q}}, \tag{2.5}$$

where $N_\nu(0)$ is the density of state at ν Fermi surface and $\sum_S$ represents summation over patches in the limit $N \to \infty$ and $\Lambda \to 0$, which can be changed into line integrals along the Fermi surfaces.

Similarly the interaction Hamiltonian in (2.3) can be expressed in terms of the density fluctuation operators as well. After a long but straightforward calculation, we arrive at the normal-ordered interaction Hamiltonian,

$$\begin{aligned} :H_I: &:= \tfrac{U}{N} \textstyle\sum_{a,\vec{q},ST\mu\nu} U^{*a\mu}_{\vec{k}_S+\vec{q}} U^{a\mu}_{\vec{k}_S} \delta n_{S\mu\vec{q}} U^{*a\nu}_{\vec{k}_T-\vec{q}} U^{a\nu}_{\vec{k}_T} \delta n_{T\nu,-\vec{q}} \\ &+ \tfrac{(2U'-J)}{N} \textstyle\sum_{\vec{q}ST\mu\nu,a\neq b} U^{*a\mu}_{\vec{k}_S+\vec{q}} U^{a\mu}_{\vec{k}_S} \delta n_{S\mu\vec{q}} U^{*b\nu}_{\vec{k}_T-\vec{q}} U^{b\nu}_{\vec{k}_T} \delta n_{S\nu,-\vec{q}}, \end{aligned}$$

where the spin index is dropped here after. The Hamiltonian (2.6) contains forward scattering only, as this is the only relevant interaction for nematic ordering. In general, other types of instabilities may exist and destroy the nematic orbital phase. However, recent Aslamazov-Larkin type vertex correction [84] and renormalization group studies have shown the nematic orbital phase to be stable, thereby justifying our approach [85].

Following [27], we write the effective action for the present bosonic theory, $S = S_t + S_I$, where

$$\begin{aligned} S_t &= -\frac{1}{2} \sum_{S,\nu\sigma,\vec{q}} \int \frac{d\omega}{2\pi} \delta n_{S,\nu\sigma,-\vec{q}} (\chi^0_{S,\nu})^{-1}(\vec{q},\omega) \delta n_{S,\nu\sigma,\vec{q}}, \\ \chi^0_{S,\nu}(\vec{q},\omega) &= N_\nu(0) \vec{v}_S \cdot \vec{q}/(\omega - \vec{v}_S \cdot \vec{q}) \\ &= N_\nu(0) \left(P \frac{\vec{v}_S.\hat{q}}{\frac{\omega}{q} - \vec{v}_S.\hat{q}} + i\pi \vec{v}_S.\hat{q}\delta(\frac{\omega}{q} - \vec{v}_S.\hat{q}) \right) \end{aligned} \tag{2.6}$$

and

$$S_I = \sum_{\vec{q}ST\mu\nu} \int \frac{d\omega}{2\pi} [\frac{U}{N} (\sum_a U^{*a\mu}_{\vec{k}_S+\vec{q}} U^{a\mu}_{\vec{k}_S} U^{*a\nu}_{\vec{k}_T-\vec{q}} U^{a\nu}_{\vec{k}_T}) + \frac{(2U'-J)}{N} (\sum_{a\neq b} U^{*a\mu}_{\vec{k}_S+\vec{q}} U^{a\mu}_{\vec{k}_S} U^{*b\nu}_{\vec{k}_T-\vec{q}} U^{b\nu}_{\vec{k}_T})] \delta n_{S\mu,\vec{q}} \delta n_{T\nu,-\vec{q}}.$$

We have introduced a small imaginary part to the denominator of χ^0_S to separate it into a real and an imaginary part, which will be helpful for later analysis. One can easily check that the interaction between quasiparticles with $\vec{k}_S$ and $\vec{k}_S$ is different from that between $\vec{k}_S$ and $R\vec{k}_S$ ($R\vec{k}_S$ denotes the new momentum obtained from rotating $\vec{k}_S$ by $\pi/2$). This directly means that the interactions contain both $l = 0$ and $l = 2$ channels which can be decoupled by introducing the auxiliary fields corresponding to l via Hubbard-Stratonovich transformations as

$$\begin{aligned} A_0(\vec{q}) &= \sqrt{\frac{1}{N}} \sum_{\nu,S_\nu} (c_{\vec{k}_{S_\nu}+\vec{q}} c_{\vec{k}_{S_\nu}} + s_{\vec{k}_{S_\nu}+\vec{q}} s_{\vec{k}_{S_\nu}}) \delta n_{S\nu,\vec{q}} \\ A_2(\vec{q}) &= \sqrt{\frac{1}{N}} \sum_{\nu,S_\nu} \pm (c_{\vec{k}_{S_\nu}+\vec{q}} c_{\vec{k}_{S_\nu}} - s_{\vec{k}_{S_\nu}+\vec{q}} s_{\vec{k}_{S_\nu}}) \delta n_{S\nu,\vec{q}}, \end{aligned} \tag{2.7}$$

where $U^{x\beta}_{\vec{k}} = U^{y\alpha}_{\vec{k}} = c_{\vec{k}}$ and $U^{y\beta}_{\vec{k}} = -U^{x\alpha}_{\vec{k}} = s_{\vec{k}}$ and the $+$ and $-$ signs in A_2 correspond to the α and β band respectively and subscripts are added to patch labels to avoid ambiguity. Integrating out the density fluctuation field δn leads to an effective action purely in terms of the auxiliary fields (The validity of integrating out the density fluctuation field can be justified by the numerical diagonalization in the next subsection, where we work directly with the bosonized Hamiltonian without integrating out the density fluctuation field. The same result is reached in both approaches.)

$$S = \int \tfrac{d\omega}{2\pi} \textstyle\sum_{\vec{q}} \begin{pmatrix} A_0(-\vec{q}) & A_2(-\vec{q}) \end{pmatrix} \begin{pmatrix} M_{00} & M_{02} \\ M_{20} & M_{22} \end{pmatrix} \begin{pmatrix} A_0(\vec{q}) \\ A_2(\vec{q}) \end{pmatrix},$$

where M_{00}, M_{22}, and M_{20} and M_{02} are given by

$$\begin{aligned}
M_{00}(\vec{q},\omega) =& - B' + \sum_{\nu,S_\nu} \frac{B'^2\chi^0_{S_\nu}}{N}(c_{\vec{k}_{S_\nu}+\vec{q}}c_{\vec{k}_{S_\nu}} + s_{\vec{k}_{S_\nu}+\vec{q}}s_{\vec{k}_{S_\nu}}) \\
& \times (c_{\vec{k}_{S_\nu}-\vec{q}}c_{\vec{k}_{S_\nu}} + s_{\vec{k}_{S_\nu}-\vec{q}}s_{\vec{k}_{S_\nu}}) \\
M_{02}(\vec{q},\omega) =& \sum_{\nu,S_\nu} \frac{BB'\chi^0_{S_\nu}}{N}(c_{\vec{k}_{S_\nu}+\vec{q}}c_{\vec{k}_{S_\nu}} + s_{\vec{k}_{S_\nu}+\vec{q}}s_{\vec{k}_{S_\nu}}) \\
& \times (c_{\vec{k}_{S_\nu}-\vec{q}}c_{\vec{k}_{S_\nu}} - s_{\vec{k}_{S_\nu}-\vec{q}}s_{\vec{k}_{S_\nu}}) \\
M_{20}(\vec{q},\omega) =& \sum_{\nu,S_\nu} \frac{BB'\chi^0_{S_\nu}}{N}(c_{\vec{k}_{S_\nu}+\vec{q}}c_{\vec{k}_{S_\nu}} - s_{\vec{k}_{S_\nu}+\vec{q}}s_{\vec{k}_{S_\nu}}) \\
& \times (c_{\vec{k}_{S_\nu}-\vec{q}}c_{\vec{k}_{S_\nu}} + s_{\vec{k}_{S_\nu}-\vec{q}}s_{\vec{k}_{S_\nu}}) \\
M_{22}(\vec{q},\omega) =& - B + \sum_{\nu,S_\nu} \frac{B^2\chi^0_{S_\nu}}{N}(c_{\vec{k}_{S_\nu}+\vec{q}}c_{\vec{k}_{S_\nu}} - s_{\vec{k}_{S_\nu}+\vec{q}}s_{\vec{k}_{S_\nu}}) \\
& \times (c_{\vec{k}_{S_\nu}-\vec{q}}c_{\vec{k}_{S_\nu}} - s_{\vec{k}_{S_\nu}-\vec{q}}s_{\vec{k}_{S_\nu}})
\end{aligned} \tag{2.8}$$

and $B = U/2 - U' + J/2$, $B' = U/2 + U' - J/2$.

It is important to recognize that the $A_2(0)$ field is associated with the orbital ordering parameter which breaks the C_4 symmetry. To see this, one can exploit the unitary matrix $U_{a\nu,\vec{k}}$ to transform $A_2(0)$ back to the orbital basis, and the resulting quantity will give the difference between the occupation number of the yz orbital and xz orbitals. As a result, we will focus on the region near OOQCP, that is, $M_{22}(0) \approx 0$, and the collective modes, if any, can be determined by the condition $M_{02}^2 - M_{00}M_{22} = 0$.

To evaluate the OOQCP condition, $M_{22}(0) = 0$, we take the limit $\omega/q \to 0$ and then $\vec{q} \to 0$ as advocated previously[27]. As a result, $\mathrm{Re}\chi^0_S(0) = -N_\nu(0)$, and the condition for the OOQCP is

$$\begin{aligned}
&\left(-1 + (U - 2U' + J)\frac{1}{2}\sum_\nu N_\nu(0) I_\nu\right) \geq 0, \\
&I_\nu = -\frac{1}{N}\sum_{S_\nu}(c^2_{\vec{k}_{S_\nu}} - s^2_{\vec{k}_{S_\nu}})^2.
\end{aligned} \tag{2.9}$$

Indeed, our condition for the OOQCP given in (2.9) is a generalization of the condition for the d-wave Pomeranchuk instability, $f_2 N(0) \leq -1$, in the continuous model[27, 86].

Now we turn to the collective modes in the critical region near the OOQCP. The low energy and long wavelength limit corresponds to $q \to 0$ and $\omega/(q\bar{v}_S) \to 0$, where $\bar{v}_S$ is the average Fermi velocity. A small q

expansion on M_{22} gives

$$M_{22}(\vec{q},\omega) = -B + \sum_{\nu,S_\nu} \frac{B^2 \chi^0_{S_\nu}(\vec{q},\omega)}{N} \left((c^2_{\vec{k}_{S_\nu}} - s^2_{\vec{k}_{S_\nu}})^2 + \cdots \right)$$

The q^2 term can be separated into real and imaginary part by the same trick. However, the imaginary part is higher order and can be neglected. Performing a similar analysis on M_{00} and M_{02}, one can find that in the small q and $\omega/(q\bar{v}_S)$ limit,

$$\begin{aligned}
M_{22} &= M^{(0)}_{22} + i\frac{\omega}{q}\widetilde{M}^{(0)}_{22} + M^{(2)}_{22} q^2 + \cdots \\
M_{00} &= M^{(0)}_{00} + i\frac{\omega}{q}\widetilde{M}^{(0)}_{00} + M^{(2)}_{00} q^2 + \cdots \\
M_{02} &= M^{(1)}_{02} q + \cdots,
\end{aligned} \tag{2.10}$$

where

$$\begin{aligned}
M^{(0)}_{22} &= -B - \sum_{\nu,S_\nu} \frac{B^2}{N} (c^2_{\vec{k}_{S_\nu}} - s^2_{\vec{k}_{S_\nu}})^2 N_\nu(0) \\
\widetilde{M}^{(0)}_{22} &= \sum_{\nu} \frac{B^2 \pi}{N\Lambda} N_\nu(0) (c^2_{\vec{k}_{S_\nu}} - s^2_{\vec{k}_{S_\nu}})^2 \\
&\quad \times \frac{\sqrt{(dk_y/dk_x)^2 + 1}}{(\omega/q - \vec{v}_{S_\nu}.\hat{q})'} |_{\omega/q = \vec{v}_{S_\nu}.\hat{q}} \\
M^{(2)}_{22} &= -\sum_{\nu,S_\nu} \frac{B^2}{N} N_\nu(0) \Big(\frac{1}{2} (c^2_{\vec{k}_{S_\nu}} - s^2_{\vec{k}_{S_\nu}}) \\
&\quad \times (c_{\vec{k}_{S_\nu}} (\vec{q}.\nabla)^2 c_{\vec{k}_{S_\nu}} + s_{\vec{k}_{S_\nu}} (\vec{q}.\nabla)^2 s_{\vec{k}_{S_\nu}}) \\
&\quad - (c_{\vec{k}_{S_\nu}} (\vec{q}.\nabla) c_{\vec{k}_{S_\nu}} - s_{\vec{k}_{S_\nu}} (\vec{q}.\nabla) s_{\vec{k}_{S_\nu}})^2 \Big)
\end{aligned} \tag{2.11}$$

where the prime in $\widetilde{M}^{(0)}_{22}$ denotes derivative with respect to k_x.

Consequently, we find that near the OOQCP (in (2.10), $M^{(0)}_{22} \approx 0$), the solution to

$$i\frac{\omega_{col}}{q} \widetilde{M}^{(0)}_{22} M^{(0)}_{00} + (M^{(0)}_{00} M^{(2)}_{22} - M^{(1)2}_{20}) q^2 = 0 \tag{2.12}$$

defines the collective $z = 3$ overdamped collective mode. This mode has a strong dependence on the Fermi surface topology and momentum $\vec{q}$. In the low-energy limit, $\omega/(q\bar{v}_S) \to 0$, the condition $\omega/q = \vec{v}_S \cdot \hat{q}$ basically requires that $\vec{v}_S$ is perpendicular to $\vec{q}$. Therefore, the Fermi surface should be smooth enough such that for an arbitrary direction of $\vec{q}$, there exists at least one perpendicular $\vec{v}_S$. This is not always the case,

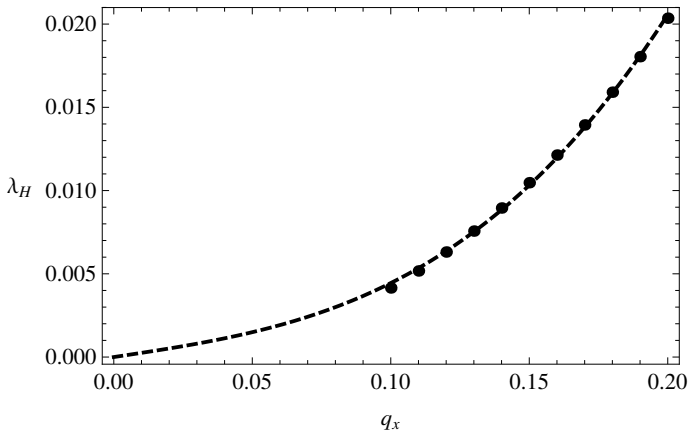

Figure 2.2: Eigenvalues of the imaginary mode of the bosonized Hamiltonian for $BN_{\alpha_1}(0) = -4.344$ and $q_y = 0$. The black dashed curve is a the fitting with the functional form, aq_x^3. The case of $q_x < 0.1$ is beyond the numerical accuracy with the choice of 2000 patches. More patches are required to access to the region of smaller q_x.

for example when the Fermi surface is a perfect square. For realistic models, $\widetilde{M}_{22}^{(0)}$ is always finite except when $q_x = \pm q_y$. This obtains because $c_{\vec{k}_S}^2 - s_{\vec{k}_S}^2$ vanishes when $\vec{k}_{S,x} = \pm\vec{k}_{S,y}$. Therefore, there will be no overdamped modes along the Brillouin zone diagonal, which matches precisely with previous studies of the Pomeranchuk instability on a square lattice[78, 79].

It is worth making a comparison between our result and the previous study on a continuous model by Lawler, *et. al.*[27]. They demonstrated that the $z = 3$ overdamped collective mode emerges close to the critical point in the continuum model when an interaction is present in the $l = 2$ channel, which is similar to the case of the itinerant ferromagnetic quantum critical point[76, 77]. It is remarkable to see that such an overdamped $z = 3$ collective mode exists in our lattice model as well, which strongly suggests that the orbital order in a lattice model is essentially equivalent to the nematic order in a continuous model. Furthermore, the existence of this overdamped $z = 3$ collective mode from the non-perturbative multidimensional bosonization technique builds a solid foundation for non-Fermi liquid behaviour since the single-particle Green function is changed fundamentally and obtains a non-perturbative form in the presence of this mode, as shown by Lawler *et. al.*[27].

2.4 Numerical Result

The collective modes can also be obtained by performing a generalized Bogoliubov transformation[87] on the bosonized Hamiltonian which allows us to make a direct comparison with the analytic result obtained above. For demonstration purposes, we choose a set of model parameters given in figure. 2.1 which have two hole pockets α_1 and α_2 but no electron pocket.We have just considered the fluctuations on the α_1 hole

Fermi pocket which is sufficient to capture the emergence of the $z = 3$ overdamped collective mode. Adding up Eqs. 2.5 and 2.6, we obtain the resulting Hamiltonian,

$$H = \frac{1}{N_{\alpha_1}(0)} \sum_{ST,\vec{q}} \left(\delta_{S,T} + N_{\alpha_1}(0) U_{S,T}(\vec{q})\right) \delta n_{T,-\vec{q}} \delta n_{S,\vec{q}}, \tag{2.13}$$

where $U_{S,T}(\vec{q}) = B/N(c_{\vec{k}_S+\vec{q}} c_{\vec{k}_S} - s_{\vec{k}_S+\vec{q}} s_{\vec{k}_S})(c_{\vec{k}_S-\vec{q}} c_{\vec{k}_S} - s_{\vec{k}_S-\vec{q}} s_{\vec{k}_S})$. The density fluctuation operator δn can be rewritten in terms of bosonic creation and annihilation operators[27, 74]

$$\begin{aligned} \delta n_{S,-\vec{q}} &= \sqrt{\vec{q}\cdot\vec{v}_S}\, a_{S,\vec{q}}\, \theta[\vec{q}\cdot\vec{v}_S] + \sqrt{-\vec{q}\cdot\vec{v}_S}\, a^\dagger_{S,\vec{q}}\, \theta[-\vec{q}\cdot\vec{v}_S] \\ \delta n_{S,\vec{q}} &= \sqrt{-\vec{q}\cdot\vec{v}_S}\, a_{S,\vec{q}}\, \theta[-\vec{q}\cdot\vec{v}_S] + \sqrt{\vec{q}\cdot\vec{v}_S}\, a^\dagger_{S,\vec{q}}\, \theta[\vec{q}\cdot\vec{v}_S] \end{aligned} \tag{2.14}$$

It can be checked that a and $a^\dagger$ must satisfy the standard commutation relation for bosons in order to satisfy the unusual commutation relation between δn[27, 74]. The Hamiltonian can now be rewritten in terms of these bosonic operators and diagonalized with a generalized Bogoliubov transformation.

The diagonalization of the bosonic Hamiltonian is done with 2000 Fermi surface patches and the interaction parameters are set to the values for the OOQCP, $(U - 2U' + J)N_{\alpha_1}(0) = -4.334$. For each momentum $\vec{q}$, we diagonalize a bosonic Hamiltonian with a size of 4000×4000. The energy of the overdamped collective mode can be identified uniquely as the only purely imaginary eigenvalue of the bosonized Hamiltonian for each $\vec{q}$ [1] Fig. 2.2 plots the magnitude of this purely imaginary eigenvalue λ_H as a function of q_x for $q_y = 0$, which can be fitted perfectly with a function of the form aq_x^3 (dashed curve). This proves that this branch of the overdamped collective modes indeed has $z = 3$. We have also checked another choice of model parameters given by Qi *et. al.*[83] as a minimal model for iron-based superconductors. In this case, the electron pockets have a much larger density of states than the hole pockets, and we find that the OOQCP is given by $U/4t \approx 1.7$, which is in a reasonable range to be experimentally relevant. We still find the same $z = 3$ overdamped collective mode from the technique presented above, which supports our overall conclusion that the overdamped critical mode with $z = 3$ is a general feature in a two-orbital model close to the OOQCP.

[1] A quadratic fermionic system can always be diagonalized by a (unitrary) Bogoliubov transformation that preserves the anti-commutation relations. However, in order to preserve the commutation relation for a bosonic system, a generalized Bogoliubov transformation is required. Such a transformation is not unitary and the resulting matrix we need to diagonalize is no longer Hermitian. It is then possible for the eigenvalues to be imaginary which signals an instability[87–89] in the system. In the study of Bose-Einstein condensation (BEC) in cold atom systems, the appearance of complex excitation energy is an important singature for the breakdown of BEC.

2.5 Conclusion

Using non-perturbative multidimensional bosonization, we have demonstrated the emergence of a $z = 3$ overdamped collective mode from a general two-orbital model in the vicinity of the orbital ordering quantum critical point. Since it has been well-established that the very existence of a $z = 3$ overdamped mode[20, 27, 78, 79] completely washes out the standard Fermi liquid description, non-Fermi liquid behaviour should generally occur in a two-orbital model or in a multiorbital model with degenerate d_{xz} and d_{yz} orbitals. Our bosonic theory provides a solid non-perturbative foundation for the interpretation of the anomalous zero-bias enhancement observed in recent point-contact spectroscopy experiments on a variety of iron-based superconductors[23, 24] as non-Fermi liquid behaviour induced by orbital fluctuations[25].

Chapter 3

Dynamical Gap and Cuprate-like Physics from Holography

We study the properties of fermion correlators in a boundary theory dual to the Reissner-Nordström AdS_{d+1} background in the presence of a bulk dipole (Pauli) interaction term with strength p. We show that by simply changing the value of the parameter p we can tune continuously from a Fermi liquid (small p), to a marginal Fermi liquid behavior at a critical value of p, to a generic non-Fermi liquid at intermediate values of p, and finally to a Mott insulator at large values of the bulk Pauli coupling. As all of these phases are seen in the cuprate phase diagram, the holographic model we study has the key elements of the strong coupling physics typified by Mott systems. In addition, we extend our analysis to finite temperature and show that the Mott gap closes. Of particular interest is that it closes when the ratio of the gap to the critical temperature is of the order of ten. This behavior is very much similar to that observed in the classic Mott insulator VO_2. We then analyze the non-analyticities of the boundary theory fermion correlators for generic values of frequency and momentum by calculating the quasi-normal modes of the bulk fermions. Not surprisingly, we find no evidence for the dipole interaction inducing an instability in the boundary theory. Finally, we briefly consider the introduction of superconducting condensates, and find that in that case, the fermion gap is driven by scalar-fermion couplings rather than by the Pauli coupling.

3.1 Introduction

Holography can offer unprecedented insight into the dynamics of strongly coupled systems. In the recent past, it has become clear that the domain of applicability of holography goes beyond high energy physics and includes strongly-correlated sytems in condensed matter physics, as well (see [52, 90–92] for reviews). Since in most cases of interest, we do not possess a microscopic understanding of the field theory dynamics under study, a phenomenological point of view (the so-called "bottom-up" approach) is taken where a minimal gravitational setup is devised for analyzing a specific strong-coupling feature of a system. In some situations where string or M-theory completion of a bottom-up construction is known, one may wonder how a bottom-up result is modified in a top-down approach. For example, a quantity of interest in strongly-correlated

condensed matter systems, which can easily be computed using holography, is the fermion spectral function (which is proportional to the imaginary part of the fermion retarded two-point function). There has recently been much discussion about this quantity in the holographic literature [48, 60, 93–95] where analyzing the Dirac equation for a charged probe fermion propagating in a gravitational background (usually a charged black hole), one can show that the retarded two-point function of the dual fermionic operator in the boundary theory shows a variety of unexpected emergent phenomena. In top-down approaches to holographic systems, the fermions are generically coupled to gravity and gauge fields in a variety of ways, beyond minimal coupling. It is certainly desirable to analyze how such non-minimal bulk couplings modify the fermion spectral function in the boundary theory, or may lead to new interesting emergent phenomena.

Recently, it was shown [96–99] that there are consistent truncations of ten and eleven dimensional supergravities to five and four dimensional bulk theories that possess an interesting class of gauge interactions and charged matter, allowing for novel condensed matter physics phenomena, such as superconductivity, to be explored in a consistent top-down approach [100–102]. The fermionic sector of these truncations has also been worked out in [103, 104] where a number of generic couplings for the fermions (with possible applications to strongly-correlated condensed matter systems) have been realized.

Motivated by these studies, we considered in [105] a generic non-minimal fermion coupling in which a spin-1/2 fermion couples to the gauge field through a dipole (Pauli) interaction of the form $F_{ab}\bar{\psi}\Gamma^{ab}\psi$. In fact, we just considered the simplest possible setup, in which a spin-1/2 fermion propagates in the background of a Reissner-Nordström AdS_{d+1} black hole. We found that as one changes the strength of this interaction, spectral weight of the dual fermionic operator is transferred between bands, and beyond a critical value of the dipole coupling, a gap emerges in the fermion density of states. We then concluded that a possible interpretation of this interaction is that it drives the dynamical formation of a (Mott) gap, in the absence of continuous symmetry breaking. In the Hubbard model, the Mott gap forms in $d > 1$ once the on-site interaction U exceeds a critical value in the half-filled system. Upon doping, spectral weight shifts from high to low energies. Consequently, we argued that the strength of the dipole interaction mimics the combined effects of doping and the on-site interaction strength U.

In this Chapter, we continue our study of the dipole interaction in more detail. We investigate the existence of Fermi surfaces as the dipole coupling p is varied. For the range of parameters considered in this Chapter, we find that there is no Fermi surface above a certain value of p. This is the range of parameters considered in [105], where the boundary theory exhibits two main features of Mott insulators, a dynamically generated gap (in the absence of continuous symmetry breaking) and spectral weight transfer. In addition, for the values of the dipole coupling p for which there is a Fermi surface in the boundary theory, we find

that at a critical value of this coupling, marginal-Fermi liquid behavior ensues. Consequently, we are able with our model (see Figure 3.1) to describe at one extreme, the Mott insulating state with a dynamically generated gap, a transition to a marginal Fermi liquid (MFL) and at the other, a Fermi-liquid-like regime in which the excitation spectrum scales linearly with the frequency. As all of these regimes are accessed simply by changing the value of the dipole coupling p, this suggests a direct parallel between p and the hole-doping level in the high-temperature copper-oxide superconductors (hereafter cuprates). In the cuprates, the strong electron correlation physics ends at a value of doping (typically optimal doping) where marginal-Fermi liquid [6] behavior ensues. Perhaps the occurence of the MFL state of the probe fermions in our holographic setup is an indication that this phenomenological model is ultimately a robust feature of the transition from strong to weakly interacting physics in doped Mott systems.

Having discussed the pole structure of the boundary theory fermion (retarded) correlators for non-zero values of p at small frequency, we analyze the non-analyticities of those correlators for generic values of frequency and momentum. We do this by numerically calculating the quasi-normal modes of the bulk fermion in the (extremal) Reissner-Nordström AdS_{d+1} background. Following the motion of the poles in the complex frequency plane as a function of momentum, we compute their dispersion relations and, for the range of parameters considered, confirm that all of the poles stay in the lower half of the complex frequency plane, for all momenta. Hence, as expected, turning on a non-zero bulk dipole coupling in our set up does not cause an instability in the boundary theory.

We consider our setup at finite temperature and find that as the temperature increases the gap closes and, moreover, the critical temperature for which this happens is much less than the value of the gap. In this regard, the closing of the gap induced by temperature parallels what one obtains in the classic Mott system VO_2 [106], namely, the gap closes at a temperature much lower than the gap.

The Chapter is organized as follows. In section 3.2 we consider a bulk fermion in the Reissner-Nordström AdS_{d+1} black hole background and couple it to the U(1) gauge field non-minimally through a dipole interaction with strength p. We then derive the Dirac equations and rewrite them as flow equations which will be more convenient for numerically calculating the boundary theory fermion correlators. In section 3.3 we investigate the existence of Fermi surfaces as a function of p by solving the Dirac equations at zero frequency. In section 3.4, we first discuss the small-frequency behavior of the poles of the boundary theory fermion (retarded) correlators when p is non-zero. We then analyze the non-analyticities of those correlators for generic values of frequency and momenta. In section 3.5 we study the effects of temperature in our holographic setup. Finally, in section 3.6, we discuss the relevance of our work to cuprate phase diagram and conclude with open questions as well as extensions for future work. In particular, we contemplate the

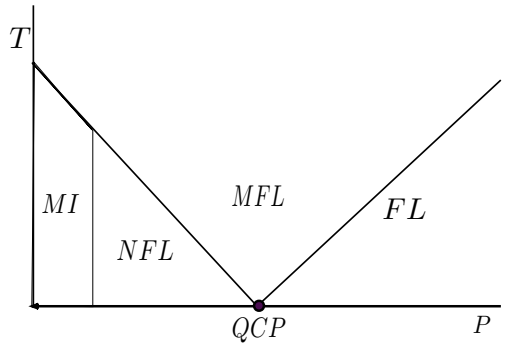

Figure 3.1: A cartoon of the phase diagram of the boundary theory considered here. MI indicates a Mott insulator, a phase with a gap in the absence of symmetry breaking. NFL denotes non-fermi liquid behavior which is distinct from the gapped spectrum of a Mott insulator. MFL indicates marginal-Fermi liquid behavior in which the "electron" self energy scales as $\omega \log \omega$ at $T = 0$, and a FL (Fermi liquid) regime in which the dispersion is linear in frequency. The tuning parameter in this model is the Pauli (dipole) coupling. Similar behavior is obtained in the non-superconducting features of the cuprate materials by tuning the hole-doping level x.

extension of our results to superconducting backgrounds, which also do not possess a finite ground state degeneracy at zero temperature.

3.2 Bulk Analysis

As we alluded to above, we consider just one form of non-minimal coupling, in which a spin-1/2 fermion is coupled to the gauge field through a dipole interaction[1] of the form $F_{ab}\bar{\psi}\Gamma^{ab}\psi$, and propagates in the background of a Reissner-Nordström AdS_{d+1} black-hole (hereafter, denoted by RN-AdS_{d+1}). Thus, we consider the bulk Lagrangian

$$\sqrt{-g}\, i\bar{\psi}(\not{D} - m - ip\not{F})\psi, \tag{3.1}$$

in $d+1 \geq 4$ dimensions where

$$\begin{aligned}
\bar{\psi} &= \psi\, \Gamma^{\underline{t}}, \\
\not{D} &= e_c^M \Gamma^c \left(\partial_M + \frac{1}{4}\omega_M^{ab}\Gamma_{ab} - iqA_M\right), \\
\not{F} &= \frac{1}{2}\Gamma^{ab} e_a^M e_b^N F_{MN},
\end{aligned} \tag{3.2}$$

with e_a^M and ω_M^{ab} being the (inverse) vielbein and the spin connection, respectively. We denote the bulk coordinate indices by capital letters $M, N, \cdots = \{t, x^i, r\}$ while the tangent space indices are denoted by

[1] In even bulk dimensions, there is a similar interaction which includes a Γ_5. We will not consider this interaction in this Chapter.

$a, b, \cdots = \{\underline{t}, \underline{x}^i, \underline{r}\}$. We will reserve the Greek indices $\mu, \nu, \ldots$ to denote boundary coordinate directions. We use Dirac matrices $\Gamma^{\underline{t}}, \Gamma^{\underline{1}}, ..., \Gamma^{\underline{r}}$ satisfying the Clifford algebra $\{\Gamma^a, \Gamma^b\} = 2\eta^{ab}$. Also, $\Gamma_{ab} = \frac{1}{2}[\Gamma_a, \Gamma_b]$. In what follows, we will rescale $p \to pL/(d-2)$ for convenience.

The RN-AdS$_{d+1}$ background has a metric and a gauge connection which can be written

$$ds^2 = \frac{r^2}{L^2}\left[-f(r)dt^2 + d\vec{x}^2\right] + \frac{L^2}{r^2}\frac{dr^2}{f(r)}, \tag{3.3}$$

$$A = \mu\left[1 - (\frac{r_0}{r})^{d-2}\right]dt, \tag{3.4}$$

where

$$\begin{aligned} f(r) &= 1 - M\left(\frac{r_0}{r}\right)^d + Q^2\left(\frac{r_0}{r}\right)^{2(d-1)}, \\ \mu &= \left(\frac{d-1}{2d-4}\right)^{1/2}\frac{Qr_0}{L^2}, \qquad\qquad M = 1 + Q^2, \end{aligned} \tag{3.5}$$

with r_0 being the horizon, given by the largest real root of $f(r_0) = 0$. The temperature T of this (black hole) background is given by

$$T = (d-2)\frac{r_0}{4\pi L^2}\left(\frac{d}{d-2} - Q^2\right). \tag{3.6}$$

From the above equation, one notes that the RN-AdS$_{d+1}$ black hole is extremal when $Q^2 = d/(d-2)$ while the density and entropy remain finite. Since the background is invariant under $A_t \to -A_t$, without loss of generality, we can choose μ, or equivalently Q, to be positive. Thus, we can take $0 < Q \leq \sqrt{d/(d-2)}$, where the equality corresponds to extremality.

To analyze the Dirac equations of the bulk fermion, we find it more convenient to go to momentum space by Fourier transforming $\psi(r, x^\mu) \sim e^{ik.x}\psi(r, k^\mu)$, where $k^\mu = (\omega, \vec{k})$. The Fourier transform of the Dirac operator $\not{D}$ is of the form

$$\begin{aligned} \not{D} = &\frac{r}{L}\sqrt{f(r)}\,\Gamma^{\underline{r}}\left[\partial_r + \frac{f'(r)}{4f(r)} + \frac{d}{2r}\right] \\ &- i\frac{L}{r\sqrt{f(r)}}\Gamma^{\underline{t}}[\omega + qA_t(r)] + i\frac{L}{r}\vec{k}\cdot\vec{\Gamma}, \end{aligned} \tag{3.7}$$

while

$$\not{F} = (d-2)\frac{\mu}{r_0}\left(\frac{r_0}{r}\right)^{d-1}\Gamma^{\underline{rt}}. \tag{3.8}$$

To decouple the Dirac equations, we introduce projectors $\Gamma_\pm = \frac{1}{2}(1 \pm \Gamma^{\underline{r}}\Gamma^{\underline{t}}\hat{k}\cdot\vec{\Gamma})$ and write $\psi_\pm(r) = r^{d/2}f(r)^{1/4}\Gamma_\pm\psi(r)$. Without loss of generality, we set $k_1 = k$ and $k_{i\neq 1} = 0$, and take the basis

$$\Gamma^{\underline{r}} = \begin{pmatrix} -\sigma_3\otimes\mathbb{1} & 0 \\ 0 & -\sigma_3\otimes\mathbb{1} \end{pmatrix},\ \Gamma^{\underline{t}} = \begin{pmatrix} i\sigma_1\otimes\mathbb{1} & 0 \\ 0 & i\sigma_1\otimes\mathbb{1} \end{pmatrix},$$
$$\Gamma^{\underline{1}} = \begin{pmatrix} -\sigma_2\otimes\mathbb{1} & 0 \\ 0 & \sigma_2\otimes\mathbb{1} \end{pmatrix}. \tag{3.9}$$

where σ_j's are the Pauli matrices, and $\mathbb{1}$ is a $2^{\frac{d-3}{2}}$-dimensional identity matrix for odd values of d, and $2^{\frac{d-4}{2}}$-dimensional for d even. Note that by choosing $k_1 = k$ and $k_{i\neq 1} = 0$ the rest of the gamma matrices do not appear in the Dirac equations. So, we did not bother to include those in (5.31). One then finds

$$\begin{aligned}\frac{r^2}{L^2}\sqrt{f(r)}\,\partial_r\psi_\pm = \frac{i\sigma_2}{\sqrt{f(r)}}\left[\omega + \mu q\left(1 - \frac{r_0^{d-2}}{r^{d-2}}\right)\right]\psi_\pm \\ - \sigma_1\left(\mu p\frac{r_0^{d-2}}{r^{d-2}} \pm k\right)\psi_\pm - \sigma_3\frac{r}{L}m\psi_\pm.\end{aligned} \tag{3.10}$$

We see that the Pauli coupling modifies the appearance of k in the above Dirac equations. To see the effects of p more clearly, consider the solutions of the Dirac equations (3.10) in the asymptotic and near horizon regimes. Asymptotically, the solutions behave as

$$\begin{aligned}\psi_\pm(r,\omega,k) = a_\pm(\omega,k)\ r^{mL}\begin{pmatrix}0\\1\end{pmatrix}\Big[1+\cdots\Big] \\ + b_\pm(\omega,k)\, r^{-mL}\begin{pmatrix}1\\0\end{pmatrix}\Big[1+\cdots\Big].\end{aligned} \tag{3.11}$$

The effect of p asymptotically is to modify the subleading terms. For $m \in [0, \frac{1}{2})$ both terms in (3.11) are normalizable and one can choose either $a_\pm$ or $b_\pm$ to be the sources for the dual fermion operator in the boundary theory. In this Chapter, we take $m \in [0, \frac{1}{2})$ and consider the conventional quantization where $a_\pm$ are the sources. Thus, the dual fermion operator has dimension $\Delta = \frac{3}{2} + m$. Choosing in-falling boundary conditions near the horizon results in a retarded correlator of the form

$$G_R(\omega,k) = \begin{pmatrix} G_+(\omega,k)\,\mathbb{1} & 0 \\ 0 & G_-(\omega,k)\,\mathbb{1} \end{pmatrix}, \tag{3.12}$$

with $G_\pm(\omega,k) = b_\pm(\omega,k)/a_\pm(\omega,k)$. Note that the Dirac equations (3.10) imply $G_+(\omega,k) = G_-(\omega,-k)$.

When the background is extremal, $f(r)$ has a double zero at the horizon, $f(r) \sim d(d-1)(1-r_0/r)^2+\cdots$, and this fact makes taking the limit of $\omega \to 0$ of the equations (3.10) near the horizon subtle. To take care of the subtlety, one realizes [60, 107] that near the horizon (in which the geometry approaches $\mathrm{AdS}_2 \times \mathbb{R}^{d-1}$ for $T = 0$) the equations for $\psi_\pm$ in (3.10) organize themselves as functions of $\zeta = \omega L_2^2/(r-r_0)$ with $L_2 = L/\sqrt{d(d-1)}$ being the radius of AdS_2. The coordinate ζ is the suitable radial coordinate for the AdS_2 part of the near horizon region, and in this region, we can write $\psi_\pm$ in terms of ζ and expand in powers of ω as follows

$$\psi_{I\pm}(\zeta) = \psi^{(0)}_{I\pm}(\zeta) + \omega\,\psi^{(1)}_{I\pm}(\zeta) + \omega^2\psi^{(2)}_{I\pm}(\zeta) + \cdots . \tag{3.13}$$

Now, substituting (3.13) into (3.10), we find that to leading order

$$\begin{aligned}\psi^{(0)\prime}_{I\pm}(\zeta) = \frac{L_2}{\zeta}\left[m\sigma_3 + \left(c_d\frac{p}{L} \pm \frac{kL}{r_0}\right)\sigma_1\right]\psi^{(0)}_{I\pm}(\zeta)\\ - i\,\sigma_2\left(1+\frac{qe_d}{\zeta}\right)\psi^{(0)}_{I\pm}(\zeta),\end{aligned} \tag{3.14}$$

where $e_d = 1/\sqrt{2d(d-1)}$, and $c_d = 1/\left[(2d-4)e_d\right]$. Equations (3.14) are identical to the equations of motion for massive spinor fields [60] with masses $(m,\tilde{m}_+)$ and $(m,\tilde{m}_-)$ in AdS_2, where $\tilde{m}_\pm$ are time-reversal violating mass terms, with the identification

$$\tilde{m}_\pm = c_d\frac{p}{L} \pm \frac{kL}{r_0}. \tag{3.15}$$

Thus, $\psi^{(0)}_{I\pm}(\zeta)$ are dual to spinor operators $\mathcal{O}_\pm$ in the IR CFT with conformal dimensions $\delta_\pm = \nu_k^\pm + \frac{1}{2}$ where

$$\begin{aligned}\nu_k^\pm &= \sqrt{m_{k\pm}^2 L_2^2 - q^2e_d^2 - i\epsilon},\\ m_{k\pm}^2 &= m^2 + \left(c_d\frac{p}{L} \pm \frac{kL}{r_0}\right)^2.\end{aligned} \tag{3.16}$$

We see that turning on p modifies the scaling in the infrared in an important way – effectively, the momentum is pushed up and down by p. We will explore the details of this in what follows.

One can write a formal expression for the fermion retarded correlator (3.12) at low frequency in terms of the retarded Green functions of the IR CFT spinor operators $\mathcal{O}_\pm$. As shown in [60], such a formal expression is extremely useful in analyzing the small ω behavior of the boundary theory Green functions. This is done by matching the inner AdS_2 and outer AdS_4 solutions in the so-called "matching region" where the $\zeta \to 0$

and $\omega/\zeta \to 0$ limits are taken. In so doing, one finds that the coefficients $a_\pm(\omega,k)$ and $b_\pm(\omega,k)$ in (3.12) are given by

$$\begin{aligned} a_\pm(\omega,k) &= \left[a_\pm^{(0)} + \omega\, a_\pm^{(1)} + \mathcal{O}\left(\omega^2\right)\right] \\ &\quad + \left[\tilde{a}_\pm^{(0)} + \omega\, \tilde{a}_\pm^{(1)} + \mathcal{O}\left(\omega^2\right)\right] \mathcal{G}_k^\pm(\omega), \end{aligned} \tag{3.17}$$

$$\begin{aligned} b_\pm(\omega,k) &= \left[b_\pm^{(0)} + \omega\, b_\pm^{(1)} + \mathcal{O}\left(\omega^2\right)\right] \\ &\quad + \left[\tilde{b}_\pm^{(0)} + \omega\, \tilde{b}_\pm^{(1)} + \mathcal{O}\left(\omega^2\right)\right] \mathcal{G}_k^\pm(\omega), \end{aligned} \tag{3.18}$$

where $a_\pm^{(n)}, \tilde{a}_\pm^{(n)}, b_\pm^{(n)}$ and $\tilde{b}_\pm^{(n)}$ are all functions of k and can, in principle, be determined numerically. Also, in the above expressions, $\mathcal{G}_k^\pm(\omega)$ denote the retarded Green functions of the dual IR CFT operators $\mathcal{O}_\pm$ which are given by [60]

$$\mathcal{G}_k^\pm(\omega) = c_\pm(k)\, \omega^{2\nu_\pm}, \tag{3.19}$$

with

$$\begin{aligned} c_\pm(k) = e^{-i\pi\nu_\pm} \frac{\Gamma(-2\nu_\pm)\Gamma(1+\nu_\pm - iqe_d)}{\Gamma(2\nu_\pm)\Gamma(1-\nu_\pm - iqe_d)} \times \\ \frac{(m+i\tilde{m}_\pm)L_2 - iqe_d - \nu_\pm}{(m+i\tilde{m}_\pm)L_2 - iqe_d + \nu_\pm}. \end{aligned} \tag{3.20}$$

Note that the expressions (3.17) are (3.18) are not valid when $2\nu_\pm$ is an integer. In such cases there would be additional terms like $\omega^n \log\omega$ (with n being a positive integer) on the right hand sides of (3.17) and (3.18).

In order to obtain $G_\pm(\omega,k)$ for generic values of ω and k, one must solve the Dirac equations (3.10) numerically. For numerical purposes, it is convenient to work with dimensionless quantities. So, we rescale r, ω and k in the Dirac equations (3.10) by defining

$$r \to r_0 u, \qquad \omega \to \frac{r_0}{L^2}\,\omega, \qquad k \to \frac{r_0}{L^2}\,k. \tag{3.21}$$

It is also more convenient to convert the Dirac equations (3.10) into the so-called flow equations [48, 108]. For that, we first write $\psi_\pm^T = (\beta_\pm, \alpha_\pm)$ and define $\xi_\pm = \beta_\pm/\alpha_\pm$, in terms of which the Dirac equations (3.10)

then reduce to the non-linear flow equations

$$\begin{aligned} u^2\sqrt{f(u)}\partial_u\xi_\pm &= -2(mL)u\,\xi_\pm \\ &\quad + [v_-(u)\mp k] + [v_+(u)\pm k]\,\xi_\pm^2, \end{aligned} \tag{3.22}$$

where

$$v_\pm(u) = \frac{1}{\sqrt{f(u)}}\left[\omega + Qq\left(1-u^{2-d}\right)\right] \pm Qp\,u^{2-d}. \tag{3.23}$$

To obtain the retarded Green functions of the boundary theory operators, one has to choose the infalling boundary condition at the horizon for the (dual) bulk fields [109, 110]. Expressed in terms of $\xi_\pm$, the infalling boundary condition for $\psi_\pm^T = (\beta_\pm, \alpha_\pm)$ at the horizon translates into

$$\xi_\pm(u=1) = \begin{cases} i & \omega \neq 0, \\ (mL_2 - \nu_\pm)/(qe_d + \tilde{m}_\pm L_2) & \omega = 0. \end{cases} \tag{3.24}$$

The matrix of Green functions (3.12) then takes the form

$$G_R(\omega,k) = \lim_{\epsilon\to 0}\,\epsilon^{-2mL}\begin{pmatrix} \xi_+\,\mathbb{1} & 0 \\ 0 & \xi_-\,\mathbb{1} \end{pmatrix}\Big|_{u=\frac{1}{\epsilon}}, \tag{3.25}$$

where one picks the finite terms as $\epsilon \to 0$. Up to normalization, the fermion spectral function is defined by

$$A(\omega,k) \equiv \mathrm{Tr}\,\mathrm{Im}\,G_R(\omega,k). \tag{3.26}$$

3.3 Continuum and Bound States

In this section, we will study the effects of small and negative values of p. As we will see, in this regime, there is a (non-Fermi-liquid) Fermi peak whose properties change as we vary p. In this regime, there is some similarity to the properties of Fermi surfaces studied in [48, 60]. As we change parameters, the scaling dimensions change, and we can pass from a non-Fermi liquid (NFL) to a marginal Fermi liquid (MFL) and on to fermions which have some resemblance to Landau Fermi liquids (FL). However, we will see clearly that there is a positive value of p beyond which the Fermi peak ceases to exist. In what follows, we will mostly set $m = 0$ and $q = 1$ (as we vary p), although similar results hold for a range of these parameters.

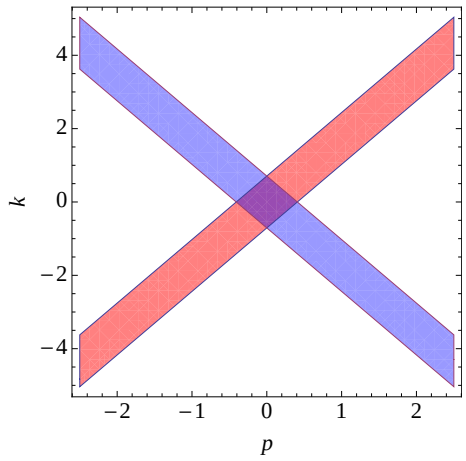

Figure 3.2: Plots of $\mathcal{I}_\pm$ versus p (for $d = 3$, $\Delta_\psi = 3/2$ and $q = 1$). The red band depicting $\mathcal{I}_-$ is where $\mathrm{Im}\, G_-(\omega, k)$ becomes oscillatory at small ω. The blue band ($\mathcal{I}_+$) shows the region where $\mathrm{Im}\, G_+(\omega, k)$ is oscillatory (at small ω).

We begin by focussing on the regime that has been called log-oscillatory in [48, 60], in which Fermi peaks do not occur. There are some important changes when $p \neq 0$ that we will explain below. When $q^2 > 2m^2L^2$, there exists a range of momenta $k \in \mathcal{I}_+$ for which the dimension of the IR CFT operator $\mathcal{O}_+$ becomes imaginary. Similarly, for $k \in \mathcal{I}_-$ the dimension of $\mathcal{O}_-$ becomes imaginary. Here, we have defined $\mathcal{I}_\pm = (\mp c_d\, p - k_o, \mp c_d\, p + k_o)$ with $k_o = \sqrt{(q^2/2) - m^2L^2}$. (Figure 3.2 shows plots of $\mathcal{I}_\pm$ versus p.) Consequently, $\mathrm{Im}\, G_\pm(0, k)$ is generically non-vanishing for $k \in \mathcal{I}_\pm$, respectively; see Figure 3.3 for plots of $\mathrm{Im}\, G_\pm(0, k)$ as a function of p. At $p = 0$, one has $\mathcal{I}_+ = \mathcal{I}_- \equiv \mathcal{I}$. This case was analyzed in [48, 60] where it was found that for $k \in \mathcal{I}$ and for small ω, both $\mathrm{Im}\, G_\pm(\omega, k)$ are periodic in $\log \omega$, with the same period.

At $p = 0$, the range of momenta for which $\mathrm{Im}\, G_\pm(\omega, k)$ become log-oscillatory at small ω is the same for each, namely $k \in \mathcal{I}$. This degeneracy does not persist for non-zero p, hence the fermion spectral function $A(\omega, k)$ will also have non-oscillatory components. For $p \in [-k_o/c_d, k_o/c_d] - \{0\}$, both $\mathrm{Im}\, G_\pm(\omega, k)$ show log-oscillatory behavior (with different periods, though) only for $k \in \mathcal{I}_+ \cap \mathcal{I}_-$. For $|p| > k_o/c_d$ where $\mathcal{I}_+ \cap \mathcal{I}_- = \emptyset$, one finds that in the regime where $\mathrm{Im}\, G_-(\omega, k)$ shows log-oscillatory behavior, $\mathrm{Im}\, G_+(\omega, k)$ is not oscillatory and vice versa.

For real $\nu_k^\pm$, the boundary conditions for $\xi_\pm(u = 1)$ at $\omega = 0$ are real. Since the equations (3.22) are real, one deduces that $\mathrm{Im}\, G_\pm(0, k) = 0$. Thus, $\mathrm{Re}\, G_\pm(0, k) = G_\pm(0, k) = b_\pm^{(0)}/a_\pm^{(0)}$. $\mathrm{Re}\, G_\pm(0, k)$ may have poles which would be given generically by the zeros of $a_\pm^{(0)}$. Each zero of $a_\pm^{(0)}$ defines a Fermi momentum k_F, given that $b_\pm^{(0)}$ do not vanish as $k \to k_\mathrm{F}$. Since $G_-(\omega, k) = G_+(\omega, -k)$, vanishing of $a_-^{(0)}$ at some $k = k_\mathrm{F}$ implies that $a_+^{(0)}$ vanishes at $k = -k_\mathrm{F}$. So, in order to find k_F, we can just analyze the zeros of $a_-^{(0)}$. From the asymptotic behavior of ψ_- which is given in (3.11), together with (3.17) and the definition of $\psi_-^T = (\beta_-, \alpha_-)$, it is easy to see that, at $\omega = 0$, $\alpha_-(u, k) = a_-^{(0)}\, u^{mL} + \cdots$ as $u \to \infty$. (Also, note that

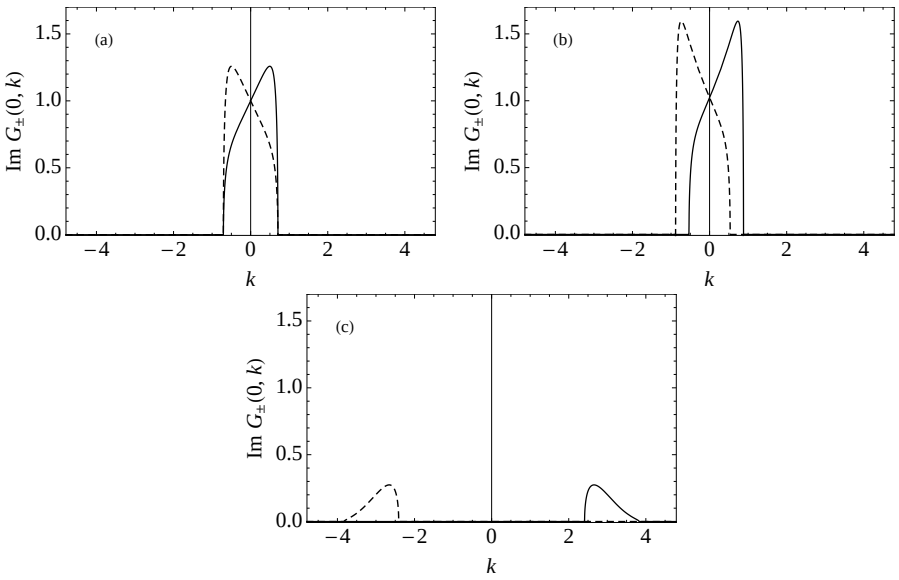

Figure 3.3: Plots of $\mathrm{Im}\, G_-(0,k)$ (solid line) and $\mathrm{Im}\, G_+(0,k)$ (dashed line) for (a) $p=0$, (b) $p=0.1$ and (c) $p=1.8$. We set $d=3$, $\Delta_\psi=3/2$ and $q=1$. Similar plots can be obtained for negative values of p by switching the solid lines with the dashed lines. Focusing on positive p, we see that the maximum value of $\mathrm{Im}\, G_\pm(0,k)$ increases as $p\to 1/\sqrt{6}$, after which (namely, for $p>1/\sqrt{6}$) it rapidly decreases.

at $\omega=0$, $\beta_-(u,k)=b_-^{(0)}\,u^{-mL}+\cdots$ as $u\to\infty$.) So the $k_{\rm F}$'s define a set of momenta for which, at $\omega=0$, $\psi_-(u,k)$ becomes normalizable (a 'bound state') as $u\to\infty$. To find the $k_{\rm F}$'s, we analyze the equation for $\alpha_-(u,k)$ as follows.

Plugging $\psi_-^T=(\beta_-,\alpha_-)$ into the Dirac equations (3.10), one obtains a set of two coupled linear differential equations for α_- and β_-. Setting $\omega=0$ and decoupling these two equations, we obtain

$$-\frac{u^2\sqrt{f(u)}}{v_-^0(u)+k}\,\partial_u\left(\frac{u^2\sqrt{f(u)}}{v_+^0(u)-k}\,\partial_u\right)\alpha_-=\alpha_-\,, \tag{3.27}$$

$$-\frac{u^2\sqrt{f(u)}}{v_+^0(u)-k}\,\partial_u\left(\frac{u^2\sqrt{f(u)}}{v_-^0(u)+k}\,\partial_u\right)\beta_-=\beta_-\,, \tag{3.28}$$

where we have set $m=0$ for convenience. In (3.27), the superscript "0" on $v_\pm(u)$ indicates that we have set $\omega=0$ in (3.23). Once again, we set $d=3$ and $q=1$ in what follows. As we vary p, we look (numerically) for the momenta $k_{\rm F}$ for which $\alpha_-(u=\infty,k_{\rm F})=0$, given an appropriate boundary condition for $\alpha_-(u,\omega=0,k)$ at the horizon. Indeed, solving (3.27) near the horizon, one easily obtains that $\alpha_-(u,k)\sim f(u)^{\pm\nu_k^-/2}$ as $u\to 1$. Because by assumption we are in a regime where ν_k^- is real and positive[2] (and, in fact, generically irrational), $f(u)^{-\nu_k^-/2}$ blows up as $u\to 1$. Thus, $\alpha_-(u\to 1,k)\sim f(u)^{\nu_k^-/2}$ is the regular horizon boundary condition that should be chosen.

[2]For $\nu_k^-=0$, one finds that $\alpha_-(u\to 1,k)=a\,(1+\cdots)+b\log(u-1)(1+\cdots)$ where the dots represent terms which vanish as $u\to 1$, and a and b are some constants. In order for $\alpha_-(u,k)$ not to blow up at the horizon, one should then choose $b=0$.

In Figure 3.4 we have plotted such values of $k_{\rm F}$ as a function of p. Starting with negative values of p (while keeping $q = 1$ fixed), $k_{\rm F}$ increases as we raise p causing it to move towards the boundary of the oscillatory region $\mathcal{I}_-$. As p approaches $1/\sqrt{6}$ from below, $k_{\rm F}$ approaches $\sqrt{2}$ (in units of r_0/L^2, from below). The blue dots in Figure 3.4 show the location of $k_{\rm F}$'s versus p and the red band depicts the oscillatory region. There is a single Fermi surface for each p as we increase p up to $p = 1/\sqrt{6}$. We have explicitly checked that $\beta_-(u = \infty, k = k_{\rm F})$ does not vanish, so $k = k_{\rm F}$ are genuine poles of $\mathrm{Re}\, G_-(0, k)$. At $p = 1/\sqrt{6}$, $k_{\rm F} = \sqrt{2}$, and as a result $\nu^-_{k_{\rm F}}$ vanishes (recall that $d = 3$, $m = 0$ and $q = 1$). (At this point, and in fact at any point in which $2\nu^{\pm}_{k_{\rm F}} \in \mathbb{Z}$, the analysis should be more carefully done, as logarithms must be included.) For $p > 1/\sqrt{6}$, we do not see a Fermi surface as $\alpha_-(u = \infty, k)$ does not vanish outside the oscillatory region. We have checked this numerically up to $p = 10$, and, given the observed behavior of $\alpha_-(u = \infty, k)$, we do not expect it to change as we increase p further. Indeed, Figure 3.5 shows plots of $\alpha_-(u = \infty, k)$ versus k for sample values of p. We have also plotted $\beta_-(u = \infty, k)$, shown by the red curves in Figure 3.5.

Following [60], the excitations around these Fermi surfaces can be analyzed. Using (3.17) and (3.18), near $k = k_{\rm F}$ and at small ω, $G_-(\omega, k)$ takes the form

$$G_-(\omega, k) \approx \frac{b^{(0)}_-(k_{\rm F})}{\partial_k a^{(0)}_-(k_{\rm F}) k_\perp + \omega\, a^{(1)}_-(k_{\rm F}) + \tilde{a}^{(0)}_-(k_{\rm F}) \mathcal{G}^-_{k_{\rm F}}(\omega)}, \tag{3.29}$$

where $k_\perp = k - k_{\rm F}$. Suppose the denominator in (3.29) vanishes at some $\omega_*(k) = \mathrm{Re}\,\omega_*(k) - i\,\mathrm{Im}\,\omega_*(k)$. For $p = 0$, the dispersion relation, the width and the residue of the pole were worked out in detail in [60]. Parts of the data in these quantities (such as the scaling of the dispersion relation) come from the IR CFT (or, equivalently, the AdS_2 part of the near horizon geometry), and other parts (such as Fermi velocity) from the UV physics. For non-zero p, the data which come from the IR CFT will be slightly modified according to (3.16) whereas the data coming from the UV physics could be substantially modified.

For $-0.53 < p < 1/\sqrt{6}$, we find that $1/2 > \nu^-_{k_{\rm F}} > 0$. As a result, the small ω excitations around $k = k_{\rm F}$ will have a (non-Fermi liquid) dispersion relation $\mathrm{Re}\,\omega_*(k) \propto k_\perp^z$ and a width $\mathrm{Im}\,\omega_*(k) \propto k_\perp^z$ where $z = 1/(2\nu^-_{k_{\rm F}})$. Thus, for this range of p, $\mathrm{Im}\,\omega_*(k)/\mathrm{Re}\,\omega_*(k)$ does not vanish as $\omega \to 0$, implying that these excitations are not stable. Note that the residue at the pole is given by $Z \propto k_\perp^{z-1}$. At $p = -0.53$, $\nu^-_{k_{\rm F}} = 1/2$ and the excitations near the Fermi surface are of the marginal Fermi liquid type. For $-1.54 < p < -0.53$, $1 > \nu^-_{k_{\rm F}} > 1/2$, hence, the small ω excitations around $k = k_{\rm F}$ will have a linear dispersion relation $\mathrm{Re}\,\omega_*(k) \propto k_\perp$ and a width $\mathrm{Im}\,\omega_*(k) \propto k_\perp^{2\nu^-_{k_{\rm F}}}$. So, for this range of p, these excitations are stable as $\mathrm{Im}\,\omega_*(k)/\mathrm{Re}\,\omega_*(k) \to 0$ as $\omega \to 0$. It is in this sense that we refer to this region as the Fermi liquid. Also, we found that $k_{\rm F}$ goes through zero at $p = -1.317$, signifying that the excitations change over from 'particle-like' to 'hole-like'.

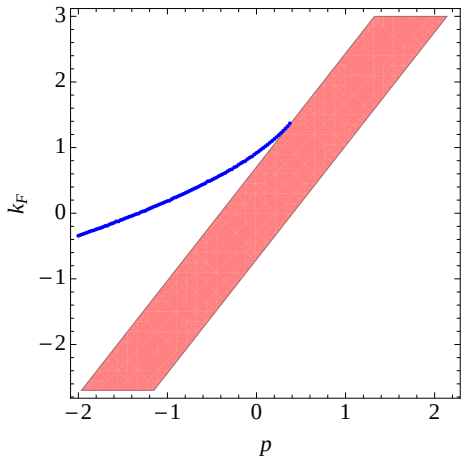

Figure 3.4: $k_{\rm F}$'s (shown by blue dots) versus p. For $p \leq 1/\sqrt{6}$ there is a single Fermi surface for each p. For $p > 1/\sqrt{6}$ we do not find Fermi surfaces. The orange band shows the oscillatory region $\mathcal{I}_-$.

Consequently, we find that simply by varying p, we can tune from a Fermi liquid, $p < -0.53$ to a marginal Fermi liquid at $p = -0.53$ to a generic non-Fermi liquid for $-0.53 < p < 1/\sqrt{6}$ and finally to a Mott insulator for p sufficiently large. Precisely how the system behaves for large values of p will now be addressed in the quasi-normal mode analysis.

3.4 quasi-normal Modes and Stability

In this section we analyze the poles of $G_\pm(\omega, k)$ and, in particular, discuss how they move in the complex ω-plane as we vary k. Since $G_+(\omega, -k) = G_-(\omega, k)$, without loss of generality, we can just focus on the poles of $G_-(\omega, k)$. We denote the poles of $G_-(\omega, k)$ by $\omega_*(k)$. At small ω, the poles of $G_-(\omega, k)$ can be worked out semi-analytically. Indeed, for $p = 0$, the small ω poles were worked out in detail in [60] for $k \in \mathcal{I}$ as well as k close to $k_{\rm F}$ where it was argued that such poles are all located in the lower half of the complex ω-plane. Since the arguments of [60] are mainly based on the data coming from the IR region (the near horizon AdS_2 region of the background), they can easily be extended to non-zero values of p, where results similar to those in the case of $p = 0$ are obtained. For example, at small ω and for $k \in \mathcal{I}_-$, where $\mathrm{Im}\, G_-(\omega, k)$ is oscillatory, the poles (for a fixed k) are exponentially separated on a straight line which is in the lower half ω-plane. (The line is diagonally oriented, *i.e.* it ends on the $\omega = 0$ branch point.) Equivalently, for those values of p for which there exists a Fermi surface, the small ω poles near $k = k_{\rm F}$ are all located in the lower half ω-plane. In particular, if $\nu^-_{k_{\rm F}} < 1/2$, then $\omega_*(k \to k_{\rm F})$ as a function of k follows a straight line in the lower half of the complex ω-plane. The semi-analytic arguments of [60], and their generalizations to non-zero p, are applicable only for small ω, and for $k \in \mathcal{I}_\pm$, or when k is near $k_{\rm F}$. Nevertheless, on general grounds, one

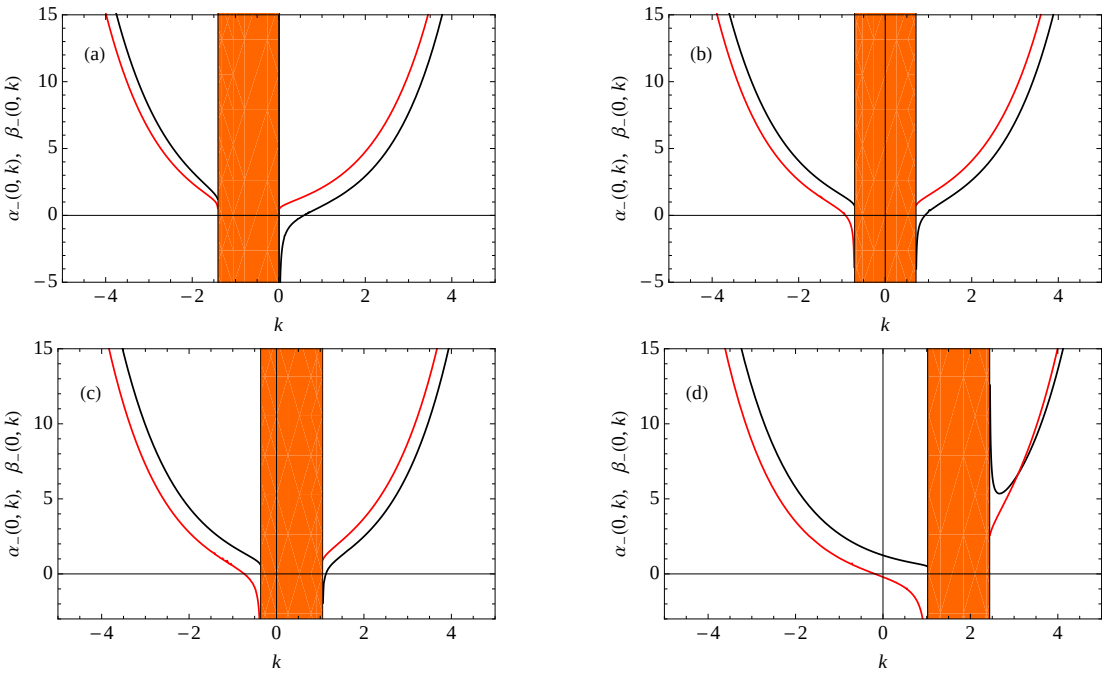

Figure 3.5: Plots of $\alpha_-(u=\infty,k)$ (black curves) and $\beta_-(u=\infty,k)$ (red curves) versus k for (a) $p=-0.4$, (b) $p=0$, (c) $p=0.2$, (d) $p=1$. The orange strip in each plot shows the oscillatory region $\mathcal{I}_-$. The plots are generated for $d=3$, $m=0$ and $q=1$. By $k\to -k$, similar plots could be obtained for $\alpha_+(u=\infty,k)$ and $\beta_+(u=\infty,k)$.

expects the poles to be located in the lower half ω-plane beyond the small ω regime (and, of course, for all values of k). To find the poles beyond the small ω regime, one is usually forced to do numerics which, in the context of the AdS/CFT correspondence, involves performing some quasi-normal mode analyses in the bulk.

Besides isolated poles, $G_\pm(\omega,k)$ at zero temperature will have a branch cut (at least for small ω) which could be understood without doing the numerics. Note that since $\mathcal{G}_k^\pm(\omega)\sim\omega^{2\nu_k^\pm}$ appears in the expressions for $a_\pm(\omega,k)$ and $b_\pm(\omega,k)$ in (3.17) and (3.18), $G_\pm(\omega,k)$ will have a branch point at $\omega=0$ for generic values of k (where $2\nu_k^\pm$ are irrational), and a branch cut, which we take to be extended in the negative imaginary axis. For those values of k for which $2\nu_k^\pm\in\mathbb{Z}$, there is still a branch cut which is due to the appearance of logarithmic terms of the form $\omega^n\log\omega$ ($n\in\mathbb{Z}$) in the expressions for $a_\pm(\omega,k)$ and $b_\pm(\omega,k)$. The branch cut seems to be a distinctive feature of the two-point retarded correlators of operators in the zero temperature d-dimensional boundary theory dual to the extremal RN-AdS$_{d+1}$ background. Indeed, the branch cut was observed explicitly in the correlators of scalar and spinor operators in [60, 111] as well as the conserved currents in the shear and sound channels in [112, 113]. As we will see below, this branch cut appears in our quasi-normal mode analysis. At finite temperature, however, the branch cut dissolves into a series of isolated poles on the negative imaginary axis.

Generically, $G_R(\omega,k)$ will have poles whenever $a_\pm(\omega,k)=0$. In the context of the AdS/CFT correspon-

dence, this problem could be addressed by computing the quasi-normal modes of $\psi_\pm$ in the RN-AdS$_{d+1}$ background, which are solutions to the Dirac equations (3.10) subject to the boundary conditions that they are infalling at the horizon and normalizable asymptotically. Except in very special cases, the generic values of the quasi-normal frequencies are usually computed numerically. We use the so-called Leaver's method [114] for this purpose. For concreteness, we take the boundary theory to be (2+1)-dimensional, *i.e.* $d = 3$. Our analysis can straightforwardly be extended to larger values of d. Also, as in the previous discussions, we consider $m = 0$ and $q = 1$.

Substituting $\psi_\pm^T = (\beta_\pm, \alpha_\pm)$ in the Dirac equations (3.10), and setting $m = 0$, one finds

$$u^2\sqrt{f(u)}\,\partial_u\beta_\pm = [v_-(u) \mp k]\,\alpha_\pm\,, \tag{3.30}$$

$$u^2\sqrt{f(u)}\,\partial_u\alpha_\pm = -\,[v_+(u) \pm k]\,\beta_\pm\,. \tag{3.31}$$

The equations for $\alpha_\pm$ are the relevant equations for obtaining the quasi-normal frequencies of $\psi_\pm$. Squaring the above equations, the decoupled equations for $\alpha_\pm$ are easily obtained

$$\frac{u^2\sqrt{f(u)}}{v_-(u)\mp k}\,\partial_u\left(\frac{u^2\sqrt{f(u)}}{v_+(u)\pm k}\,\partial_u\right)\alpha_\pm = -\alpha_\pm. \tag{3.32}$$

As we alluded to above, without loss of generality, we can focus on the quasi-normal frequencies of ψ_- and just analyze the equation for α_- in (3.32).

In what follows, we switch to a new radial coordinate $z = 1/u$ which is more convenient for doing the numerics in this section. In terms of the new radial coordinate, the horizon is at $z = 1$ and the asymptotic boundary at $z = 0$. The equation for α_- in (3.32) then becomes

$$\frac{\sqrt{f(z)}}{v_-(z)+k}\,\partial_z\left(\frac{\sqrt{f(z)}}{v_+(z)-k}\,\partial_z\right)\alpha_- = -\alpha_-. \tag{3.33}$$

To compute the quasi-normal modes of ψ_-, the behavior of α_- should be infalling at the horizon and normalizable at the boundary. As mentioned above, we use Leaver's method [114] to compute the quasi-normal frequencies. For that, we first pull out the leading behavior of α_- at the horizon as well as the boundary and write

$$\alpha_-(z) = e^{i\frac{\omega}{6(1-z)}}\,f(z)^{-i\left(\frac{\omega}{9}+\frac{q}{4\sqrt{3}}\right)}\,z\,\tilde{\alpha}_-(z). \tag{3.34}$$

Note that $\tilde{\alpha}_-(z=1)$ is a constant which could be set equal to unity as the equation for α_- is homogeneous.

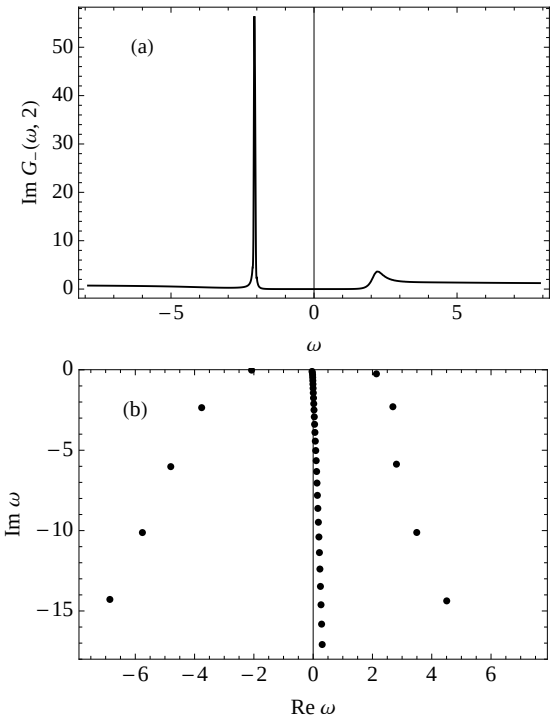

Figure 3.6: (a) $\mathrm{Im}\, G_-(\omega, k)$ as a function of ω for $k = 2$. (b) The quasi-normal frequencies of α_- for $k = 2$. $d = 3$, $p = 5$, $q = 1$ and $m = 0$ in both plots. Also, $M = 250$.

Next, we write $\tilde{\alpha}_-(z)$ as a power series in z around a point $z_0 = 1/2$ (so that the radius of convergence of the series covers both the horizon and the boundary)

$$\tilde{\alpha}_-(z) = \sum_{m=0}^{M} \tilde{\alpha}^-_m(\omega, k) \left(z - \frac{1}{2}\right)^m . \tag{3.35}$$

Substituting (3.35) and (3.34) into (3.33), one obtains

$$\sum_{m=0}^{M} A^-_{mp}(\omega, k)\, \tilde{\alpha}^-_m(\omega, k) = 0, \tag{3.36}$$

where $A^-_{mp}(\omega, k)$ are the elements of a $(M + 1)$ by $(M + 1)$ matrix $A^-(\omega, k)$. The quasi-normal frequencies (for a fixed k) are then the solutions to

$$\det\ A^-(\omega, k) = 0. \tag{3.37}$$

The bottom plot in Figure 3.6 shows the quasi-normal frequencies of α_- for $p = 5$ and $k = 2$. To generate this plot we set $M = 250$. Due to space limitations, the plot only shows a handful of the quasi-

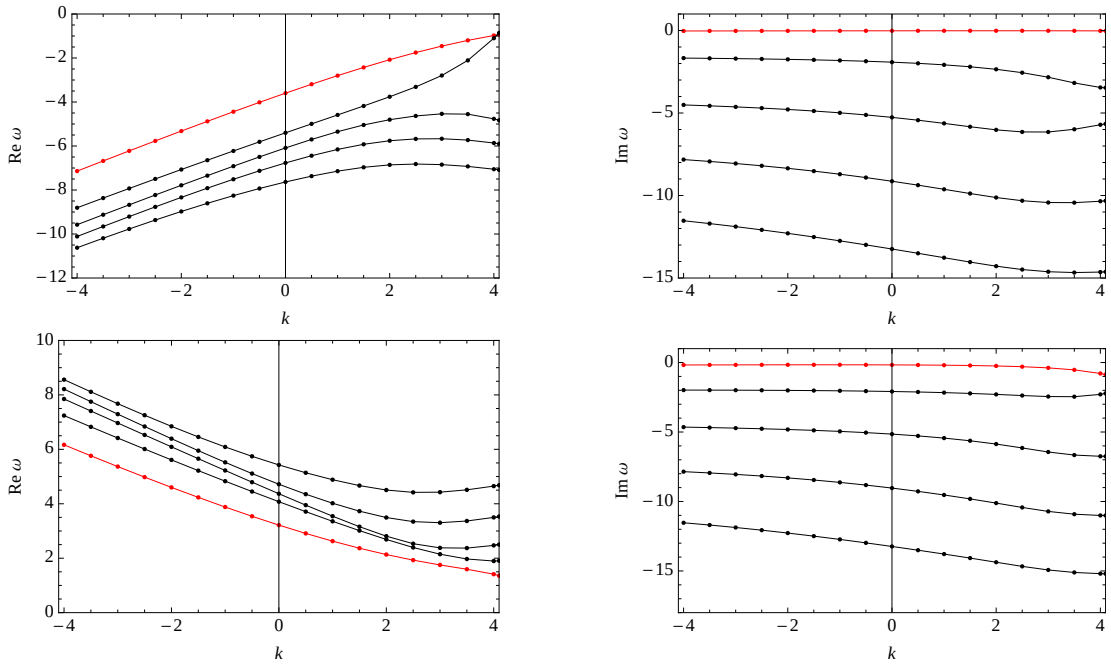

Figure 3.7: The top two plots show the dependence on k (dispersion relation) of the real and imaginary parts of the first five quasi-normal modes (depicted in Figure 3.6(b)) on the left hand side of the negative imaginary axis. The bottom two plots show the dispersion relation of the real and imaginary parts of the first five quasi-normal modes of Figure 3.6(b) which are on the right hand side of the negative imaginary axis. The plots are generated for $d = 3$, $p = 5$, $m = 0$ and $q = 1$ and $M = 250$. The red data corresponds to the mode closest to the real axis in the complex ω-plane.

normal frequencies. As M is increased, the poles located along the negative imaginary axis become closer to one another, suggesting that their existence is due to taking M to be finite, and in the limit of $M \to \infty$ they should indeed form the branch cut we mentioned earlier. On the other hand, increasing M does not seem to change the qualitative behavior of the poles which are oriented almost diagonally on each side of the negative imaginary axis. Notice that the poles are all located on the lower half ω-plane. As may be seen from the plot, the branch cut bends to the right for large negative values of $\mathrm{Im}\,\omega$. This behavior is different from the cases studied in [112, 113] where the unbroken parity symmetry of the boundary theory forces the branch cut of the retarded correlators to stay on the negative imaginary axis. Indeed, the bending of the branch cut is similar to what was observed in [111] for the retarded correlators of charged scalar operators in the presence of a magnetic field. The top plot in Figure 3.6 shows $\mathrm{Im}\,G_{-}(\omega, k = 2)$ as a function of ω. The location of the peak on the left hand side and the bump on the right hand side match quite well with the two quasi-normal frequencies which are closest to the real axis. It is apparent that all of the other quasi-normal modes are relatively wide and individually have small residue.

The dispersion relation, $\omega_*(k)$, of the quasi-normal frequencies shown in Figure 3.6(b) can be computed numerically by following their motion in the complex ω-plane as k is varied. As shown in Figure 3.7, the two quasi-normal frequencies which are closest to the real axis have markedly different dispersion relations than

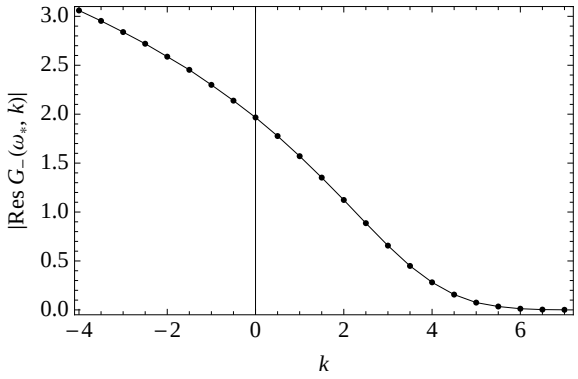

Figure 3.8: $|\mathrm{Res}\, G_-(\omega_*, k)|$ as a function of k for the leading negative-frequency pole in Figure 3.6(b) which is closest to the real axis and located to the left of the negative imaginary axis. We set $d = 3$, $p = 5$, $q = 1$ and $m = 0$.

the rest (higher resonances). The effects of these higher resonances become important as one goes beyond the small frequency and momentum approximation. For large $|k|$, the imaginary part of the quasi-normal frequencies is approximately constant (and negligible compared to the real part). In contrast, for large $|k|$, the real part is proportional to k, with the constant of proportionality being equal to ± 1 (within our numerical precision). This behavior is expected because at large frequency and momentum, the vacuum of the boundary theory is effectively Lorentz-invariant. So, the dispersion relation of the excitations should effectively be relativistic at large frequency and momentum where the effect of charge density is negligible.

To have a better understanding of the spectrum, it is important to know how the residues (at the poles) behave as a function of k. In order to numerically compute the residues of $G_-(\omega, k)$ at $\omega = \omega_*(k)$, we first developed series expansions for $\alpha_-(z; \omega, k)$ and $\beta_-(z; \omega, k)$ both near the horizon around $z = 1 - \epsilon$ and near the boundary around $z = \delta$. We then numerically integrated the (decoupled) differential equation for $\alpha_-(z; \omega, k)$ and $\beta_-(z; \omega, k)$ from $z = 1 - \epsilon$ to $z = \delta$ and matched the numerically integrated solutions and their (first) derivatives with their boundary series expansions at $z = \delta$. In so doing, we were able to compute the residues of $G_-(\omega, k)$ at $\omega = \omega_*(k)$ for a fixed k, denoted by $\mathrm{Res}\, G_-(\omega_*, k)$. Repeating the same steps for different k's, one can numerically obtain the dependence of the residues on k. We computed the k-dependence of the residues of $G_-(\omega, k)$ for the leading negative-frequency pole (closest to the real axis). Shown in Figure 3.8 is the absolute value of $\mathrm{Res}\, G_-(\omega_*, k)$ as a function of k for this pole. Also, the plots in Figure 3.9 show a close up of the real and imaginary parts of the dispersion relation of this pole.

Comparing the plot of the residue to Figure 3.6(a), it is now apparent why the gap forms: as the leading negative-frequency quasi-normal mode approaches $\omega = 0$, its residue dies off quickly. Since no other mode has appreciable spectral weight, this accounts for the suppression of the spectral weight near $\omega = 0$. For larger values of p, the residue falls off more rapidly, and consequently the gap widens.

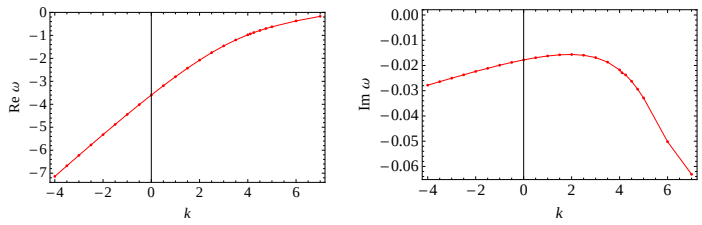

Figure 3.9: A close-up of of the real (left plot) and imaginary (right plot) parts of the dispersion relation of the leading pole shown in Figure 3.6(b) which is closest to the real axis and located to the left of the negative imaginary axis.

3.5 Finite Temperature

So far, our analysis has been at zero temperature. However, there are important aspects of Mott insulators that transpire at finite temperature. In particular, there are Mott insulators [106] exhibiting a transition to a conducting state as the temperature is increased. The classic example of this is VO_2. Below $T_* = 340K$, VO_2 becomes insulating with a gap of $\Delta = 0.6$ eV. This ratio of the gap to the critical temperature Δ/T_* is approximately 20. This behavior should be contrasted with systems such as superconductors in which $U(1)$ symmetry is broken and $\Delta/T_c \approx 1 - 2$. That Δ/T_* well exceeds unity is one of the unresolved puzzles with VO_2. It points to strong correlations being the source of the gap rather than the breaking of some spontaneous symmetry as in the case of superconductivity. Optical conductivity studies [115] reveal that spectral weight as far away as 6 eV contributes to the formation of the Drude peak at zero frequency once the Mott gap closes. Such UV-IR mixing is a ubiquitous feature of Mott systems. While we have argued that our holographic setup can capture the high-low energy spectral weight transfer, we have not yet addressed the finite temperature aspects of the Mott problem.

The boundary theory we are investigating here can easily be studied at finite temperature by considering the RN-AdS_4 background away from extremality, namely for $0 < Q < \sqrt{3}$. Using the same procedures outlined above, we obtained the spectral function and studied the density of states as a function of temperature. As Figure 3.10 reveals, the Mott gap observed here does in fact close as the temperature increases. Further, the transition is sharp. To estimate the ratio of the zero-temperature gap to the temperature at which the gap closes, T_*, we take a close-up of the density of states and study its evolution as a function of temperature, see Figure 3.11. Indeed for $p = 6$ (or $p = 7$), we find that $\Delta/T_* \sim 10$. Though smaller than Δ/T_* in vanadium oxide, it does illustrate that dynamically generated gap we have found here does possess non-trivial temperature dynamics.

For the record, we have shown in Figure 3.12 the quasi-normal frequencies of α_- (bottom plot) as well as $\mathrm{Im}\, G_-(\omega, k)$ (top plot) for $k = 2$, $p = 5$ and $T/\mu = 0.16$. Notice that the branch cut at zero temperature

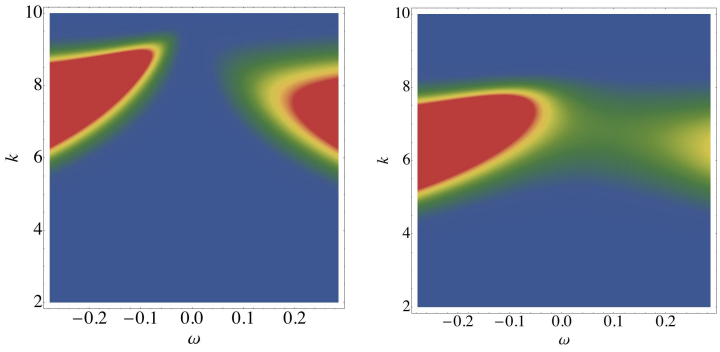

Figure 3.10: A close-up of the density plots of $\mathrm{Im}\, G_-(\omega, k)$ for $p = 6$ and $T/\mu \simeq 5.15 \times 10^{-3}$ (left) and $T/\mu \simeq 3.98 \times 10^{-2}$ (right). A gap is still seen in the plot on the left while it is closed in the plot on the right.

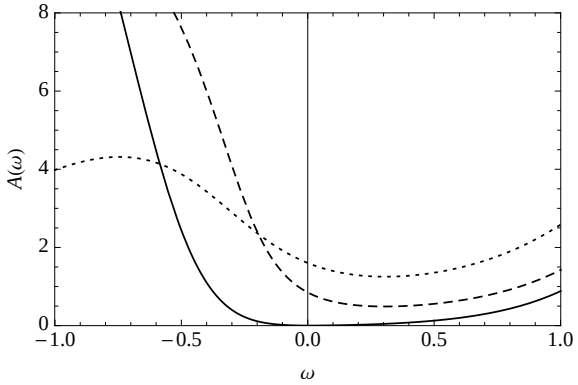

Figure 3.11: A close-up of the density of states $A(\omega)$ at $p = 6$ for $T/\mu \simeq 0.44$ (dotted), 0.16 (dashed) and 5.15×10^{-3} (solid).

has dissolved at finite temperature into a series of isolated poles on the negative imaginary axis[3]. Also, as it can easily be seen from the plots in Figure 3.12, the (real part of the) two quasi-normal frequencies of α_- which are closest to the real axis match quite well with the location of the peak on the left hand side and the bump on the right hand side in $\mathrm{Im}\, G_-(\omega, k = 2)$. The other quasi-normal frequencies represent poles in $\mathrm{Im}\, G_-(\omega, k = 2)$ which are relatively wide and have small residue. Although not shown, to the extent that we have checked, all the poles stay on the lower half ω-plane as k is varied.

3.6 Discussion

We have studied extensively the dichotomous behavior of the boundary theory fermion correlators in the presence of a bulk Pauli coupling in our holographic set up. For the boundary theory dual to the extremal RN-AdS$_4$ background, we showed that as we vary p from large negative values up to a small positive value

[3]Note that in order to generate the bottom plot in Figure 3.12, the expression in (3.34) should be appropriately modified to reflect the fact that the system is at finite temperature. This is tied to the fact that at finite temperature $f(r)$ has a single zero at the horizon.

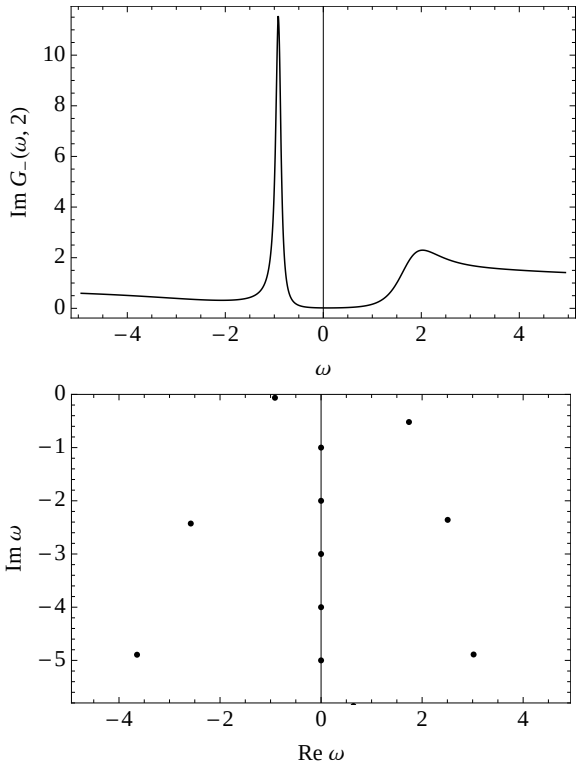

Figure 3.12: The plots in (a) and (b) show, for $k = 2$ and $T/\mu = 0.16$, $\mathrm{Im}\, G_-(\omega, k)$ as a function of ω and the quasi-normal frequencies of α_-, respectively. Here, $d = 3$, $p = 5$, $q = 1$, $m = 0$, and $M = 250$.

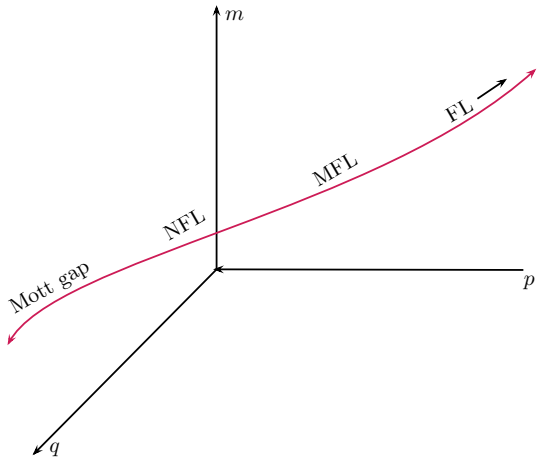

Figure 3.13: A cartoon of the zero temperature "phase diagram" in the m, q, p parameter space. Different regions of the phase diagram correspond to each of the principal structures in the cuprate phase diagram (compare to Figure 3.1).

of $p = 1/\sqrt{6}$ (while keeping $m = 0$ and $q = 1$ fixed), the behavior of the excitations change from Fermi liquid like (for $p < -0.53$), though not in the precise Landau sense in which the width of the excitations is quadratic in frequency, to a marginal Fermi liquid at $p = -0.53$ and on to a non-Fermi liquid for $-0.53 < p \leq 1/\sqrt{6}$. In the context of the earlier work [60] in which such behavior was observed by changing the scaling dimension, as well as the charge, of the boundary theory fermion operator, the Pauli coupling offers a different route to the physics that has a more direct connection with Mott physics. Our argument here is based on the fact that for large positive values of p a Mott gap arises (as evidenced by a vanishing of the quasiparticle residue shown in Figure 3.8) in the spectrum of the boundary theory fermion operator without the apparent breaking of a continuous symmetry. This is Mott physics. Now, we have seen these features by holding m and q fixed while varying p. It is clear that the basic properties that we have seen will persist throughout a domain in the m, q, p parameter space. In Figure 3.13, we suggest that some locus through the parameter space can be identified with doping in the cuprate phase diagram: each of the principle features of the cuprates is present. It is interesting to compare this heuristic phase diagram with that of the cuprates. As is evident, there is a continuous evolution from a Mott insulator in the undoped state to a Fermi liquid in the overdoped regime. In between these extremes lie non-superconducting non-Fermi liquid states characterized by a pseudogap (a suppression of the density of states without any long-range superconductivity) and a strange metal in which the resistivity is a linear function of temperature. Our work suggests that the Pauli coupling mimics the role of the doping.

It is natural to investigate how the introduction of a superconducting condensate would complement the physics that we have discussed here. A suitable charged background at zero-temperature was studied in [116], following [46, 47]. For a range of parameters (namely, for $m_\phi^2 - 2q_\phi^2 < -3/2$ where m_ϕ and q_ϕ are the mass and the charge of the bulk scalar field, respectively), a bulk solution with a non-zero charged scalar condensate is preferred over the Reissner-Nordström solution. (Indeed, for this range of parameters, the Reissner-Nordström solution is unstable against turning on the scalar field in the bulk.) This solution is asymptotically AdS_4, and for $m_\phi = 0$ has a near horizon geometry that is also AdS_4 with a finite speed of light $c_{\rm IR}$ and a finite dynamical exponent. The horizon of the zero-temperature solution (which is the Poincaré horizon of AdS_4) is at $r = 0$, hence there is no residual entropy at zero temperature. Preliminary studies of the effect of the Pauli coupling on the boundary theory fermion correlators [4] indicates that the main contributor to the gap in the fermion spectral density in the superconducting phase is the so-called Majorana scalar-fermion coupling (denoted by η_5 in [118]). As there are limited tools available for the study of "electrons" at strong coupling, the model proposed here could offer key insight into how superconductivity

[4] See [117–122] where the authors analyze fermion correlators (in the absence of the Pauli interaction) in some superconducting backgrounds.

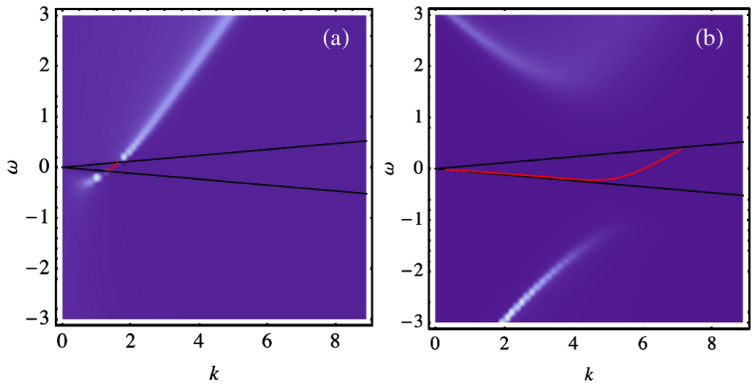

Figure 3.14: Density plot of the boundary theory fermion spectral function for (a) $p = 0$ and (b) $p = 3$.. Here, $q_\phi = 1.5$, $L = 1$, and $\mu = 2\sqrt{3}$.

emerges from a background in which all energy scales are coupled. As a first step, we set $\eta_5 = 0$, and briefly discuss here the effect of the Pauli coupling on fermion correlators in a boundary theory dual to the superconducting background of [116]. Suppose $m_\phi = 0$, and $q_\phi > \sqrt{3}/2$, so that the near horizon geometry is AdS_4 (with a characteristic radius $L_{\rm IR}$), and assume there exists a (2+1)-dimensional IR CFT dual to this AdS_4 near-horizon geometry. For definiteness, we set $q_\phi = 2q$, where q is the charge of the bulk fermion[5]. The Dirac equation for $\psi_\pm$ (as well as the corresponding flow equations for $\xi_\pm$) and the IR boundary conditions can easily be worked out. A crucial difference compared to the case of the RN-AdS_4 is that here the dimension of the IR CFT operators dual to $\psi_\pm(r \to 0)$ does not depend on p. Depending on the sign of $s^2 \equiv -\omega^2/c_{\rm IR}^2 + k^2$, the Green functions $G_\pm(\omega, k)$ exhibit different behaviors. (Note that one still has $G_-(\omega, k) = G_+(\omega, -k)$.) For $s^2 > 0$ (IR space-like region), the horizon boundary conditions for $\xi_\pm$ are real and since the flow equations are also real, one concludes that the boundary theory fermion spectral density is zero in this region, except when there are bound states (by which we mean poles of $\mathrm{Re}\, G_\pm(\omega, k)$ in the $s^2 > 0$ region) of the Dirac equation. For $s^2 < 0$ (IR time-like region), on the other hand, the horizon boundary conditions are complex resulting generically in a non-vanishing fermion spectral density. The IR space-like region is the primary feature of the finite $c_{\rm IR}$ theory that distinguishes it from the RN-AdS_4 theory. In particular, there is no analogue here of the log-oscillatory region (at $\omega = 0$), and thus no analogous mechanism for the disappearance of zero-frequency poles as p is increased. Indeed as we describe below, as p is increased, the zero-frequency pole moves but persists. What this implies is that in the presence of superconductivity where the U(1) symmetry is spontaneously broken, the gap in fermion spectral density is determined by the Majorana scalar-fermion coupling η_5.

[5]This condition is not required when $\eta_5 = 0$. We consider this condition so that our analysis here can be generalized to the case where $\eta_5 \neq 0$. Also, note that the convention of charge in [116, 118] is different than our convention in previous sections by a factor of two, namely $q_{\rm here} = 2q_{\rm there}$. In this discussion, we use the convention of [116, 118] for q and q_ϕ.

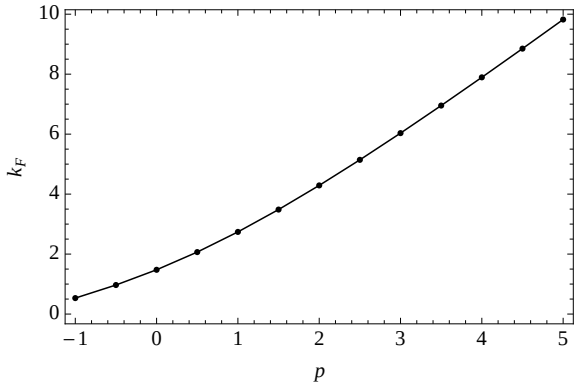

Figure 3.15: k_F as a function of p. Here, $q_\phi = 1.5$, $L = 1$, and $\mu = 2\sqrt{3}$.

Figure 3.14 shows a density plot of the fermion spectral function for $p = 0$ (left) and $p = 3$ (right), where $q_\phi = 1.5$ and $\mu = 2\sqrt{3}$. The density plot for $p = 0$, which has been previously obtained in [118], is also shown for the purpose of comparison with the density plot for a non-zero value of p such as $p = 3$. As the plot in Figure 3.14(b) shows, turning on a non-zero value of p results in a suppression in the spectral density of the incoherent excitations (those in the IR time-like region) and pushes them away from the boundary (the IR light-like region, depicted by solid black lines). But, since at $\omega = 0$ there is a Fermi peak (and indeed an infinite number of long-lived bound states for other values of ω in the IR space-like region), turning on p does not result in the formation of a gap. In fact, for the above-mentioned parameters, we find that, for $p = 3$, $k_{\rm F} \approx 6.0$. For $p = 0$, the Fermi peak, for the same parameters, is at $k_{\rm F} \approx 1.5$ [118]. Turning on p moves around the location of this Fermi peak as shown in Figure 3.15.

We note again that there are regions of parameter space (in particular, q_ϕ and m_ϕ) where the preferred geometry is either Reissner-Nordström or the superconducting geometry. Our results indicate that while the ferimon gap in the superconducting geometry is controlled by the Majorana scalar-fermion coupling [116], a Mott gap can still form in the Reissner-Nordström regime. The decoupling of these two effects is promising in the context of the cuprate phase diagram.

Chapter 4

Neutral Order Parameters in Metallic Criticality in d=2+1 from a Hairy Electron Star

We use holography to study the spontaneous condensation of a neutral order parameter in a (2+1)-dimensional field theory at zero-temperature and finite density, dual to the electron star background of Hartnoll and Tavanfar. An appealing feature of this field theory is the emergence of an IR Lifshitz fixed-point with a finite dynamical critical exponent z, which is due to the strong interaction between critical bosonic degrees of freedom and a finite density of fermions (metallic quantum criticality). We show that under some circumstances the electron star background develops a neutral scalar hair whose holographic interpretation is that the boundary field theory undergoes a quantum phase transition, with a Berezinski-Kosterlitz-Thouless character, to a phase with a neutral order parameter. Including the backreaction of the bulk neutral scalar on the background, we argue that the two phases across the quantum critical point have different z, a novelty that exists in certain quantum phase transitions in condensed matter systems. We also analyze the system at finite temperature and find that the phase transition becomes, as expected, second-order. Embedding the neutral scalar into a higher form, a variety of interesting phases could potentially be realized for the boundary field theory. Examples which are of particular interest to condensed matter physics include an antiferromagnetic phase where a vector condenses and break the spin symmetry, a quadrupole nematic phase which involves the condensation of a symmetric traceless tensor breaking rotational symmetry, or different phases of a system with competing order parameters.

4.1 Introduction

Condensed matter physics is replete with examples of ordered states described by a neutral operator acquiring a non-zero vacuum expectation value. Systems exhibiting magnetism [123], itinerant or otherwise, or more complicated ordered phases such as quadrupolar nematic states [124] are just a few examples of such ordered states. Our focus in this Chapter is to use holography to describe the onset of such neutral ordered states in itinerant-like $d = 2 + 1$ dimensional strongly-correlated systems with a finite dynamical exponent z. The standard method for treating the onset of magnetism in a Fermi liquid is to introduce a neutral bosonic

order parameter at the level of a Hubbard-Stratonovich field in some fermionic model and then integrate out the fermions [125, 126]. Because the fermions are gapless, and hence inherently part of the low-energy degrees of freedom, they should not *a priori* be integrated out in the Wilsonian sense. Indeed, it is now well known [127–129] that this procedure is highly problematic in two spatial dimensions. For example, in the case of $d = 2 + 1$ and $z = 2$, the fermions introduce an infinite number [127] of non-local marginal perturbations rendering any truncation of the resultant bosonic action at the Gaussian level moot. In the renormalization group sense, the critical theory in terms of the neutral bosonic order parameter does not possess any coupling constant from which a controlled expansion can be obtained. It turns out that even a $1/N$ expansion is of no use [128, 129] as the naive power counting fails, and an infinite number of planar diagrams contributes to the fermionic self energy. Recent attempts [58] have been made to shed light on this problem by using holography where a strongly coupled quantum theory is mapped onto a weakly interacting dual theory of gravity[1]. The boundary theory considered in [58] is dual to the Reissner-Nordström AdS_{d+1} black hole background (RN-AdS_{d+1}) and flows in the IR to a (0+1)-dimensional CFT with a dynamical exponent $z = \infty$. Hence, such a theory may have less direct bearing on real condensed matter systems, compared to a theory which flows in the IR to a fixed-point with finite z. Another drawback of this theory is the existence of a finite entropy density at zero temperature.

All is not lost with holography in this context, however. Indeed, holography is ideally suited to treating this problem as the failures of the existing conventional treatments [127–129] stem from the inherent strongly-coupled nature of the underlying theory. We show here that it is possible to construct a holographic setup in which a neutral bosonic operator condenses in an itinerant-like electron fluid with a finite value of z, and in $d = 2 + 1$. Interestingly, the case we consider also includes $z = 2$. A finite value of z in the IR is achieved by replacing the $\mathrm{AdS}_2 \times \mathbb{R}^{d-1}$ near-horizon geometry of the RN-AdS_{d+1} background with one that is of, say, Lifshitz type [130] as in [54]. Our work here then represents a holographic description of quantum criticality in a metallic system in two spatial dimensions with $z = 2$, and with a neutral bosonic order parameter.

It was realized in [47] that a neutral scalar field with a mass square satisfying the Breitenlohner-Freedman (BF) bound [57] of the asymptotic AdS_{d+1} can cause an instability in the extremal, or near-extremal, RN-AdS_{d+1} background if its effective mass square in the AdS_2 region of the near horizon geometry violates the BF bound of AdS_2. As a result, the RN-AdS_{d+1} background could become unstable to forming a neutral scalar hair[2]. The holographic interpretation of this hairy background is that the boundary theory is in a

[1] See [52, 90–92] for reviews of holography with applications to strongly-correlated condensed matter-like phenomena.

[2] This mechanism is identical to the one used for the construction of holographic superconductors [46, 47, 100, 131]. As discussed in [132, 133], there is another way of making the AdS_2 region unstable even if the effective mass square of the scalar field, either charged or neutral, satisfies the BF bound of AdS_2. This mechanism involves deforming the boundary theory by relevant multi-trace operators [134, 135], which are, in this context, constructed out of the operator dual to the scalar field.

phase where the operator dual to the bulk neutral scalar field condenses. Such a condensate was explicitly constructed in [58] for the boundary theory dual to the RN-AdS$_{d+1}$ background, where it was shown that the operator condenses below some critical temperature as long as its conformal dimension is in a certain range. The phase transition at finite temperature was shown to be second-order with mean-field exponents. Moreover, in the standard quantization, the critical temperature goes to zero as the conformal dimension of the operator approaches a critical dimension from below. At zero temperature, on the other hand, by varying the conformal dimension of the operator, the boundary theory undergoes a quantum phase transition of the Berezinski-Kosterlitz-Thouless (BKT) type near the quantum critical point. The authors of [58] then used the condensation of the neutral scalar operator as a starting point to construct an antiferromagnetic phase in the boundary theory. This was accomplished by embedding the bulk neutral scalar field into a triplet whose dual operator condenses in such a way as to break the SU(2) spin symmetry to U(1) (see also [95]). The fluctuations of this antiferromagnetic order parameter (two Goldstone modes) were then analyzed in [58] and their dispersion relations were determined.

As mentioned above, the boundary theory considered in [58] flows in the IR to a (0+1)-dimensional CFT with a dynamical exponent $z = \infty$. This is an unwelcome feature in modeling metallic quantum criticality using holography. In this Chapter, we ask ourselves whether it is possible to condense a neutral scalar operator in a boundary field theory which flows in the IR to a fixed-point with finite z. We find that the answer is yes. To achieve this goal, one first replaces the AdS$_2 \times \mathbb{R}^{d-1}$ near horizon geometry of the RN-AdS$_{d+1}$ background with, say, a Lifshitz geometry. Consequently, the background is asymptotically AdS$_{d+1}$ while in the IR it has Lifshitz scaling. For simplicity, and with an eye towards condensed matter applications, we assume that the boundary theory is $d = 2 + 1$ dimensional. A background with such properties was recently constructed by Hartnoll and Tavanfar in [54] following [136, 137]. As in [54], we refer to this background as the electron star background, or simply the star background. Compared to other backgrounds which are asymptotically AdS$_4$ and Lifshitz in the IR [138], the electron star background has the appealing feature that the IR Lifshitz scaling is due to the strong interaction between critical bosonic degrees of freedom and a finite density of fermions, which is of utmost importance in metallic quantum criticality.

The (2+1)-dimensional boundary theory dual to the electron star background is a zero-temperature, but finite density, field theory which flows in the IR to a (2+1)-dimensional Lifshitz fixed-point with a finite z. We construct a neutral scalar hair for the electron star background and show that upon varying the UV conformal dimension of the dual scalar operator, or any other knob in the boundary theory which allows the effective mass square of the bulk scalar in the far-interior Lifshitz region to change, the boundary field

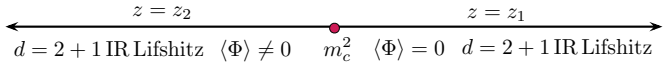

Figure 4.1: A cartoon of the phase transition in our hologrphic setup as a function of the mass square, m^2, of the bulk neutral scalar field ϕ. Once m^2 violates the BF bound, m_c^2, of the far-interior Lifshitz region of the electron star background, the boundary theory goes into a phase where the dual operator Φ spontaneously condenses. The backreaction of the scalar on the geometry changes the value of the dynamical exponent z. The condensation of Φ is controlled by the IR characteristics of the background which remains $d = 2 + 1$ Lifshitz across the transition.

theory undergoes a quantum phase transition to a phase with a neutral order parameter. Figure 4.1 shows a cartoon of the phase transition. A key characteristic we find is that the dynamical exponent changes across the transition. We analyze the nature of the phase transition at zero temperature and argue that it has a BKT character. We then consider the setup at finite temperature and show that below some critical temperature, the neutral order parameter condenses and moreover the transition is of the standard mean field type. While the focus of this Chapter is mainly on the condensation of a single neutral scalar operator in the boundary theory, we discuss, very briefly, its applications for the holographic modeling of phases with vector or tensor order parameters, or systems with multiple order parameters. For example, following [58], an antiferromagnetic phase of the boundary theory in our case can easily be constructed by embedding the bulk neutral scalar into a triplet which is charged under the SU(2) spin symmetry, and allowing the dual neutral vector operator condense and break SU(2) down to U(1). Constructing a quadrupole nematic phase, where the order parameter is a symmetric traceless tensor which breaks the SO(2) rotational symmetry, is more difficult. We comment on the challenges of constructing such a phase using the embedding of the bulk neutral scalar into a symmetric traceless tensor.

The Chapter is organized as follows. We start the next section by reviewing the electron star background of [54], and its finite-temperature variant [139, 140]. In section 4.3 we consider a neutral scalar field as a probe in the electron star background and show that under some circumstances this gravitational system undergoes a phase transition to a background with a neutral scalar hair. The holographic interpretation of the transition is that the boundary field theory undergoes a quantum phase transition of the BKT type from a $\mathbb{Z}_2$-symmetric phase to a phase with a neutral order parameter, which spontaneously breaks this symmetry. We then consider the backreaction of the neutral scalar on the star background and show that the aforementioned two phases have different dynamical exponents. Section 4.4 extends the analysis to the finite temperature case. In the last section we discuss various applications of our holographic setup and conclude with open questions and directions for future work.

4.2 The Background

The boundary theory that we wish to study is dual to the so-called electron star background. The zero-temperature background was constructed in [54], and was later extended to finite temperature in [139, 140]. In this section we briefly review the star background both at zero and finite temperature, and set the stage for later calculations.

4.2.1 Zero-Temperature Background

Consider an ideal fluid of charged fermions in a (3+1)-dimensional space-time with a negative cosmological constant $\Lambda = -3/L^2$. The equations of motion of the system read

$$R_{MN} - \frac{1}{2}R\, g_{MN} + \Lambda\, g_{MN} = \kappa^2 T_{MN}, \tag{4.1}$$

$$\nabla^M F_{MN} = e^2 J_N, \tag{4.2}$$

where $\kappa^2 = 8\pi G_{\rm N}$, e is the fermion charge and

$$\begin{aligned} T_{MN} = {} & \frac{1}{e^2}\Big(F_{MP}F_N^P - \frac{1}{4} g_{MN}\, F_{PQ}F^{PQ}\Big) \\ & + (\rho + p)\, u_M u_N + p\, g_{MN}, \end{aligned} \tag{4.3}$$

$$J_M = \sigma\, u_M, \tag{4.4}$$

with ρ, p, σ and u_a being, respectively, energy density, pressure, charge density and four-velocity (satisfying the normalization $u_M u^M = -1$) of the fluid. Throughout the Chapter, we denote the bulk indices by capital letters $M, N, \cdots = \{t, x, y, r\}$ while the boundary theory directions are denoted by the Greek indices $\mu, \nu, \ldots = \{t, x, y\}$.

To solve the above equations, we take the ansatz for the metric and the gauge field to be of the following form

$$\frac{ds^2}{L^2} = -f(r)dt^2 + \frac{1}{r^2}\left(dx^2 + dy^2\right) + g(r)dr^2, \tag{4.5}$$

$$A = \frac{eL}{\kappa} h(r) dt, \tag{4.6}$$

where the asymptotic boundary is at $r \to 0$. In addition, an equation of state for the fluid must also be specified. Suppose the fluid is composed of zero temperature charged fermions with mass $m_{\rm f}$, with the

density of states

$$n(E) = \beta E \sqrt{E^2 - m_{\rm f}^2}, \tag{4.7}$$

where β is a constant of order one. The authors of [54] then assumed a locally flat approximation where, at each r-slice, the fermion dynamics are determined by the local chemical potential

$$\mu_{\rm loc}(r) = \frac{e}{\kappa} \frac{h(r)}{\sqrt{f(r)}}, \tag{4.8}$$

and argued that such an approximation is self-consistent in a regime of parameters where gravity can be treated classically with an order-one backreaction of the fermions on the geometry. Given this approximation one can then use (4.7) to compute the fluid energy density, pressure and charge density as function of r. Obviously, $n(E) = \rho(r) = p(r) = \sigma(r) = 0$ for $r \leq r_s$ where r_s is the boundary of the fluid given by solving $\mu_{\rm loc}(r_s) = m_{\rm f}$.

It is more convenient to rescale $\rho \to \rho/(L^2\kappa^2)$, $p \to p/(L^2\kappa^2)$, $\sigma \to \sigma/(L^2 e\kappa)$, $\beta \to (\kappa^2/e^4L^2)\beta$, $m_{\rm f} \to (e/\kappa)\, m_{\rm f}$ and $\mu_{\rm loc} \to (e/\kappa)\, \mu_{\rm loc}$, with the new quantities being all dimensionless. Putting everything together, the equations of motion then take the form

$$\frac{1}{r}\left(\frac{f'(r)}{f(r)} + \frac{g'(r)}{g(r)} + \frac{4}{r}\right) + \frac{g(r)h(r)}{\sqrt{f(r)}}\sigma(r) = 0, \tag{4.9}$$

$$\frac{f'(r)}{rf(r)} - \frac{h'(r)^2}{2f(r)} + [3 + p(r)]\, g(r) - \frac{1}{r^2} = 0, \tag{4.10}$$

$$h''(r) + \frac{g(r)}{\sqrt{f(r)}}\left(\frac{r}{2}h(r)h'(r) - f(r)\right)\sigma(r) = 0. \tag{4.11}$$

In the far-interior region $r \to \infty$, the solution is of the Lifshitz type [54]. As argued there, in order for the Lifshitz solution to make sense, one should have $0 \leq m_{\rm f} < 1$. The solution in the interior region $r_s < r < \infty$ (where the fluid energy density, pressure and charge density are all non-zero) can easily be worked out by perturbing the Lifshitz solution, and demanding the perturbation to grow as $r \to 0$, but not blow up as $r \to \infty$. In so doing, one finds

$$f(r) = \frac{1}{r^{2z}}\left(1 + \mathfrak{f}_1 r^{\alpha_-} + \cdots\right), \tag{4.12}$$

$$g(r) = \frac{\mathfrak{g}}{r^2}\left(1 + \mathfrak{g}_1 r^{\alpha_-} + \cdots\right), \tag{4.13}$$

$$h(r) = \frac{\mathfrak{h}}{r^z}\left(1 + \mathfrak{h}_1 r^{\alpha_-} + \cdots\right), \tag{4.14}$$

where $z = z(m_{\rm f}, \beta)$ is the dynamical critical exponent

$$\mathfrak{g}^2 = \frac{36 z^4 (z-1)}{\left[(1-m_{\rm f}^2)\, z - 1\right]^3 \beta^2}, \qquad \mathfrak{h}^2 = \frac{z-1}{z}, \tag{4.15}$$

and $\mathfrak{g}_1$, $\mathfrak{h}_1$ and all higher order perturbation coefficients are determined in terms of $\mathfrak{f}_1$, which itself could be set to any value by rescaling r, t, x, y. Also, α_- is determined in terms of $m_{\rm f}$ and z, the expression of which can be found in [54]. The dependence of z on $m_{\rm f}$ and β is complicated, but satisfies $z \geq (1-m_{\rm f}^2)^{-1} \geq 1$. (A numerical plot of z in terms of β for some sample values of $m_{\rm f}$, along with the explicit forms of its asymptotic expressions can also be found in [54].) The solution in the exterior region $0 < r \leq r_s$ (with the fluid energy density, pressure and charge density all being zero) is RN-AdS$_4$ where the metric and gauge field functions are given by

$$\begin{aligned} &f(r) = \frac{1}{r^2}\Big(c^2 - M r^3 + \frac{1}{2} Q^2 r^4\Big), \quad g(r) = \frac{c^2}{r^4 f(r)}, \\ &h(r) = \mu - Q r. \end{aligned} \tag{4.16}$$

Matching $f(r)$, $g(r)$, $h(r)$ and $h'(r)$ of the interior and exterior solutions at $r = r_s$ will then determine the constants c, M, Q and μ. Note that the constant c is introduced because choosing a particular value of $\mathfrak{f}_1$ in the interior solution fixes the normalization of time. The electron star background is a family of asymptotically AdS$_4$ solutions parametrized by $m_{\rm f}$ and β. The far-interior region of the background is generically Lifshitz. But, in some limits of the β-$m_{\rm f}$ parameter space, the far-interior region is characterized by a geometry other than Lifshitz. For example, an AdS$_2 \times \mathbb{R}^2$ solution (where $z = \infty$) can be recovered either by taking $\beta \to 0$ while keeping $m_{\rm f}$ fixed, or by taking the $m_{\rm f} \to 1$ limit from below. Another interesting limit of the far-interior solution is AdS$_4$ (with $z = 1$) which is obtained by taking $\beta \to \infty$ at $m_{\rm f} = 0$.

In this Chapter, we exclude the two limiting AdS$_2 \times \mathbb{R}^2$ and AdS$_4$ interior solutions by taking $m_{\rm f} \in (0, 1)$. In other words, the far-interior solution is Lifshitz with a finite $z > 1$. In this case, one obtains $\mathfrak{g} > 1$, which turns out to be crucial in our subsequent discussions. Note that the zero-temperature electron star background has zero entropy density.

4.2.2 Finite-Temperature Background

The details of the finite-temperature version of the electron star background are as follows [139, 140]. Temperature is introduced by making the Euclidean time coordinate periodic with a period $1/T$, where T is the temperature. This then requires a horizon at some finite radius $r = r_0$ in the interior of the

geometry. As argued in [139, 140], in the regime of validity of the electron star background $e \sim \kappa/L \ll 1$, the effect of temperature on the fermion density of state could be neglected. Therefore, the density of states is given by (4.7) and with the same planar ansatz for the metric and the gauge field as before, one has to solve the equations (4.9)–(4.11) in order to determine the finite temperature background. Again, for large enough $m_{\rm f}$, the fluid energy density, pressure and charge density vanish everywhere. As a result, a RN-AdS$_4$ background will satisfy those equations. On the other hand, if $m_{\rm f}$ is small enough, there exists a critical radius $r = r_c$ for which $m_{\rm f}$ equals the local chemical potential $\mu_{\rm loc}$ at that radius. This happens at a critical temperature $T = T_*$. The quantities r_c and T_* are determined by solving the two equations $\mu_{\rm loc}(r_s) = m_{\rm f}$ and $\mu'_{\rm loc}(r_s) = 0$, with prime denoting derivative with respect to r.

For $T < T_*$, there exists a finite width $r_2 > r > r_1$ for which the fluid has non-zero energy density, pressure and charge density. The radii r_1 and r_2 are solutions to $\mu_{\rm loc}(r_{1,2}) = m_{\rm f}$. Thus, the finite-temperature electron star background is divided into three regions. In the so-called inner region of the background, $r_0 \geq r \geq r_2$, the solution is a RN-AdS$_4$ black hole with

$$\begin{aligned} f(r) &= \frac{1}{r^2}\Big(1 - M_0 r^3 + \frac{1}{2}Q_0^2 r^4\Big), \quad g(r) = \frac{1}{r^4 f(r)}, \\ h(r) &= \mu_0 - Q_0 r, \end{aligned} \tag{4.17}$$

where r_0 is the horizon radius given by the largest real root of $f(r) = 0$, $\mu_0 = Q_0 r_0$ and $M_0 r_0^3 = 1 + \mu_0^2 r_0^2/2$. The temperature of the black hole is given by $T = (4\pi c)^{-1}\,|df(r_0)/dr|$, where the parameter c is introduced for later convenience. The quantity μ_0 is the inner region chemical potential which is proportional to the charge Q_0 hidden "inside" the black hole horizon. Note that μ_0 does not correspond to the chemical potential of the boundary field theory. Indeed, $\mu_0 r_0$ can be used as a tuning parameter to change the temperature and the chemical potential of the boundary field theory. In the intermediate region $r_2 > r > r_1$, the fluid pressure, energy density and charge density are all non-zero. The background in this intermediate region is obtained by solving the equations (4.9)–(4.11). In the exterior region, namely $r_1 \geq r$, the background is again described by a RN-AdS$_4$ solution with

$$\begin{aligned} f(r) &= \frac{c^2}{r^2}\Big(1 - M r^3 + \frac{1}{2}Q^2 r^4\Big), \quad g(r) = \frac{c^2}{r^4 f(r)}, \\ h(r) &= c\,(\mu - Q r)\,, \end{aligned} \tag{4.18}$$

where the boundary theory quantities c, M, Q and μ are determined by matching the solutions at $r = r_1$ and r_2. Note that μ is the chemical potential of the boundary field theory.

In summary, for $m_{\rm f} \in (0,1)$, as the temperature is lowered, the RN-AdS$_4$ background undergoes a phase transition to a finite-temperature electron star background. It was shown in [139, 140] that this phase transition is third order. Also, it is worth emphasizing that an appealing feature of the finite-temperature electron star background is that, unlike the RN-AdS$_4$ solution, the entropy density s approaches zero as $s \sim T^{2/z}$ in the $T \to 0$ limit [140], where, for given allowed values of the parameters $m_{\rm f}$ and β, the dynamical critical exponent z agrees with the one obtained from the zero-temperature electron star background with the same values of $m_{\rm f}$ and β.

4.3 Neutral Scalar Order Parameter at Zero Temperature

In this section we analyze the spontaneous condensation of a neutral scalar operator in a strongly-coupled (2+1)-dimensional zero-temperature boundary field theory with a finite density of fermions, which is dual to the the zero-temperature electron star background reviewed in the previous section. In the context of the AdS/CFT correspondence, the question of whether a scalar operator can spontaneously condense in a strongly-coupled boundary theory maps to the question of whether the gravitational background can develop a scalar hair. So, we are naturally led to investigate whether the electron star background can develop a neutral scalar hair.

4.3.1 Neutral Scalar Hair for the Electron Star

We introduce the scalar field ϕ in the electron star background by considering the action

$$S_\phi = -\frac{1}{2\kappa^2\lambda}\int d^4x\sqrt{-g}\left[\frac{1}{2}(\nabla\phi)^2 + V(\phi)\right], \tag{4.19}$$

where the potential $V(\phi)$ takes the form

$$V(\phi) = \frac{1}{4L^2}\left[\left(\phi^2 + m^2L^2\right)^2 - m^4L^4\right]. \tag{4.20}$$

We choose the mass square of the scalar, m^2, to be negative but above the BF bound of the asymptotic AdS$_4$ region. Namely, the mass of the scalar is assumed to be in the range $-9/4 < m^2L^2 < 0$. Note that since m^2 is taken to be negative, the field ϕ should be expanded asymptotically around the maximum[3] of the Mexican-hat potential $V(\phi)$, *i.e.* $\phi = 0$. As we will explain below, it is important that $V(\phi)$ has (at least) a

[3]Expanding ϕ in the asymptotic region around either of the two minima of $V(\phi)$ corresponds to a positive m^2. We will not consider such a case in this Chapter, as, with the mechanism explained in the Chapter, we do not expect to see a condensation of the dual neutral scalar operator in the boundary theory.

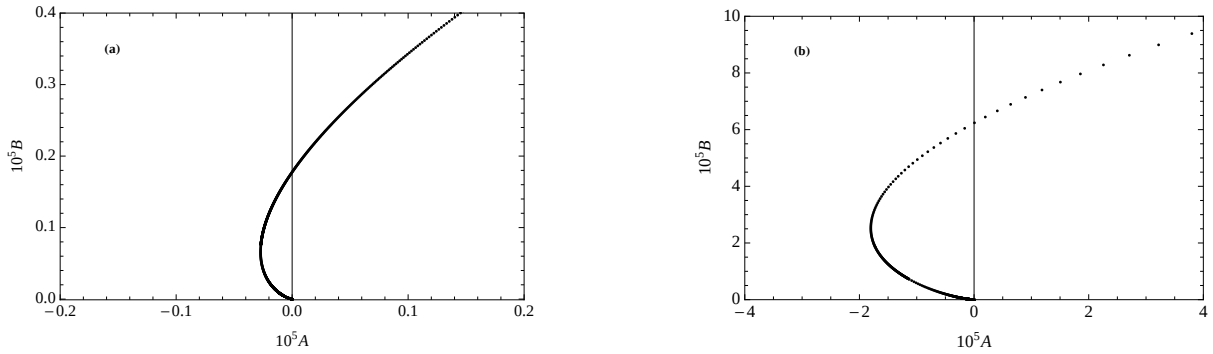

Figure 4.2: Plots of B versus A for the neutral scalar field ϕ with a mass square $m^2L^2 = -2.20$ on an electron star background with $m_{\rm f} = 0.36$ and (a) $z = 2$ and (b) $z = 3$. The BF bounds in the far-interior of the star (with $m_{\rm f} = 0.36$) for $z = 2$ and $z = 3$ are $m_{\rm c}^2L^2 \simeq -2.12$ and -2.02, respectively. Since B is non-zero at $A = 0$, the plots show the spontaneous condensation of the dual operator Φ in the respective boundary theories.

minimum [58]. Note that the constant term in $V(\phi)$ is there to ensure zero contribution to the cosmological constant of the electron star background, $\Lambda = -3/L^2$, for $\phi = 0$. Also, λ is a coupling constant chosen, at first, to be large in order for the probe approximation to be valid. We later relax this assumption when we consider the backreaction of the scalar on the electron star background. The same scalar action was used in [58] to study the condensation of a neutral scalar order parameter in the boundary theory dual to the RN-AdS$_4$ background, both at zero and finite temperature[4].

The action (4.19) is invariant under a $\mathbb{Z}_2$ symmetry: $\phi \to -\phi$. This symmetry is broken in a phase of the boundary theory where the operator dual to ϕ spontaneously condenses. The symmetry group can easily be enlarged by considering more scalar fields, and depending on which dual operators condense, a variety of interesting symmetry breaking patterns could be realized in the boundary theory. Such holographic setups can potentially be used to capture the relevant physics of the strongly-correlated systems with competing order parameters. In this section, we deal with just one neutral scalar field with an action given in (4.19).

The equation of motion for ϕ reads

$$\frac{1}{\sqrt{-g}}\partial_M\left(g^{MN}\sqrt{-g}\,\partial_N\phi\right) = V'(\phi), \tag{4.21}$$

where prime here denotes derivative with respect to ϕ. Given the background metric in (4.5) and choosing the ansatz $\phi = \phi(r)$, equation (4.21) takes the form

$$\frac{r^2}{\sqrt{f(r)g(r)}}\,\partial_r\left(\frac{1}{r^2}\sqrt{\frac{f(r)}{g(r)}}\partial_r\phi\right) = L^2V'(\phi). \tag{4.22}$$

[4]See also [133] for a discussion of condensing neutral scalar operators in holographic setups using multi-trace deformations.

We are after a non-trivial solution which is regular as $r \to \infty$ and normalizable as $r \to 0$. Note that $r \to \infty$ is the far-interior of the background which is Lifshitz, while $r \to 0$ is the boundary of the background which is AdS_4. From (4.12) and (4.13), the metric functions in the interior region take the form $f(r) = r^{-2z} + \cdots$ and $g(r) = \mathfrak{g}\, r^{-2} + \cdots$, where the dots represent the sub-leading terms as $r \to \infty$. Hence, the equation of motion for ϕ in the far-interior region reduces to

$$\frac{1}{\mathfrak{g}} r^{3+z} \partial_r \left(r^{-(1+z)} \partial_r \phi \right) = L^2 V'(\phi). \tag{4.23}$$

Demanding a *non-trivial regular* solution in the far interior forces ϕ to sit at a minimum of the potential $V(\phi)$. This can easily be shown following [58]. Suppose the non-trivial regular solution in the far interior of the background behaves as $\phi = \phi_0 + \delta\phi$ where $\delta\phi \sim r^{\delta}$ with $\delta < 0$, so that $\phi \to \phi_0$ as $r \to \infty$. One then easily deduces that the left-hand side of the equation (4.23) vanishes, resulting in $V'(\phi_0) = 0$. So, the scalar field must sit at an extremum of the potential. Now linearizing equation (4.23) around $\phi = \phi_0$, we find

$$\frac{1}{\mathfrak{g}} r^{z+3} \partial_r \left(r^{-(1+z)} \partial_r \delta\phi \right) - L^2 V''(\phi_0) \delta\phi = \mathcal{O}(\delta\phi^2). \tag{4.24}$$

The general solution of the above equation takes the form $\delta\phi(r) = a\, r^{\delta_+} + b\, r^{\delta_-}$ with

$$\delta_\pm = \frac{1}{2} \left[(2+z) \pm \sqrt{(2+z)^2 + 4\mathfrak{g} L^2 V''(\phi_0)} \right]. \tag{4.25}$$

Because the solution $a\, r^{\delta_+}$ blows up in the $r \to \infty$ limit, we set $a = 0$. In order for $b\, r^{\delta_-}$ to be a regular solution in the interior, one has to have $V''(\phi_0) > 0$ (note that $\mathfrak{g}$ is positive). This then proves that the scalar field must sit at a minimum of $V(\phi)$, if one demands a non-trivial regular solution for $\phi(r)$ as $r \to \infty$. Thus, the regular solution takes the following form in the far-interior region of the background

$$\phi(r) = \phi_0 + b\, r^{\delta_-} (1 + \cdots), \qquad r \to \infty, \tag{4.26}$$

with

$$\delta_- = \frac{1}{2} \left[(2+z) - \sqrt{(2+z)^2 - 8\mathfrak{g}\, m^2 L^2} \right]. \tag{4.27}$$

Asymptotically as $r \to 0$, from (4.16), we have $f(r) = c^2 r^{-2} + \cdots$ and $g(r) = r^{-2} + \cdots$. The scalar

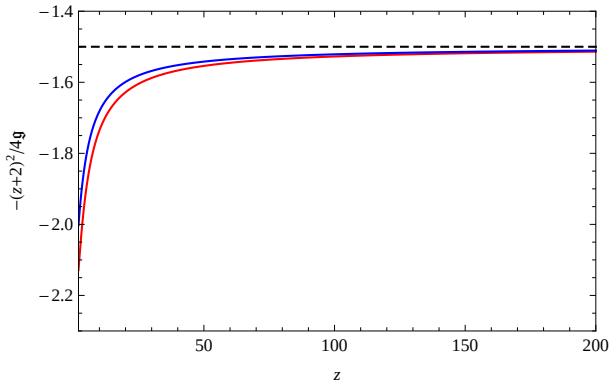

Figure 4.3: Plots of $m_c^2 L^2 = -(z+2)^2/4\mathfrak{g}$ as function of z for $m_{\rm f} = 0.36$ (red) and $m_{\rm f} = 0.7$ (blue). Here L is the curvature radius of the asymptotic AdS_4 region. As z increases the curves asymptote to the dashed line, which represents the scalar BF bound in AdS_2.

equation of motion (4.21) then becomes

$$r^4 \partial_r \left(\frac{1}{r^2} \partial_r \phi \right) - \phi(\phi^2 + m^2 L^2) = 0, \qquad r \to 0. \tag{4.28}$$

Linearizing equation (4.28) around $\phi = 0$, the general solution will be of the form

$$\phi = A\, r^{3-\Delta}(1 + \cdots) + B\, r^{\Delta}(1 + \cdots), \tag{4.29}$$

where $\Delta = \frac{3}{2} + \sqrt{m^2 L^2 + \frac{9}{4}}$. For $-\frac{9}{4} < m^2 L^2 < -\frac{5}{4}$, either A or B could be called the source and the other one the vacuum expectation value (vev) of the dual operator Φ [55]. We choose to work in the so-called "standard quantization" where we take A to be the source for Φ, and B as the vev of Φ, denoted by $\langle \Phi \rangle$. (Note that for $m^2 L^2 \geq -\frac{5}{4}$, only the standard quantization exists.) Hence, Δ is the dimension of the neutral scalar operator Φ, which is the holographic dual of the bulk neutral scalar field ϕ. Given the boundary condition (4.26) for ϕ in the interior, for each value of b, the equation (4.22) could be numerically integrated to the asymptotic $r \to 0$ region from which both A and B could be determined. Repeating the process for different values of b, the dependence of A and B on b, and thus the dependence of B on A, could easily be obtained. Since we are interested in the condensation of the operator Φ without turning on a source, we look for solutions where B remains finite at $A = 0$.

In performing the numerics in this section, it is more convenient to define a dimensionless radial coordinate by rescaling $r \to r_s r$. As a result, we also make b, A and B dimensionless by redefining $b \to r_s^{-\delta_-} b$, $A \to r_s^{\Delta-3} A$ and $B \to r_s^{-\Delta} B$. We also set $L = 1$ in our numerics throughout this Chapter. Figure 4.2 shows B versus A for the bulk neutral scalar with $m^2 L^2 = -2.2$ on two different electron star backgrounds, one which flows in the IR to a theory with $z = 2$ and the other to a theory with $z = 3$. For both of the

star backgrounds, we set $m_{\rm f} = 0.36$. As the plots in Figure 4.2 demonstrate B is non zero when A is zero, indicating that the neutral operator Φ spontaneously condenses in the two boundary theories (which are the holographic duals of the two electron star backgrounds). Said another way, the aforementioned two electron star backgrounds have each formed a neutral scalar hair.

The reasoning behind the formation of a neutral scalar hair for the electron star background is similar to the RN-AdS$_4$ case discussed in [47, 58]. Recall that the (2+1)-dimensional boundary field theory under consideration flows in the IR to a (2+1)-dimensional Lifshitz fixed-point with a finite dynamical critical exponent z. Let's denote the dimension of the operator Φ at the IR Lifshitz fixed-point by $\Delta_{\rm IR}$. One can then easily show that

$$\Delta_{\rm IR} = \frac{1}{2}\left[(2+z) + \sqrt{(2+z)^2 + 4\mathfrak{g}\, m^2 L^2}\right]. \tag{4.30}$$

In the discussion below equation (4.20), we have assumed that the mass square of ϕ satisfies $-\frac{9}{4} < m^2L^2 < 0$, where the lower bound is the BF bound of the asymptotic AdS$_4$ region of the electron star background. Since for the IR Lifshitz fixed-point with $z > 1$ one has $\mathfrak{g} > 1$, there is always a range of mass square for which the expression under the square root in (4.30) becomes complex, while still satisfying the BF bound of the asymptotic AdS$_4$ region. Namely, for

$$-\frac{9}{4} < m^2L^2 < m_c^2L^2, \quad \text{with} \quad m_c^2L^2 = -\frac{(z+2)^2}{4\mathfrak{g}}, \tag{4.31}$$

the bulk neutral scalar field becomes tachyonic in the far-interior region or equivalently, in the language of the the dual field theory, the scaling dimension of Φ at the IR Lifshitz fixed-point $\Delta_{\rm IR}$ becomes imaginary, signaling a potential instability in the theory. Note that $-(z+2)^2/4\mathfrak{g}$ is the scalar BF bound in the far-interior Lifshitz geometry of the electron star background. Figure 4.3 shows plots of this bound as a function of z for $m_{\rm f} = 0.36$ (red) and $m_{\rm f} = 0.7$ (blue). One sees from the plots in Figure 4.3 that as z increases, $m_c^2L^2$ approaches the value -3/2, which equals the scalar BF bound in an AdS$_2$ background. (Note that L is the curvature radius of the asymptotic AdS$_4$ region.) Such behavior is expected, and is due to the fact that for a fixed value of $m_{\rm f} \in (0,1)$ and in the $z \to \infty$ limit, the far-interior region of the electron star background becomes AdS$_2 \times \mathbb{R}^2$ [54]. In other words, the electron star background reverts back to the RN-AdS$_4$ solution.

In both of the plots in Figure 4.2, the mass square of the bulk scalar $m^2L^2 = -2.2$ violates the BF bound of the far-interior Lifshitz region of each of the two star backgrounds while satisfying the BF bound of their asymptotic AdS$_4$ regions. Hence, we see from the plots that the neutral scalar operator Φ spontaneously condenses in each of the two boundary theories, and breaks the aforementioned $\mathbb{Z}_2$ symmetry. On the

other hand, if the mass square is above the BF bound in the far-interior Lifshitz region, no spontaneous condensation for Φ is seen[5] in the boundary theory, and, as a result, the $\mathbb{Z}_2$ symmetry is intact. The plot in Figure 4.4 shows the behavior of B as a function of m^2L^2 for the bulk neutral scalar in an electron star background with $m_{\rm f} = 0.36$ and $z = 2$. As the plot shows, B approaches zero as m^2L^2 approaches $m_c^2L^2 \simeq -2.12$ from below. In general, by tuning the mass square of the bulk scalar across the critical value $m_c^2L^2$, we obtain a hairy electron star background. Or, simply put in the language of the boundary theory, varying the dimension Δ of the operator Φ across a critical dimension Δ_c, the boundary theory at low energies goes through a quantum phase transition, from an uncondensed ($\mathbb{Z}_2$-symmetric) phase, $\langle\Phi\rangle = 0$, to a phase with a neutral scalar order parameter, $\langle\Phi\rangle \neq 0$, in which the $\mathbb{Z}_2$ symmetry is spontaneously broken. Here, $\Delta_c = \frac{1}{2}\left(3 + \sqrt{9 - (z+2)^2/\mathfrak{g}}\right)$.

A few comments are in order. We would like to emphasize that the inequality $\mathfrak{g} > 1$ plays an important role here. Indeed, should $\mathfrak{g} < 1$, the BF bound in the interior Lifshitz region, for the case of $z > 1$, would be less than the scalar BF bound in the asymptotic AdS_4 region, and, as a result, there would be no possibility for the phase transition of the kind we just described above.

The two phases described above have the same dynamical critical exponent z. This is just an artifact of the probe approximation we have employed so far where the backreaction of the bulk neutral scalar field on the electron star background in neglected. In a subsection to follow, we will take into account such a backreaction and show that the aforementioned zero-temperature quantum phase transition is indeed between two phases with different z. This is a particular novelty in certain quantum phase transitions in condensed matter systems. Phase transitions in which the critical dynamical exponent changes across the critical point have been suggested to underlie magnetism in the cuprates [141, 142] and in nematic-smectic transitions [143].

The existence of the neutral scalar hair is essentially goverened by the physics in the far-interior region of the electron star background. More concretely, in the standard quantization, it is the effective mass square of the neutral scalar field in the Lifshitz region which determines whether the electron star background becomes unstable to forming a neutral scalar hair. Since the bulk scalar field is neutral, its effective mass in the Lifshitz region is the same as the mass m in the asymptotic AdS_4 region. So, tuning m^2L^2 across the BF bound in the Lifshitz region, $m_c^2L^2 = -(z+2)^2/4\mathfrak{g}$, the electron star background undergoes a phase

[5]Adding a double-trace deformation of the type $g\int d^3x\,\Phi^2$ (with $g < 0$) to the boundary theory action, and choosing the alternative quantization where the dimension of the operator Φ satisfies $1/2 < \Delta < 3/2$, makes it possible for Φ to condense even if the mass square of the dual bulk neutral scalar is above the BF bound of the far-interior Lifshitz region. It would be interesting to explore, along the lines of [133], the consequences of the aforementioned double-trace deformation for the holographic setup under consideration here. In the standard quantization, however, the mass square of the neutral scalar being below the BF bound of the far-interior Lifshitz region is the necessary and sufficient condition for the condensation of Φ in the theory dual to the zero-temperature electron star background.

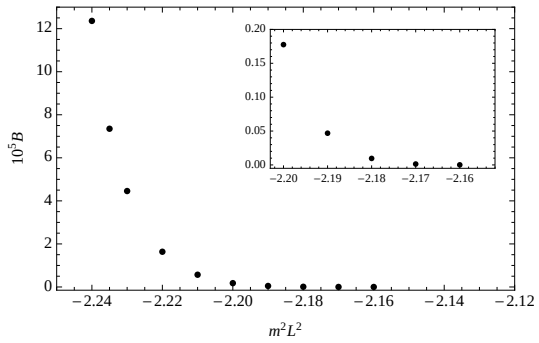

Figure 4.4: B versus m^2L^2 for the neutral scalar field ϕ on an electron star background with $m_{\rm f} = 0.36$ and $z = 2$. Due to numerical limitations we could not access the region of mass square very close to the BF bound, $m_c^2L^2 \simeq -2.12$, of the far-interior of the star. The inset shows a close up of the behavior of B for larger values of m^2L^2.

transition to the formation of a neutral scalar hair. Tuning the mass square of the scalar in the asymptotic region is not the only way to achieve this phase transition. For example, a simple way for tuning the effective mass square of the neutral scalar field in the far-interior Lifshitz region is to couple the scalar to the square of the Weyl tensor in the action (4.19), by adding to the potential $V(\phi)$ a term of, say, the following form [59]

$$\delta V = -\frac{1}{2}L^2 l^2 \phi^2 W^2, \tag{4.32}$$

where $W^2 = W_{MNPQ}W^{MNPQ}$ with W_{MNPQ} being the Weyl tensor. The effect of this new coupling is to make the mass of the scalar to depend on the radial coordinate r. Asymptotically, $W^2 \to 0$ as $r \to 0$. So the mass of the scalar in the asymptotic AdS_4 region is untouched by the coupling (4.32). In the far-interior region, one can easily show that $W^2 \to 4z^2(-1+z)^2/(3\mathfrak{g}^2L^4)$ as $r \to \infty$, hence, the mass square of the scalar in the Lifshitz region is shifted by a constant proportional to l^2. Thus, the effective mass square of the scalar in the Lifshitz region can be varied simply by varying l. The coupling l could be tuned such that the effective mass square in the Lifshitz region violates the BF bound there, in which case it is not hard to show that the electron star background develops a neutral scalar hair. Neither tuning m nor tuning l is an operation that could be performed in a single theory. If one thinks of backgrounds such as the electron star background, or RN-AdS_4, as coming from, say, M-theory, then the couplings m, l, $\cdots$ are generally fixed. In this regard, tuning m or l seems unnatural. Nevertheless, we continue to tune m^2L^2 in order to be able to obtain the aforementioned phase transition. As the transition owns its existence to what the effective mass square of the scalar is in the far-interior region, we do expect the qualitative features of the phase transition to stay the same regardless of whether it has been obtained by tuning m, l, or a UV knob (such as a magnetic field) that could be continuously changed within a single theory. A simple way to introduce

such a knob that can be continuously varied in a single theory has been explained in [58].

4.3.2 Free Energy of the Condensed Phase

In this section we determine the free energy density of the boundary theory in the condensed phase $\langle\Phi\rangle \neq 0$. The free energy is given by the on-shell action, up to boundary counter terms. Assuming the bulk scalar field does not back-react on the background, the free energy of the condensed phase is just the sum of two contributions: one coming from the electron star background and the other from the neutral scalar field. We work in the grand canonical ensemble where the boundary theory chemical potential μ is held fixed. As shown in [54], the free energy density of the theory dual to the zero-temperature electron star background is given by $\Omega_1 = M - \mu Q = -M/2$, with M and Q being the energy and charge densities, respectively. Thus, we only need to determine the free energy density contributed by the boundary theory operator Φ, denoted hereafter by Ω_2.

Up to boundary counter terms, Ω_2 is simply given by the action (4.19) evaluated on-shell. To make the expressions less cluttered, we drop the coefficient $1/(2\kappa\lambda)$ from the action. We also set $L = 1$ in this discussion. Upon integrating by parts and using the equation of motion (4.21), the action (4.19) takes the form

$$S_{\text{o.s.}} = \int d^3x \left\{ \frac{1}{2} \left(\sqrt{-g}\, g^{rr} \phi\, \phi' \right) \Big|_{r=\epsilon} + \frac{1}{4} \int_{\epsilon}^{\infty} dr \sqrt{-g}\, \phi^4 \right\}, \tag{4.33}$$

where prime denotes derivative with respect to r and ϵ is a cutoff introduced to regulate the above integral, as it is naively divergent. We will eventually send ϵ to zero.

If we work in an ensemble where the source is kept fixed, *i.e.* $\delta\phi = 0$, the on-shell action (4.33) needs to be supplemented by a counter term

$$S_{\text{c.t.}} = -\frac{c}{2}(3-\Delta) \int d^3x \sqrt{-\gamma}\, \phi^2|_{r=\epsilon}, \tag{4.34}$$

to cancel the divergence. Note that γ is the induced metric on the boundary. Adding the above counter term to (4.33), and taking the $\epsilon \to 0$ limit, the renormalized on-shell action S_{ren} becomes

$$\begin{aligned} S_{\text{ren}} &= S_{\text{o.s.}} + S_{\text{c.t.}} \\ &= V \left[\frac{c}{2}(2\Delta - 3)AB + \frac{1}{4} \int_0^{\infty} dr \sqrt{-g}\, \phi^4 \right], \end{aligned} \tag{4.35}$$

where $V = \int d^3x$, and we have substituted the asymptotic expansion of the scalar field at the boundary. Since $\Omega_2 = -S_{\rm ren}/V$ is the free energy density contributed by the operator Φ, the free energy density of the system $\Omega = \Omega_1 + \Omega_2$ then reads

$$\Omega = -\frac{M}{2} - \frac{c}{2}(2\Delta - 3)AB - \frac{1}{4}\int_0^\infty dr\sqrt{-g}\,\phi^4. \tag{4.36}$$

If instead we work in an ensemble where the response is fixed, *i.e.* $\delta\phi' = 0$, then one has to add an additional counter term, analogous to the Gibbons-Hawking term [144, 145], to the on-shell action in order to render the variational problem well-defined. The total counter term for this case becomes

$$\begin{aligned} S_{\rm c.t.} = &- \int d^3x\, \left(\sqrt{-g}\, g^{rr}\phi\,\phi'\right)\Big|_{r=\epsilon} \\ &+ \frac{c}{2}(3-\Delta)\int d^3x\sqrt{-\gamma}\,\phi^2|_{r=\epsilon}. \end{aligned} \tag{4.37}$$

Going through the same steps as before, we write the free energy density of the system as

$$\Omega = -\frac{M}{2} + \frac{c}{2}(2\Delta - 3)AB - \frac{1}{4}\int_0^\infty dr\sqrt{-g}\,\phi^4. \tag{4.38}$$

The condensed phase, $\langle\Phi\rangle \neq 0$, corresponds, in the standard quantization, to $A = 0$ and $B \neq 0$ while the uncondensed phase is given by $A = B = 0$. Indeed, in the latter phase, there is only the trivial solution $\phi(r) = 0$ in the bulk. The change in free energy is then given by

$$\Omega_{\rm condensed} - \Omega_{\rm uncondensed} = -\frac{1}{4}\int_0^\infty dr\sqrt{-g}\,\phi^4. \tag{4.39}$$

Therefore, we see that when the operator Φ condenses, the free energy of the system is actually lower than that of the uncondensed phase. Figure 4.5 shows a plot of the change in free energy density, $\Delta\Omega = \Omega_{\rm condensed} - \Omega_{\rm uncondensed}$, versus m^2L^2. Clearly, the condensed phase has a lower free energy than the uncondensed phase, the difference approaches zero when the critical point is approached from below.

4.3.3 Zero-Temperature Phase Transition

In this subsection we analyze the nature of this zero-temperature phase transition and argue that it has a BKT character, meaning that close to the critical point in the condensed phase $\langle\Phi\rangle \sim \mu^\Delta \exp(-c_1/\sqrt{\nu_c - \nu})$, where ν is a parameter that can be tuned across the critical point and $c_1 > 0$.

Consider the boundary theory dual to the AdS_{d+1} background, with a UV scale. For this theory,

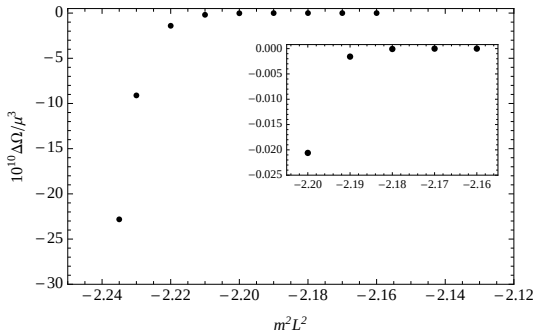

Figure 4.5: Plot of $\Delta\Omega/\mu^3$ versus m^2L^2. For the background, we set $z = 2$ and $m_{\rm f} = 0.36$. Numerical difficulties prevented us from obtaining more data points for the values of m^2L^2 very close to the critical value $m_c^2L^2 \simeq -2.12$.

the authors of [146] have argued on general grounds that if the mass square of a bulk scalar is slightly below the BF bound, an IR scale $\Lambda_{\rm IR}$ will be generated, which is related to the UV scale $\Lambda_{\rm UV}$ via $\Lambda_{\rm IR} = \Lambda_{\rm UV}\exp(-c_2/\sqrt{\nu_c - \nu})$ with $c_2 > 0$. Concrete examples of this phenomenon were constructed in [58, 147] using a background with an AdS_2 near horizon geometry. Also, it was argued in [147] that the same phenomenon would occur in a boundary theory dual to a Lifshitz-like background [147]. As shown below, the discussion in [58, 146] for a BKT-type phase transition can handily be generalized to our case as well.

Consider the equation of motion for ϕ given by equation (4.23). Linearizing around $\phi = 0$ in the far-interior Lifshitz region of the electron star background, this equation can be put in the form

$$\chi''(r) = \frac{\mathfrak{g}}{r^2}\left[-r^{2z}\omega^2 + \left(m^2 - m_c^2\right)L^2 - \frac{1}{4\mathfrak{g}}\right]\chi(r), \tag{4.40}$$

where we assumed a time-dependence of $e^{-i\omega t}$ for ϕ, and defined $\phi(r) = r^{(z+1)/2}\chi(r)$. Note that in the above equation $m_c^2L^2 = -(2+z)^2/4\mathfrak{g}$ is the BF bound of the far-interior Lifshitz region. For the mass square below the BF bound, there will exist a negative-energy bound state if $0 < r < \infty$. On the other hand, if the geometry is cut by some suitably chosen UV and IR "walls", denoted by $r_{\rm UV}$ and $r_{\rm IR}$ such that $r_{\rm IR} \geq r \geq r_{\rm UV}$, the existence of negative-energy bound states could be prevented. This is actually the case in our setup. The far-interior Lifshitz region does not extend all the way to the boundary, and at some radius matches to the exterior geometry. Also, the IR wall is provided by the condensate, whose existence is essentially due to the stabilizing effect of the quartic term in the scalar potential (4.20).

Since we are interested in the onset of an instability we look at the $\omega = 0$ solutions. As argued in [58, 146] the exact form of the boundary conditions for ϕ at the walls are not important and could be taken to be Dirichlet. So, we choose $\phi(r_{\rm UV}) = \phi(r_{\rm IR}) = 0$. The zero-energy solution satisfying the Dirichlet boundary

condition at $r_{\rm UV}$ is found to be [58, 146]

$$\phi(r) = r^{(z+2)/2} \sin\left[\sqrt{\mathfrak{g}\,(m_c^2 L^2 - m^2 L^2)}\log\frac{r}{r_{\rm UV}}\right]. \tag{4.41}$$

To satisfy the boundary condition at $r_{\rm IR}$, one should then have

$$r_{\rm IR} = r_{\rm UV}\exp\left[\frac{\pi}{\sqrt{\mathfrak{g}\,(m_c^2 L^2 - m^2 L^2)}}\right]. \tag{4.42}$$

Note that $r_{\rm IR}/r_{\rm UV} = \Lambda_{\rm UV}/\Lambda_{\rm IR}$. For $r_{\rm IR}$ given by the above formula, the ground state has zero energy. So, there will be no negative-energy bound states. On the other hand, for larger $r_{\rm IR}$ there will be a negative-energy ground state, hence instability. For the mass square of the dual bulk scalar slightly less than the BF bound, the IR Lifshitz fixed-point is still scale invariant over a large energy scale. For energies below $\Lambda_{\rm IR}$, the operator Φ wants to condense and end the instability. For the mass square slightly less than the BF bound, the IR (mass) dimension of Φ according to (4.30) is almost $(z+2)/2$. So, following the argument given in [58], and given that $\Lambda_{\rm UV} \sim \mu$, one then concludes

$$\langle\Phi\rangle \sim \mu^{\Delta}\exp\left[-\frac{(z+2)\pi}{2\sqrt{\mathfrak{g}\,(m_c^2 L^2 - m^2 L^2)}}\right]. \tag{4.43}$$

Note that there are also an infinite number of states, characteristic of Efimov states [58, 147, 148], with $\langle\Phi\rangle_n \sim \mu^{\Delta}\exp\left[-(1+z/2)n\pi/\sqrt{\mathfrak{g}\,(m_c^2 L^2 - m^2 L^2)}\right]$, where $n = 2, 3, 4, \cdots$. The ground state, however, is given by (4.43). The scaling of the condensate as in (4.43) signifies that the underlying transition is of the BKT-type.

4.3.4 Backreaction

In this section, we consider the backreaction of the neutral scalar field on the electron star background, and show that if the mass square of the scalar is below the BF bound of the far-interior region, the dual operator in the boundary theory condenses. Moreover, in the condensed phase the value of the dynamical critical exponent z is different from that of the uncondensed phase.

To consider the effect of backreaction of the scalar field on the background, we need to modify the expression for T_{MN} in (4.3) by including the energy-momentum tensor of the scalar. Note that since the scalar field is neutral, the current J_N is unchanged. The ansatz that we take for the metric and the gauge field is the same as in (4.5) and (4.6), respectively. For the scalar, as in the previous sections, we take the ansatz $\phi = \phi(r)$. Substituting the ansatz into the Einstein-Maxwell-fluid-scalar equations of motion, one

obtains

$$0 = \frac{1}{r}\left(\frac{f'(r)}{f(r)} + \frac{g'(r)}{g(r)} + \frac{4}{r}\right) + \left[p(r) + \rho(r)\right] g(r) + \frac{1}{2\lambda}\phi'(r)^2, \tag{4.44}$$

$$0 = p'(r) + \frac{1}{2}\frac{f'(r)}{f(r)}\left[p(r) + \rho(r)\right] - \frac{h'(r)}{\sqrt{f(r)}}\,\sigma(r), \tag{4.45}$$

$$0 = \frac{f'(r)}{rf(r)} - \frac{h'(r)^2}{2f(r)} + \left[3 + p(r)\right] g(r) - \frac{1}{r^2} + \frac{1}{4\lambda}\phi'(r)^2 - \frac{g(r)}{2\lambda}L^2 V(\phi), \tag{4.46}$$

$$0 = h''(r) + \frac{r}{2}\left[p(r) + \rho(r)\right] g(r)h'(r) - g(r)\sqrt{f(r)}\sigma(r) + \frac{1}{4\lambda}rh'(r)\phi'(r)^2, \tag{4.47}$$

$$0 = \phi''(r) + \frac{1}{2}\left(\frac{f'(r)}{f(r)} - \frac{g'(r)}{g(r)} - \frac{4}{r}\right)\phi'(r) - g(r)L^2 V'(\phi). \tag{4.48}$$

As before, to solve the above equations, we need to specify the equation of state for the fermion fluid. Compared to the case without the scalar backreaction, the equation (4.45) is unchanged . This is due to the fact that in our model, the neutral scalar does not couple directly to the fermion fluid. Thus, the fermion density of states is given by (4.7). Also, similar to the case without the scalar backreaction, we adopt a locally flat approximation where the fermion dynamics is determined by the local chemical potential, whose form is given in (4.8). As a result, the formulae for σ, ρ, and p are the same as before, with the understanding that the metric and the gauge field functions in these expressions are now the backreacted ones. We do not write the formulae for σ, ρ, and p here as they can be found in [54]. It can easily be verified that the expressions for σ, ρ, p satisfy the equation (4.45). Thus, in order to determine the backreacted background, one has to solve the remaining equations, namely the equations (4.44), (4.46), (4.47) and (4.48).

In the far-interior region $r \to \infty$, we anticipate a Lifshitz-type geometry. This is due to the fact that the local charge density screens the electric field making it massive, and massive vector fields usually give rise to Lifshitz geometries [130]. Indeed, in the region $r \to \infty$, the following

$$\begin{aligned} \frac{ds^2}{L^2} &= -\frac{dt^2}{r^{2z}} + \frac{1}{r^2}\left(dx^2 + dy^2\right) + \frac{\mathfrak{g}}{r^2}dr^2, \\ A &= \frac{eL}{\kappa}\frac{\mathfrak{h}}{r^z}dt, \qquad\qquad \phi = \phi_0, \end{aligned} \tag{4.49}$$

is an exact solution to the equations of motion, with $\phi_0 = 0, \pm\sqrt{-m^2L^2}$. The expressions for $\mathfrak{g}$ and $\mathfrak{h}$ are identical to the ones given in (4.15) except that, with the scalar backreaction included, and when $\phi_0 = \pm\sqrt{-m^2L^2}$, the dynamical exponent z acquires contributions from two more parameters mL and λ, namely, $z = z(m_{\rm f}, \beta, mL, \lambda)$. Note that for $\phi_0 = 0$, z does not depend on either mL or λ. For example, without the scalar backreaction, $z = 2$ for $m_{\rm f} = 0.36$ and $\beta = 19.95$. Including the scalar backreaction, z is modified to approximately 2.025 for $m^2L^2 = -2.2$, $\lambda = 10$ and the same values of $m_{\rm f}$ and β.

Since the far-interior solution is of the Lifshitz type, following essentially the same argument as before, one can analyze equation (4.48) to show that demanding a non-trivial regular solution for $\phi(r \to \infty)$ requires the scalar to sit at a minimum of $V(\phi)$. This is exactly the case when z acquires contributions from mL and λ. The form of this non-trivial regular solution in the far-interior region is simply given by (4.26), with z and $\mathfrak{g}$ given by their new backreacted values.

In order to flow up to the asymptotic region, we perturb away from the far-interior Lifshitz solution (4.49) by taking the ansatz

$$f(r) = \frac{1}{r^{2z}}\left(1 + \mathfrak{f}_1 r^{\alpha} + \cdots\right), \tag{4.50}$$

$$g(r) = \frac{\mathfrak{g}}{r^2}\left(1 + \mathfrak{g}_1 r^{\alpha} + \cdots\right), \tag{4.51}$$

$$h(r) = \frac{\mathfrak{h}}{r^z}\left(1 + \mathfrak{h}_1 r^{\alpha} + \cdots\right), \tag{4.52}$$

$$\phi(r) = \phi_0 + b\, r^{\delta} + \cdots . \tag{4.53}$$

We demand the perturbation to grow as $r \to 0$ and not blow up as $r \to \infty$. We also discard the perturbation which gives rise to turning on a finite temperature. Substituting the above ansatz back into the equations of motion, and taking into account the above consideration for the type of perturbation, we then find that the expressions for $\mathfrak{f}_1$, $\mathfrak{g}_1$, $\mathfrak{h}_1$ and α take the same form as in the case with no scalar backreaction, although their numerical values are changed due to the change in z. Similarly, the expression for δ is the same as δ_- in (4.27). Thus, similar to the case without backreaction, the scalar field sits at a minimum of $V(\phi)$, which results in z acquiring a contribution from mL and λ. The perturbation described above can then be thought of as an irrelevant deformation of the (2+1)-dimensional IR Lifshitz fixed-point, which is assumed to be the holographic dual of the bulk solution (4.49) with ϕ_0 siting at the bottom of the potential.

Note that the backreacted geometry is asymptotically AdS_4, and the leading-order expansion of ϕ (expanded around $\phi = 0$) in that region is the same as in (4.29). Thus, if the non-trivial regular solution for ϕ in the far-interior region could be matched to a normalizable solution in the asymptotic region, then the boundary theory dual to this background would be in a condensed phase where the dynamical exponent z is different from the value when the boundary theory is in an uncondensed phase. So, one can by tuning a knob, which, for simplicity, could be taken to be the conformal dimension of the operator Φ, drive the boundary theory from an uncondensed phase, $\langle\Phi\rangle = 0$, with $z = z_1$ to a condensed phase, $\langle\Phi\rangle \neq 0$, where $z = z_2 \neq z_1$.

In order to find a normalizable solution for ϕ in the asymptotic region, we scan different values of b (or, more precisely, the scale-invariant combination $b/\mathfrak{f}_1^{\delta/\alpha}$) to determine whether there is any solution for which

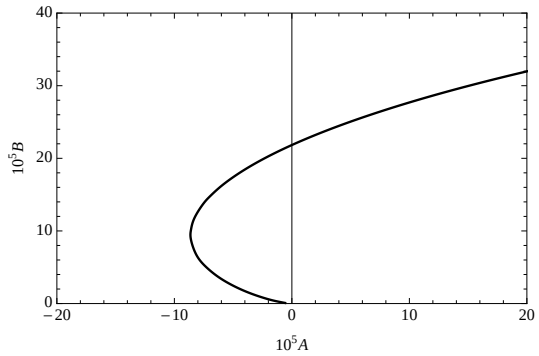

Figure 4.6: Plot of B versus A for $\lambda = 1000$. Here $z = 4$, $m_{\rm f} = 0.36$ and $m^2L^2 = -2.2$. The BF bound of the far-interior region is $m_c^2 L^2 \simeq -1.952$.

$A = 0$ while $B \neq 0$. Figure 4.6 shows a plot of B against A for the case of $z = 4$ and $\lambda = 1000$. As the plot shows, the qualitative behavior of B against A is similar to the case when the scalar backreaction is ignored. The plots show that the boundary theory dual to the backreacted background is in a phase where $\langle\Phi\rangle \neq 0$.

4.4 Neutral Scalar Condensation at Finite Temperature

In this section we extend our studies of the condensation of the operator Φ to finite temperature. The boundary field theory in this case is dual to the finite-temperature electron star background [139, 140]. As we alluded to earlier, a finite-temperature electron star background exists only for temperatures less than a critical temperature T_*. For $T > T_*$, the background is a non-extremal RN-AdS$_4$. The condensation of a neutral scalar operator for the theory dual to a non-extremal RN-AdS$_4$ background was already addressed in [58]. Hence, the temperatures we consider in this section are always in the range $T < T_*$ for which the electron-star background is the preferred solution.

The operator Φ is dual to the neutral scalar field ϕ whose bulk action is given in (4.19). The assumption regarding the mass m of the scalar field is as before. Also, we first consider the case where the scalar backreaction is ignored, namely, for large λ. The equation of motion for the scalar field is given in (4.22). We are after a non-trivial solution which is regular as $r \to r_0$ and normalizable as $r \to 0$. Such a solution in the bulk characterizes a phase of the boundary theory where the dual operator Φ condenses. At finite temperature, demanding a non-trivial regular solution for the scalar ϕ close to the horizon does not require the scalar to be sitting at the bottom of the potential. This can easily be verified by expanding equation (4.22) close to the horizon. Note that close to the horizon, in the so-called inner region of the finite-temperature electron star background, the metric functions are given by (4.17). Indeed, once expanded close to the

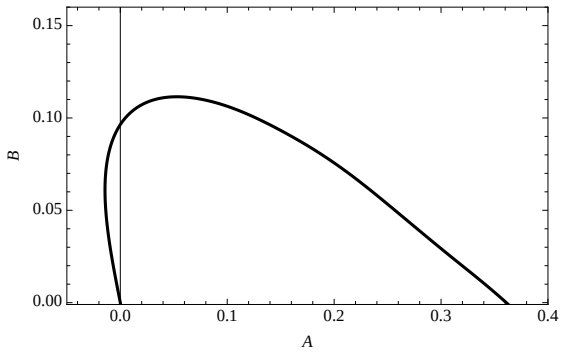

Figure 4.7: Plot of B versus A for $m^2L^2 = -2.2$ and $T/T_c \simeq 0.443$. For the background, we set $m_{\rm f} = 0.7$ and $\beta = 10$.

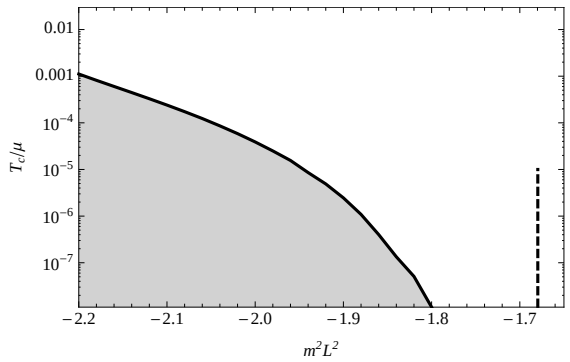

Figure 4.8: T_c versus m^2L^2. For the background, we set $m_{\rm f} = 0.7$ and $\beta = 10$. The shaded region represent the condensed phase, and the dashed line marks the BF bound of the far-interior region as $T \to 0$.

horizon, equation (4.22) admits a regular solution of the form

$$\phi(r) = \phi_0 + \phi_1(r_0 - r) + \phi_2(r - r_0)^2 + \cdots ,$$

where ϕ_1, ϕ_2 and all other coefficients are determined in terms of ϕ_0.

The asymptotic behavior of ϕ (expanded around $\phi = 0$) will be given by the same expression as in (4.29), as both the zero- and finite-temperature electron star backgrounds are asymptotically AdS_4. As in the zero-temperature case in the previous section, we choose to work in the standard quantization where A is the source and B is the vev of the dual operator Φ. Thus, by varying ϕ_0, one can search for a normalizable solution asymptotically with $A = 0$ and $B \neq 0$. For numerical computations in this section, we define a dimensionless radial coordinate by rescaling $r \to r_0 r$, and also work with dimensionless coefficients A and B defined through $A \to r_0^{\Delta-3}A$ and $B \to r_0^{-\Delta}B$. Our numerics show that the operator Φ condenses below some critical temperature T_c as long as the mass squared of the scalar field satisfies $-9/4 < m^2L^2 \leq m_c^2L^2$. Note that the lower limit is there to ensure stability in the asymptotic AdS_4 region. Figure 4.7 shows a plot of B versus A for $m^2L^2 = -2.2$ on an electron star background with $m_{\rm f} = 0.7$ and $\beta = 10$. For the plot, $T/T_c \simeq 0.443$. Notice that as $\phi_0 \to -\phi_0$, $A \to -A$ and $B \to -B$. So, without loss of generality, we have

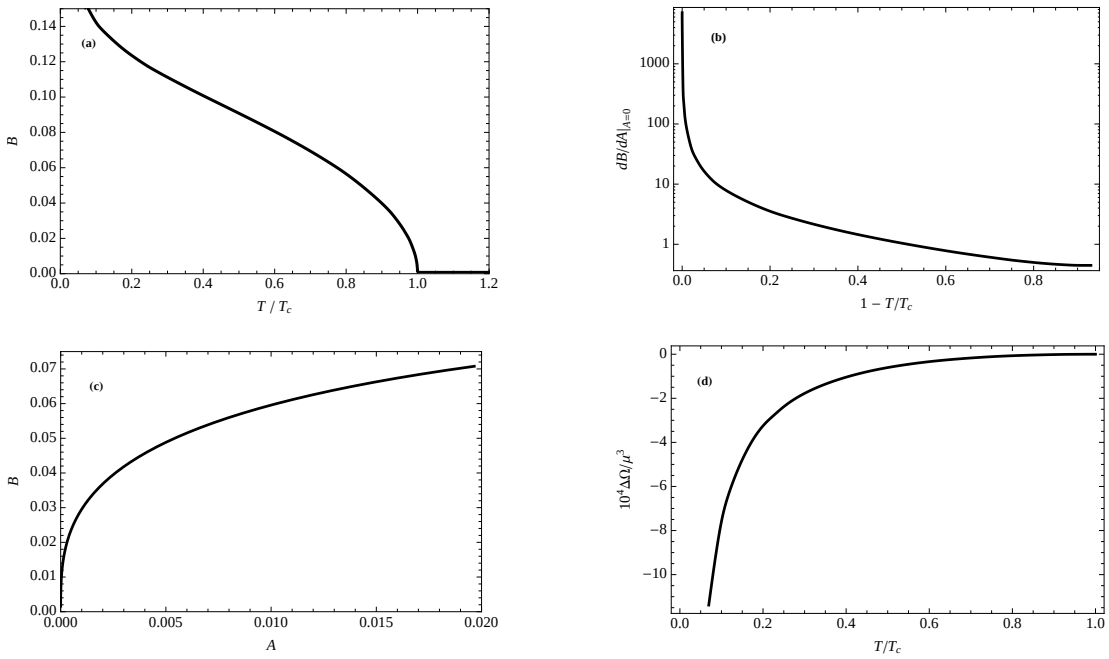

Figure 4.9: Plots of (a) B versus T/T_c, (b) dB/dA at $A = 0$ as function of $1 - T/T_c$ (c) B versus A at $T = T_c$ and (d) $\Delta\Omega$ versus T/T_c. We set $m^2L^2 = -2.2$ and for the background, $m = 0.7$ and $\beta = 10$. From these plots, the critical exponents β_c, γ_c, δ_c, and ν_c are found to be $\beta_c \simeq 0.506$, $\gamma_c \simeq 1.015$, $\delta_c \simeq 3.07$ and $\nu_c \simeq 2.061$ which indicate a second-order phase transition with mean field exponents.

just plotted half the curve of B versus A in Figure 4.7, the half for which ϕ_0 is non-negative. Our numerics also show that $T_c \to 0$ as m^2L^2 approaches the critical value from below, as shown in Figure 4.8, although, due to numerical difficulties, we could not probe larger values of m^2L^2, namely the ones very close to $m_c^2L^2$. Moreover, as shown in the plots of Figure 4.9, we find that close to T_c, $B \sim (1 - T/T_c)^{\beta_c}$ with $\beta_c \simeq 0.506$, $dB/dA|_{A=0} \sim (1 - T/T_c)^{-\gamma_c}$ with $\gamma_c = 1.015$, and at $T = T_c$, $B \sim A^{1/\delta_c}$ with $\delta_c \simeq 3.07$. Also, Figure 4.9(d) shows a plot of the change in the free energy density $\Delta\Omega = \Omega_{\text{condensed}} - \Omega_{\text{uncondensed}}$ versus the temperature. It shows that whenever there is a condensed phase, its free energy is always lowered when compared to the uncondensed phase. Hence, the condensed phase is energetically favored over the uncondensed phase. As temperature approaches T_c from below, the difference in free energy approaches zero as $\Delta\Omega \sim (1 - T/T_c)^{\nu_c}$, with the numerically obtained value of $\nu_c \simeq 2.061$.

The numerically obtained critical exponents β_c, γ_c, δ_c and ν_c are indicative of a second-order phase transition with mean field exponents. The finite-temperature phase transition obtained here is indeed similar to the result found in [58] for the scalar condensation in the boundary theory dual to the non-extremal RN-AdS_4 background. This is perhaps not surprising as the nature of this phase transition at finite temperature could be traced back to the analyticity of A and B as a function of ϕ_0 close to the horizon [58].

4.4.1 Backreaction at Finite Temperature

We now take into account the backreaction of the neutral scalar field on the finite-temperature electron star background. Again, since the neutral scalar does not couple directly to the fermion, the fermion density of states is given by (4.7). This assumes that the effect of the temperature on the fermionic density of states is negligible. We also assume that the fermion dynamics are determined by the local chemical potential, with a form given in (4.8), with the same formulae for σ, ρ, p given as in the case without scalar backreaction. Similar to the case without scalar backreaction, the finite-temperature background is divided into three regions. The radii r_1 and r_2 which separate the three different regions are solutions to the equation $\mu_{\rm loc}(r) = m_{\rm f}$. Our discussion of the backreacted background in the following will be brief as its characteristics are very much similar to the case without the backreaction of the neutral scalar. In the inner region, $r_0 \geq r \geq r_2$, the solution is obtained by solving the equations (4.44), (4.46), (4.47) and (4.48) with $p = \rho = \sigma = 0$, namely

$$0 = \frac{1}{r}\left(\frac{f'(r)}{f(r)} + \frac{g'(r)}{g(r)} + \frac{4}{r}\right) + \frac{1}{2\lambda}\phi'(r)^2, \tag{4.54}$$

$$0 = \frac{f'(r)}{rf(r)} - \frac{h'(r)^2}{2f(r)} + \left[3 - \frac{1}{2\lambda}L^2V(\phi)\right]g(r) - \frac{1}{r^2} + \frac{1}{4\lambda}\phi'(r)^2, \tag{4.55}$$

$$0 = h''(r) + \frac{1}{4\lambda}rh'(r)\phi'(r)^2, \tag{4.56}$$

$$0 = \phi''(r) + \frac{1}{2}\left(\frac{f'(r)}{f(r)} - \frac{g'(r)}{g(r)} - \frac{4}{r}\right)\phi'(r) - g(r)L^2V'(\phi). \tag{4.57}$$

Our objective in this subsection is to study the condensation of the operator Φ in the boundary theory dual to the backreacted finite-temperature electron-star background. This means that we are after a solution for ϕ which is regular at the horizon (as well as normalizable in the asymptotic region). So, we start by taking the following ansatz for the expansion of the solution near the horizon

$$g(r) = \frac{g_0}{r - r_0} + g_1 + \cdots, \tag{4.58}$$

$$f(r) = f_0(r - r_0) + f_1(r - r_0)^2 + \cdots, \tag{4.59}$$

$$h(r) = h_0(r - r_0) + h_1(r - r_0)^2 + \cdots, \tag{4.60}$$

$$\phi(r) = \phi_0 + \phi_1(r - r_0) + \phi_2(r - r_0)^2 + \cdots. \tag{4.61}$$

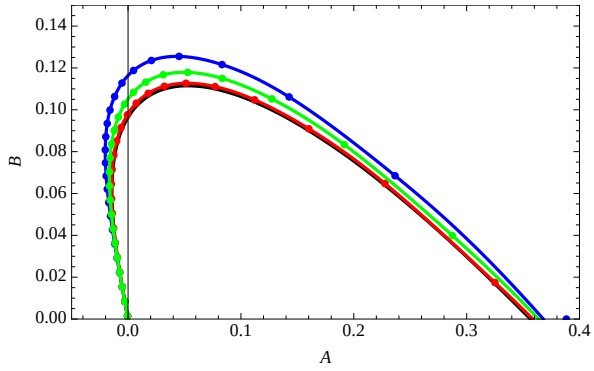

Figure 4.10: Plots of B as function of A. The black curve corresponds to the case without the backreaction of the scalar field, while the blue, green and red curves correspond to the scalar backreaction with $\lambda = 10, 20$ and 100 respectively. The mass square of the scalar is $m^2L^2 = -2.2$ for all the curves. For the non-backreacted case, $T/\mu \simeq 0.00045$ with $m_{\rm f} = 0.7$ and $\beta = 10$.

It is more convenient to rescale the radial coordinate such that the horizon is at $r_0 = 1$. Substituting the ansatz back into the equations (4.54)-(4.57), one finds that all of the coefficients in the above expansion are determined in terms of h_0, f_0 and ϕ_0. Note that the value one chooses for f_0 fixes the normalization of time. In the intermediate region $r_2 > r > r_1$ where the fluid energy density, pressure and charge density are all non-zero, one has to solve the equations (4.44), (4.46), (4.47) and (4.48). In the outer region $r \leq r_1$, the space-time is given, once again, by the solution to the equations (4.54)-(4.57). The outer-region solution is asymptotically AdS_4, with the leading expansion of the scalar field given by (4.29). Note that in the backreacted case, the temperature of dual field theory is given by $(4\pi c)^{-1}|df(r_0)/dr\sqrt{1/f(r_0)g(r_0)}|$, where c is given by $\sqrt{r^4 f(r)g(r)}|_{r\to 0}$. Also, the chemical potential of the dual theory is given by $h(r \to 0)/c$.

The condensed phase (in the standard quantization) is once again characterized by $A = 0$ and $B \neq 0$. The plots in Figure 4.10 show the behavior of B versus A for different values of the coupling λ. As the plots show, the condensed phase persists even as λ decreases, where the backreaction of the neutral scalar field becomes more important. As a test of our numerics for $\lambda \to \infty$, the curves produced with the scalar backreaction present approach the curve obtained for the case without the scalar backreaction. We have checked that even if the scalar backreaction is included, the finite-temperature phase transition between the condensed and uncondensed phases is still second-order with mean-field exponents.

4.5 Discussion

The Hertz-Millis [125, 126] theory is an attempt to describe quantum criticality in a metallic system in the presence of some type of magnetic order described by a neutral order parameter. In obtaining the low-energy theory in terms of the bosonic neutral order parameter, the fermions, which are gapless, are integrated out. This procedure has no guarantee of working since the fermions belong to the low-energy sector. In

$d = 2 + 1$, this procedure is fatal as an infinite [127–129] number of marginal operators are generated by the integration procedure. Holography obviates integrating out the fermions because they can be included non-perturbatively in the background. While the geometry remains AdS_4 asymptotically, the fermions deform the space-time in the interior giving rise to an IR Lifshitz fixed-point in which the dynamical exponent is inherently finite. What we have shown is that the condensation of the neutral scalar operator in the boundary theory dual to the electron star background is controlled by the IR Lifshitz fixed-point whenever the mass square of the neutral scalar field in the bulk violates the BF bound. Figure 4.1 shows explicitly that the boundary theory undergoes a quantum phase transition simply by tuning the mass square of the bulk scalar field. It is the condensation of the scalar that gives rise to the new IR scale, see equation (4.43), that depends exponentially on the distance from the critical point. Consequently, the underlying $T = 0$ transition is of the BKT form. At finite temperature, we find that the phase transition is second-order and is described by mean-field exponents. Backreaction of the condensed scalar on the geometry leads to a change in the dynamical exponent across the phase transition. This is a particularly attractive feature of this theory as there are a variety of systems [141, 143] in which the condensation of a neutral field changes the dynamical exponent across the phase transition.

There are a number of immediate applications of our work. First, our model can be used to described antiferromagnetic phases in condensed matter systems with finite dynamical critical exponents. To do so, we would simply follow the analysis discussed in [58] by embedding the neutral scalar field into a triplet charged under an SU(2) gauge symmetry in the bulk; see also the discussion in [95]. This bulk SU(2) symmetry are to model the SU(2) spin symmetry in the dual boundary theory. The antiferromagnetic ordering then corresponds to the spontaneous breaking of the SU(2) spin symmetry to U(1) in the low energy limit. To holographically model the transition to the antiferromagnetic phase, where there is a staggered spin order parameter with zero spin density, we introduce in the bulk an SU(2) gauge field A^a_M along with a triplet ϕ^a charged under the SU(2) gauge group. Here, $a = 1, 2, 3$. (Note that ϕ^a is neutral under the U(1) gauge group.) A^a_M is dual to the spin density in the boundary theory which will be set to zero, while ϕ^a is dual to the staggered order parameter. By embedding the neutral scalar field ϕ into ϕ^a, we can explicitly break the SU(2) spin symmetry when the mass of the scalar field falls below the BF bound of the far-interior Lifshitz region. Further, by studying perturbations around the symmetry breaking solution, one can find that there are two gapless Goldstone mode with linear dispersion relations. The argument presented in [58] is independent of the form of metric and can be applied to electron star solution also.

Second, we could also model nematic order. As mentioned in the introduction, nematic order [124] is an instance of a neutral tensor condensate. The order parameter for a nematic phase is a traceless symmetric

second-rank tensor. Indeed, one way for holographically constructing such a phase would be similar to the holographic setups studied in [121, 149, 150] for d-wave superconductivity, except that the order parameter here is neutral. Thus, one introduces a massive neutral traceless symmetric rank-two tensor field in the bulk. A rotation in the (x, y)-plane can be used to set one component of the tensor field equal to zero. The equation of motion for the remaining component, after a field redefinition, will be identical to the equation of motion for a neutral scalar field. So, the analysis for the condensation of the dual tensor operator in the boundary theory is essentially mapped to the analysis for the condensation of a neutral scalar operator that we presented in this Chapter. It would be interesting to see the Pomeranchuk instability [86**?**] in this holographic setup as the quantum critical point is approached. Of course, this would require coupling the tensor field to a fermion. One should look at our heuristic description of a holographic quadrupolar nematic phase from an effective field theory point of view, mainly because, as of now, there is no consistent action describing the dynamics of a massive spin-two field which would be causal and free of ghost in a space-time which is not Einstein; see [61, 150] for more discussions.

Third, there are numerous examples in condensed matter as well as particle physics (most notably in QCD) in which several ordering tendencies compete. In the instances in which competing order involves neutral condensates in metallic systems, the holographic method used here can be tailored to capture the relevant physics. The $\mathbb{Z}_2$ symmetry in the case of a single neutral scalar field can easily be enlarged by including more scalar fields in the action (4.19) and then choosing the interactions to be invariant under the desired symmetry. Depending on which dual operators condense, a variety of interesting symmetry breaking patterns could be potentially realized in the boundary theory.

Finally, another extension would be the inclusion of probe fermions coupled to the neutral scalar field. For the RN-AdS$_4$ background, fermion correlators in the dual boundary theory have been studied extensively; see, for example, [48, 60, 93–95, 105, 111, 117–122, 151–154]. A similar kind of analysis can be done here for the electron star background. In fact, the results on the electron star background would in principle be more relevant to condensed matter systems because the IR theory is controlled by a Lifshitz fixed-point and moreover, the entropy density of the system goes to zero at zero temperature. While some work along these lines has been initiated in [155], probe fermions which couple to an order parameter, either charged or neutral, have not been included. Including such couplings could give rise to a non-trivial dispersion for the fermions around the Fermi surface. One interesting effect that could be studied in this approach is whether or not a neutral condensate with a non-trivial momentum structure could, upon coupling to the probe fermions, give rise to a Fermi arc structure indicative of the pseudogap phase of the cuprates. This is particularly appealing since most models [156] of the pseudogap involve some type of neutral order parameter. Recent

holographic constructions [121, 122] of Fermi arcs are not particularly relevant to the pseudogap phase of the cuprates because in these construction the existence of the Fermi arcs are due to the coupling between the probe fermion and a charged superconducting order parameter.

Chapter 5

Pomeranchuk Instability in a non-Fermi Liquid from Holography

The Pomeranchuk instability, in which an isotropic Fermi surface distorts and becomes anisotropic due to strong interactions, is a possible mechanism for the growing number of experimental systems which display transport properties that differ along the x and y axes. We show here that the gauge-gravity duality can be used to describe such an instability in fermionic systems. Our holographic model consists of fermions in a background which describes the causal propagation of a massive neutral spin-two field in an asymptotically AdS spacetime. The Fermi surfaces in the boundary theory distort spontaneously and become anisotropic once the neutral massive spin-two field develops a normalizable mode in the bulk. Analysis of the fermionic correlators reveals that the low-lying fermionic excitations are non-Fermi liquid-like both before and after the Fermi surface shape distortion. Further, the spectral weight along the Fermi surface is angularly dependent and can be made to vanish along certain directions.

5.1 Introduction

To a surprising extent, the electronic properties of most metals are well described by Landau Fermi liquid theory. The key building blocks of this theory are quasi-particles and a Fermi surface, the surface in momentum space that demarcates filled from empty states. For a system of weakly interacting electrons, the shape of the Fermi surface is isotropic. On the other hand, if the interactions among the quasi-particles are strong enough, other possibilities might emerge. Pomeranchuk [86] showed that forward scattering among quasi-particles with non-trivial angular momentum and spin structure can lead to an instability of the ground state towards forming an anisotropic Fermi surface. For example, the simplest form of a two-dimensional nematic Fermi liquid can be thought of, in the continuum limit, as a realization of the Pomeranchuk instability in the angular momentum $l = 2$ and spin $s = 0$ particle-hole channel whereby a circular Fermi surface spontaneously distorts and becomes elliptical with a symmetry of a quadrupole (d-wave). Such an instability, depicted in Figure 5.1(a), is often referred to in the literature as the quadrupolar Pomeranchuk instability[1].

[1]The instabilities in other channels, including the antisymmetric spin channel, are also interesting. (Note that there is no Pomeranchuk instability in the $l = 1$, $s = 0$ channel.) In this Chapter, however, we only focus on the quadrupolar Pomeranchuk

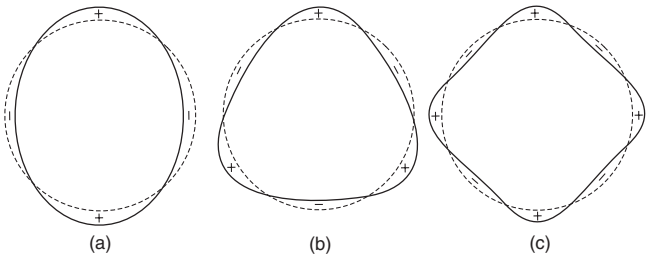

Figure 5.1: (a) Examples of the Pomeranchuk instability in (a) $l = 2$, (b) $l = 3$ and (c) $l = 4$ channels. The + and − signs on the anisotropic Fermi surfaces show the momentum gain and loss compared to the isotropic Fermi surfaces (which are shown above by the dashed lines).

In practice, however, the instability breaks the discrete point group symmetry of the underlying lattice. As such, systems undergoing a Pomeranchuk instability exhibit manifestly distinct transport properties along the different crystal axes. Experimentally several instances of anisotropic transport in strongly correlated electronic systems have been reported [157–160] and occupy much of the current focus in correlated electron matter. Although it is unclear at present whether the Pomeranchuk mechanism is the only root cause[2], it nevertheless offers a framework where such anisotropies can be characterized in detail. So far, much of the work in this direction has focused on reaching the nematic phases of correlated electron matter, via the Pomeranchuk instability, in a weakly interacting Fermi fluid [162, 163]. A natural question to ask is whether a nematic phase could be approached, via a Pomeranchuk instability, from a non-Fermi liquid phase. To answer the question, one has to address the origin of the Pomeranchuk instability beyond the Fermi liquid framework. Unlike Fermi liquids, there is no notion of stable quasi-particles in non-Fermi liquids. Nevertheless, non-Fermi liquids have sharp Fermi surfaces. Consequently, a Pomeranchuk instability, viewed simply as a spontaneous shape distortion of the underlying Fermi surface, is still a theoretical possibility.

We explore here how such an instability can be studied using the gauge-gravity duality, hereafter referred to as holography. The duality, which maps certain d-dimensional strongly coupled quantum field theories to $(d+1)$-dimensional semiclassical gravitational theories in asymptotically AdS spacetimes, is a promising tool in modeling some features of strongly correlated condensed matter systems. For reviews on the applications of holography for condensed matter physics, see [50–52, 90–92, 164]. We take the system to be $d = 2 + 1$ dimensional, as this is the most interesting case experimentally [157–160]. Also, we consider the case where the broken phase is a nematic (non-)Fermi liquid with the symmetry of a quadrupole. In other words, we only explore the possibility of a quadrupolar Pomeranchuk instability. Such an instability is characterized by an order parameter which is a neutral symmetric traceless tensor $\mathcal{O}_{ij}$ where i and j denote spatial indices. Thus, in order to use holography to realize the transition to such a phase in the boundary theory, one has to

instability and the resulting nematic phase.

[2]Nematic phases could also be obtained by the melting of stripe phases; see [124, 161] and references therein.

turn on a neutral massive spin-two field $\varphi_{\mu\nu}$ in the bulk and show that, under some circumstances, it develops a non-trivial normalizable profile in the bulk radial direction. From the point of view of the physics in the bulk, there is a serious hurdle that one needs to overcome in order to successfully describe the propagation of a massive spin-two field, which has to do with the existence of extra unwanted degrees of freedom (ghosts) and superluminal modes. Eliminating ghosts and superluminal modes within a theory that also allows for the condensation of the operator dual to the massive spin-two field is the first step. In addition, a coupling of the correct type must be introduced in the bulk between the massive spin-two field and the fermions in order to bring about the shape distortion of the Fermi surface in the boundary. We present here a minimal model which can address each of these problem, and show that the isotropic Fermi surface of the boundary non-Fermi liquid gets spontaneously distorted and becomes elliptical. We also find that the broken (nematic) phase is a non-Fermi liquid. We interpret this transition as a holographic realization of the quadrupolar Pomeranchuk instability in non-Fermi liquids.

The outline of this Chapter is as follows. Section II sets up the Lagrangian for the neutral massive spin-two field. Included here will be an explicit mechanism for obtaining a normalizable profile for the bulk spin-two field. Section III contains the fermonic degrees of freedom as well as the results illustrating that the low-lying excitations are non-Fermi liquid in nature as well as the shape distortion of the underlying Fermi surface.

5.2 Background

Since we want to explore the possibility of a transition from a non-Fermi liquid to a nematic Fermi liquid phase in the boundary, the first step is to construct a background which consistently incorporates a neutral massive spin-two field $\varphi_{\mu\nu}$. This field is dual to the operator whose vacuum expectation value (vev) is the order parameter for the nematic phase.

5.2.1 BGP Lagrangian

In flat $(d+1)$-dimensional Minkowski spacetime, Fierz and Pauli suggested [165] a Lagrangian for a free neutral massive spin-two field which is quadratic in derivatives and correctly describes the propagating degrees of freedom for such a field. Generalizing to curved spacetimes, Buchbinder, Gitman and Pershin (BGP)[61], following [166], proposed a simple Lagrangian (quadratic in the massive spin-two field, and also quadratic in derivatives) which describes the causal propagation of the correct number of degrees of freedom of a neutral massive spin-two field in a fixed Einstein background in arbitrary dimensions. In four bulk

dimensions, their Lagrangian for $\varphi_{\mu\nu}$, denoted by $\mathcal{L}_{\rm BGP}$, reads

$$\begin{aligned}\frac{\mathcal{L}_{\rm BGP}}{\sqrt{-g}} = \frac{1}{4}\Big\{ &- \nabla_\mu\varphi_{\nu\rho}\nabla^\mu\varphi^{\nu\rho} + \nabla_\mu\varphi\nabla^\mu\varphi \\ &+ 2\nabla_\mu\varphi_{\nu\rho}\nabla^\rho\varphi^{\nu\mu} - 2\nabla^\mu\varphi_{\mu\nu}\nabla^\nu\varphi \\ &- m^2\big(\varphi_{\mu\nu}\varphi^{\mu\nu} - \varphi^2\big) + \frac{R}{2}\,\varphi_{\mu\nu}\varphi^{\mu\nu} - \frac{R}{4}\,\varphi^2\Big\}.\end{aligned} \tag{5.1}$$

Here R is the Ricci scalar. Also, we have defined $\varphi = \varphi^\mu_\mu$. Several comments are warranted here. First, it is crucial that the fixed background satisfies the Einstein relation (which, in four bulk dimensions, reads) $R_{\mu\nu} = \Lambda g_{\mu\nu}$, with Λ being the cosmological constant, otherwise some constraint equations become dynamical which would give rise to extra propagating degrees of freedom for $\varphi_{\mu\nu}$. In our context this restriction simply implies that one should ignore the backreaction of $\varphi_{\mu\nu}$, as well as other bulk fields that will be introduced later, on the metric of the fixed Einstein background. Second, in the flat spacetime limit, the above Lagrangian becomes the Fierz-Pauli Lagrangian [165]. Third, the massless limit of the BGP Lagrangian, *i.e.* $m^2 = 0$, has an emergent gauge symmetry (diffeomorphism) which is unique to the graviton: $\varphi_{\mu\nu} \to \varphi_{\mu\nu} + \nabla_{(\mu}\xi_{\nu)}$ with ξ_μ being an infinitesimal vector. Indeed, as pointed out in [61], this symmetry has been used to settle the ambiguity associated with the definition of the mass of $\varphi_{\mu\nu}$. Fourth, for $m^2 = R/6$ (here $d+1 = 4$) the above Lagrangian has another emergent gauge symmetry [167]: $\varphi_{\mu\nu} \to \varphi_{\mu\nu} + (\nabla_\mu\nabla_\nu + g_{\mu\nu}R/12)\epsilon$ with ϵ being an infinitesimal scalar gauge parameter. In the following, we always assume that $m^2 \neq 0$ and $m^2 \neq R/6$. Excluding these two special values for the mass, the equations of motion and constraints obtained from (5.1) are given by [61]

$$0 = \big(\nabla^2 - m^2\big)\,\varphi_{\mu\nu} + 2R^\rho{}_\mu{}^\sigma{}_\nu\varphi_{\rho\sigma}, \tag{5.2}$$

$$0 = \nabla^\mu\varphi_{\mu\nu}, \tag{5.3}$$

$$0 = \varphi, \tag{5.4}$$

$$0 = \dot{\varphi}, \tag{5.5}$$

$$\begin{aligned}0 =& g^{00}\nabla_0\nabla_i\varphi^i_\nu - g^{0i}\nabla_0\nabla_i\varphi^0_\nu - g^{0i}\nabla_i\nabla_0\varphi^0_\nu \\ &- g^{ij}\nabla_i\nabla_j\varphi^0_\nu - 2R^{\rho\,0\,\sigma}{}_\nu\,\varphi_{\rho\sigma} + m^2\varphi^0_\nu.\end{aligned} \tag{5.6}$$

The above expressions give the correct number of propagating degrees of freedom for a massive spin-two field in (3+1)-dimensions. Such a field transforms in the five-dimensional irreducible representation of SO(3), with SO(3) being the little group of the Lorentz group SO(3,1).

As we alluded to earlier, in order to satisfy the constraint $R_{\mu\nu} = \Lambda g_{\mu\nu}$, we will work in a regime where

matter fields do not backreact on the bulk geometry. So, we take the Schwarzschild AdS_4 black hole as our background geometry ($\Lambda = -3$)

$$\begin{aligned} ds^2 &= g_{\mu\nu} dx^\mu dx^\nu \\ &= r^2 \left(-f(r)\, dt^2 + dx^2 + dy^2\right) + \frac{dr^2}{r^2 f(r)}, \end{aligned} \tag{5.7}$$

where $f(r) = 1 - (r_0^3/r^3)$ with r_0 being the horizon radius, given by the largest real root of $f(r_0) = 0$. Note that we are working in units where we set the curvature radius L of AdS_4 equal to unity. Also, note that in the coordinates we have chosen above, the asymptotic boundary of the spacetime is at $r \to \infty$. The temperature of the black hole is given by $T = 3r_0/(4\pi)$.

To solve for $\varphi_{\mu\nu}$, we only consider the configuration where $\varphi_{\mu\nu} = \varphi_{\mu\nu}(r)$ for all $\mu, \nu \in \{t, r, x, y\}$. Analyzing the equations (5.2)–(5.6), one can show [121, 150] that it is consistent to put $\varphi_{\mu\nu}(r)$ in the form

$$\varphi_{\mu\nu}(r) = \begin{pmatrix} \mathbf{0} & \mathbf{0} \\ \mathbf{0} & \varphi_{ij}(r) \end{pmatrix}, \tag{5.8}$$

where $\varphi_{ij}(r)$, with $i, j = x, y$, is a symmetric traceless two-by-two matrix. Defining the "director" $\vec{\varphi}(r) = \varphi_{xx}(r) + i\varphi_{xy}(r)$, under a rotation θ in the (x,y)-plane, $\vec{\varphi}(r)$ transforms as

$$\vec{\varphi}(r) \to e^{2i\theta} \vec{\varphi}(r). \tag{5.9}$$

One can then choose a particular value of θ to set either $\varphi_{xx}(r)$ or $\varphi_{xy}(r)$ equal to zero, or make them equal.

Suppose now there exists a (2+1)-dimensional field theory dual to the gravitational setup under consideration here. Focusing for the moment on the bulk neutral massive spin-two field $\varphi_{\mu\nu}$, holography tells us that it should be dual to some operator in the boundary theory. Since $\varphi_{\mu\nu}$ is a bulk field with spin greater than zero, its number of components does not naively match the number of components of the dual operator. But, as explained in [150], since $\varphi_{\mu\nu}$ can be put in the form (5.8), it is φ_{ij} which sources a neutral symmetric traceless operator $\mathcal{O}_{ij}$ in the boundary theory. (The vev of the operator $\mathcal{O}_{ij}$ determines the nematicity of the (2+1)-dimensional boundary theory.) More concretely, equation (5.2) implies that $\varphi_{ij}(r)$ takes the following form near the boundary as $r \to \infty$

$$\varphi_{ij}(r) = A_{ij}\, r^{\Delta - 1}\big(1 + \cdots\big) + B_{ij}\, r^{2-\Delta}\big(1 + \cdots\big), \tag{5.10}$$

with A_{ij} and B_{ij} being symmetric traceless tensors. A_{ij} is the source for the boundary theory operator $\mathcal{O}_{ij}$ while B_{ij} is proportional to its vev, $\langle \mathcal{O}_{ij} \rangle$. In (5.10), Δ denotes the UV scaling dimension of $\mathcal{O}_{ij}$, which is related to the mass of the bulk field $\varphi_{\mu\nu}$ via

$$\Delta = \frac{3}{2} + \sqrt{\frac{9}{4} + m^2}. \tag{5.11}$$

Note that for $m = 0$, *i.e.* when $\varphi_{\mu\nu}$ is the graviton, equation (5.11) yields $\Delta = 3$ which is the dimension of $T_{\mu\nu}$, the energy-momentum tensor operator, of the (2+1)-dimensional boundary theory. There is a Breitenlohner-Freedman bound [57] for the propagation of $\varphi_{\mu\nu}$ in an asymptotically AdS_4 geometry which reads $m^2 \geq 0$ [150, 168, 169]. Equation (5.11) then implies that $\Delta \geq 3$. In our discussions in this Chapter, we will always take the mass squared of $\varphi_{\mu\nu}$ in the asymptotic AdS_4 region of the geometry to satisfy the condition $m^2 > 0$. Note that the condition $m^2 \neq R/6 = -2$ is then trivially satisfied.

Given the ansatz (5.8), we are interested in solutions in which $\varphi_{\mu\nu}(r)$, or rather $\varphi_{ij}(r)$, is regular near the horizon and normalizable as $r \to \infty$. More concretely, near the horizon, we look for a solution of the equation (5.2) which is regular as $r \to r_0$, namely

$$\varphi_{ij}(r) = a_{ij} + b_{ij}(r - r_0) + c_{ij}(r - r_0)^2 + \cdots , \tag{5.12}$$

where the coefficient tensors b_{ij}, c_{ij}, $\cdots$ are all determined in terms of a_{ij}. In the boundary as $r \to \infty$, we demand $\varphi_{ij}(r)$ to be normalizable

$$\varphi_{ij}(r) = B_{ij}\, r^{2-\Delta}\big(1 + \cdots\big). \tag{5.13}$$

If a solution with the above two boundary conditions exists, then the boundary theory would be in a phase where the neutral symmetric traceless operator $\mathcal{O}_{ij}$ (which is the operator dual to φ_{ij}) spontaneously condenses. It is easy to show that given the set of equations (5.2)–(5.6), such a solution does not exist. As we will explain in the next section, one way forward is to minimally modify the BGP Lagrangian (5.1) such that the new action yields the correct number of causal propagating degrees of freedom for $\varphi_{\mu\nu}$, and also permits the aforementioned spontaneous condensation to occur.

5.2.2 Modifying the BGP Lagrangian

Undoubtedly, there are many ways to modify the BGP Lagrangian to facilitate spontaneous condensation of the operator dual to $\varphi_{\mu\nu}$. Instead of categorizing all such modifications, we take perhaps the simplest

possibility. Gubser [59] has shown that coupling a neutral scalar field to the square of the Weyl tensor leads to a scalar hair on an asymptotically flat Schwarzschild black hole. This coupling is of interest here because the square of the Weyl tensor vanishes at the boundary ($r \to \infty$) and hence does not affect the scaling dimension of the dual boundary operator. To this end, we modify the BGP Lagrangian (5.1) as follows

$$\mathcal{L}_\varphi = \mathcal{L}_{\rm BGP} + \frac{\ell^2}{4}\sqrt{-g}\, C_{\mu\nu\rho\sigma}C^{\mu\nu\rho\sigma}\left(\varphi_{\gamma\delta}\varphi^{\gamma\delta} - \varphi^2\right), \tag{5.14}$$

with $C_{\mu\nu\rho\sigma}$ the Weyl tensor. In the below, we show that the above modification to the BGP Lagrangian, though not unique, offers a valid description of the neutral massive spin-two field $\varphi_{\mu\nu}$, meaning that $\varphi_{\mu\nu}$ still propagates causally in a fixed Einstein spacetime with the correct number of degrees of freedom. In what follows, we show that the equations of motion for $\varphi_{\mu\nu}$ obtained from the new Lagrangian now admits non-trivial normalizable solutions (whose near horizon and asymptotic boundary behaviors are given by (5.12) and (5.13), respectively).

5.2.3 Einstein spacetime

In this subsection, we demonstrate that adding a coupling of the form $\ell^2 C_{\gamma\delta\rho\sigma}C^{\gamma\delta\rho\sigma}(\varphi_{\mu\nu}\varphi^{\mu\nu} - \varphi^2)$ to the BGP Lagrangian, given that the background spacetime is an Einstein manifold, does not induce any extra degrees of freedom for the neutral massive spin-two field $\varphi_{\mu\nu}$ nor violate its causal propagation. Our discussion below closely follows that of [61], where it has been shown that neutral massive spin-two field in an Einstein spacetime, such as the AdS_{d+1} Schwarzschild black hole, has the correct number of degrees of freedom and propagates causally. In our discussion below, we keep the number of dimensions of the bulk spacetime (denoted by $d+1$) arbitrary.

Consider the following Lagrangian [166]

$$\begin{aligned}\mathcal{L} = \frac{1}{4}\Big\{ &- \nabla_\mu\varphi_{\nu\rho}\nabla^\mu\varphi^{\nu\rho} + \nabla_\mu\varphi\nabla^\mu\varphi - 2\nabla^\mu\varphi_{\mu\nu}\nabla^\nu\varphi \\ &+ 2\nabla_\mu\varphi_{\nu\rho}\nabla^\rho\varphi^{\nu\mu} - m_0^2(\varphi_{\mu\nu}\varphi^{\mu\nu} - \varphi^2) \\ &+ 2a_1 R\,\varphi_{\mu\nu}\varphi^{\mu\nu} + 2a_2 R\,\varphi^2 + 2a_3 R^{\mu\lambda\nu\rho}\varphi_{\mu\nu}\varphi_{\lambda\rho} \\ &+ 2a_4 R^{\mu\nu}\varphi_{\mu\lambda}\varphi^\lambda_\nu + 2a_5 R^{\mu\nu}\varphi_{\mu\nu}\varphi\Big\},\end{aligned} \tag{5.15}$$

where $\varphi = \varphi^\mu_\mu$. The above Lagrangian is the most general two-derivative action for a neutral massive spin-two field $\varphi_{\mu\nu}$ (up to the quadratic order in $\varphi_{\mu\nu}$, though) in a curved background. The coefficients in the first two rows of (5.15) are fixed because in the flat spacetime limit, one demands the Lagrangian to go over to the

Fierz-Pauli Lagrangian [165], which is known to have the correct number of causally-propagating degrees of freedom for a neutral massive spin-two field. Indeed, in order for a massive spin-two field (represented by a symmetric tensor $\varphi_{\mu\nu}$) to have the correct number of propagating degrees of freedom in a $(d+1)$-dimensional spacetime, one needs $2(d+2)$ constraint equations to kill the extra degrees of freedom.

Now, add to the above Lagrangian an additional coupling of the form $\ell^2 C^2(\varphi_{\mu\nu}\varphi^{\mu\nu} - \varphi^2)$ and define the Lagrangian

$$\mathcal{L}_\varphi = \mathcal{L} + \frac{1}{4}\ell^2 C^2 \left[\varphi_{\mu\nu}\varphi^{\mu\nu} - \varphi^2\right], \tag{5.16}$$

where, in order to make the expressions less cluttered, we defined $C^2 = C_{\gamma\delta\rho\sigma}C^{\gamma\delta\rho\sigma}$. For $\ell = 0$, the analysis has been performed in [61], where, in order to get rid of the extra degrees of freedom of $\varphi_{\mu\nu}$, one obtains a one-parameter family of solutions for the coefficients $a_1, \cdots, a_5$ (labeled by an arbitrary real parameter ξ) which can be represented as

$$a_1 = \frac{\xi}{d+1}, \quad a_2 = \frac{1-2\xi}{2d+2}, \quad a_3 = a_4 = a_5 = 0, \tag{5.17}$$

provided that the background metric $g_{\mu\nu}$ satisfies the Einstein relation $R_{\mu\nu} = 2\Lambda g_{\mu\nu}/(d-1)$, and $m_0^2 \neq 2(\xi-1)/(d+1)$. Defining $m^2 = m_0^2 + 2(1-\xi)R/(d+1)$ and given the above solution for a_i's, the Lagrangian (5.15) takes the form given in the expression (5.1), the so-called BGP Lagrangian.

For $\ell \neq 0$, one can easily obtain the constraint equations following [61]. Basically, constraints come from the equations of motion and their derivatives which do not contain two time derivatives of spin-two field $\ddot{\varphi}_{\mu\nu}$. The equations of motion read

$$\tilde{E}_{\mu\nu} = E_{\mu\nu} + \ell^2 C^2 \left(\varphi_{\mu\nu} - g_{\mu\nu}\varphi\right) = 0, \tag{5.18}$$

where $E_{\mu\nu}$ denotes the equations of motion for the $\ell = 0$ case. The explicit form of $E_{\mu\nu}$ is given in [61]. Since $E_{\mu 0}$ does not involve second time-derivatives of $\varphi_{\mu\nu}$, and obviously the new term in (5.18) does not involve any second time-derivative of $\varphi_{\mu\nu}$ either, the equations $\tilde{E}_{\mu 0} = 0$ actually give us $d+1$ (primary) constraints.

In order to obtain the secondary constraints, we take the covariant derivative of the equations of motion

$$\nabla^\mu \tilde{E}_{\mu\nu} = 0. \tag{5.19}$$

Again, neither $\nabla^\mu E_{\mu\nu}$ nor $\nabla^\mu \left[C^2(\varphi_{\mu\nu}\varphi^{\mu\nu} - \varphi^2)\right]$ involves two time-derivatives of the spin-two field. Thus, the equations (5.19) give us $d+1$ secondary constraints. Following [61], the equations (5.19) should contain $\dot{\varphi}_{\mu 0}$ through a rank d matrix in order for their derivatives to define d accelerations $\ddot{\varphi}_{i0}$:

$$\begin{aligned} E_{\mu 0,}{}^{\mu} &= \mathcal{A}\,\dot{\varphi_{00}} + \mathcal{B}^j \dot{\varphi_{j0}} + \cdots , \\ E_{\mu i,}{}^{\mu} &= \mathcal{C}_i\,\dot{\varphi_{00}} + \mathcal{D}_i^j \dot{\varphi_{j0}} + \cdots , \\ \operatorname{rank} \hat{\Phi}_\mu^\nu &\equiv \operatorname{rank} \begin{Vmatrix} \mathcal{A} & \mathcal{B}^j \\ \mathcal{C}_i & \mathcal{D}_i^j \end{Vmatrix} = d. \end{aligned} \tag{5.20}$$

The explicit form for $\hat{\Phi}_\mu^\nu$ when $\ell = 0$ appears in [61]. The additional non-vanishing contributions to $\mathcal{A}$, $\mathcal{B}^j$, $\mathcal{C}_i$ and $\mathcal{D}_j^i$ are given by

$$\delta\mathcal{B}^j = -\ell^2 C^2 g^{j0}, \qquad \delta\mathcal{D}_j^i = \ell^2 C^2 g^{00}\delta_j^i. \tag{5.21}$$

Hence, in order for the rank of $\hat{\Phi}_\mu^\nu$ to be d, we require $m_0^2 - \ell^2 C^2 + 2(1-\xi)R/(d+1) \neq 0$, where ξ is arbitary parameter. We now have $2d+2$ constraints.

One of the remaining constraints can be obtained from a linear combination of the equations of motion and the primary and secondary constraints:

$$\begin{aligned} &\frac{m_0^2 - \ell^2 C^2}{d-1}\tilde{E}_\mu^\mu + \nabla^\mu\nabla^\nu \tilde{E}_{\mu\nu} + \frac{2(1-\xi)}{(d+1)(d-1)} R\tilde{E}_\mu^\mu \\ &= \frac{\varphi}{d-1}\left[\frac{2(1-\xi)}{d+1}R + m_0^2 - \ell^2 C^2\right] \\ &\times \left[\frac{d+1-2\xi d}{d+1}R + (m_0^2 - \ell^2 C^2)d\right] \\ &+ 2\ell^2(\nabla^\nu C^2)(\nabla^\mu\varphi_{\mu\nu} - \nabla_\nu\varphi) \\ &+ \ell^2(\nabla^\mu\nabla^\nu C^2)(\varphi_{\mu\nu} - g_{\mu\nu}\varphi) \approx 0. \end{aligned} \tag{5.22}$$

This equation can be used as a constraint since it does not contain $\ddot{\varphi}_{\mu\nu}$. It contains $\dot{\varphi}_{\mu\nu}$ which can be removed by the equations $\nabla^\mu\tilde{E}_{\mu\nu} = 0$. After such a removal, the time-derivative of (5.22) does not contain $\ddot{\varphi}_{\mu\nu}$ and can be used as the last constraint. We then have in total $2d+4$ constraints and hence the correct number of propagating degrees of freedom.

Following the discussion in [61], it can be seen easily that the characteristic matrix remains unchanged for $\ell \neq 0$, due to the fact that the Weyl squared coupling does not affect any of the terms with two time-derivatives. So, the equations remain hyperbolic and causal even for the $\ell \neq 0$ case. The resulting equations

of motion are

$$\left(\nabla^2 - m^2 + \ell^2 C^2\right)\varphi_{\mu\nu} + 2R^{\rho}{}_{\mu}{}^{\sigma}{}_{\nu}\varphi_{\rho\sigma} = 0. \tag{5.23}$$

where, as we have defined before, $m^2 = m_0^2 + 2(1-\xi)R/(d+1)$.

5.2.4 Normalizable Solution

From the previous section, the relevant equation for determining whether there exists a normalizable solution for $\varphi_{\mu\nu}$ is

$$\left(\nabla^2 - m^2 + \ell^2 C_{\gamma\delta\rho\sigma}C^{\gamma\delta\rho\sigma}\right)\varphi_{\mu\nu} + 2R^{\rho}{}_{\mu}{}^{\sigma}{}_{\nu}\varphi_{\rho\sigma} = 0. \tag{5.24}$$

Note that the background metric must again satisfy the Einstein relation. Since we have taken the spacetime to be the Schwarzschild AdS_4 black hole, the square of the Weyl tensor is $C_{\mu\nu\rho\sigma}C^{\mu\nu\rho\sigma} = 12(r_0/r)^6$. One can easily show that, given the constraints presented in the previous section and the equation (5.24), it is again consistent to put $\varphi_{\mu\nu}$ in the form given in (5.8). Notice that as shown above, the square of the Weyl tensor evaluated on the background vanishes as $r \to \infty$. This then implies that the relationship between the asymptotic mass m of φ_{ij} and the UV dimension Δ of the dual operator $\mathcal{O}_{ij}$ is still given by (5.11). Also, the mass of φ_{ij} in the asymptotic AdS_4 region satisfies the same Breitenlohner-Freedman bound as before. Thus, regardless of the value of the coupling ℓ^2, the asymptotic AdS_4 region of the background remains stable.

As Figure 5.2 illustrates, there exists a normalizable solution with $A_{ij} = 0$ and $B_{ij} \neq 0$. (We have used the gauge in (5.9) to set $\varphi_{xx} = \varphi_{xy}$.) The holographic interpretation of this normalizable solution is that $\mathcal{O}_{ij}$ has spontaneously condensed in the boundary theory. While it may be possible to obtain a normalizable solution for $\varphi_{\mu\nu}$ using an alternative mechanism, we believe that the details of how the dual operator condenses in the boundary theory should be irrelevant to the Pomeranchuk instability as we discuss in the next section.

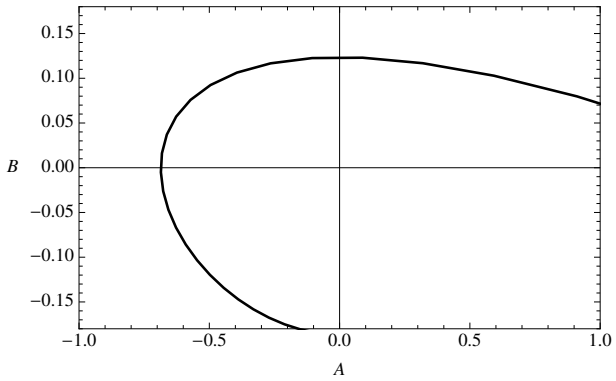

Figure 5.2: A plot of B_{ij} verse A_{ij} for $\ell^2 = 1.0866$ and $m^2 = 1/100$. The values of B_{ij} and A_{ij} have been rescaled so that they are dimensionless. The gauge in (5.9) has been used to set $\varphi_{xx} = \varphi_{xy}$.

5.2.5 Maxwell's Lagrangian

Since we will be considering the boundary theory at a finite chemical potential μ for a U(1) charge, we need to introduce in the bulk an Abelian gauge field A_μ with the Lagrangian

$$\mathcal{L}_{\rm M} = -\frac{1}{4}\sqrt{-g}\, F_{\mu\nu}F^{\mu\nu}. \tag{5.25}$$

The equations of motion for A_μ is then

$$\nabla^\mu F_{\mu\nu} = 0. \tag{5.26}$$

We will only be interested in the case where A_t is non-zero and, moreover, depends only on the radial coordinate r. So, we take the ansatz $A_\mu = A_t(r)\delta_{\mu 0}$. Given our assumption that A_μ does not back react on the metric (5.7), the solution to (5.26) is easily obtained to be

$$A = \mu\Big(1 - \frac{r_0}{r}\Big)dt, \tag{5.27}$$

where the boundary conditions at the horizon and the asymptotic boundary have been fixed by demanding $A_t(r_0) = 0$ and $A_t(r \to \infty) = \mu$.

5.3 Fermions

In this section, we study the shape distortion of the Fermi surface as a result of the condensation of the boundary theory operator $\mathcal{O}_{ij}$. We start by introducing a bulk spinor field ψ with mass m_ψ and charge q which is dual to a boundary theory fermionic operator $\mathcal{O}_\psi$ with a UV scaling dimension Δ_ψ and charge q.

Note that the bulk spinor ψ is a four-component Dirac spinor while the dual operator $\mathcal{O}_\psi$ is a two-component Dirac spinor. In this Chapter, we take $m_\psi \in [0, \frac{1}{2})$ and choose the so-called "conventional quantization" where the scaling dimension of the fermionic operator is related to the mass of the bulk spinor field through $\Delta_\psi = \frac{3}{2} + m_\psi$.

5.3.1 Fermion Lagrangian and Equation of Motion

In our discussions below, the bulk spinor field ψ is treated as a probe where its backreaction on the background metric, gauge field and neutral massive spin-two field is ignored. The Dirac Lagrangian,

$$\mathcal{L}_{\text{Dirac}} = -\sqrt{-g}\, i\bar{\psi}(\not{D} - m)\psi, \tag{5.28}$$

describes the bulk spinor field, where $\bar{\psi} = \psi^\dagger \Gamma^{\underline{t}}$ and $\not{D} = e_c^\mu \Gamma^c \left(\partial_\mu + \frac{1}{4}\omega_\mu{}^{ab}\Gamma_{ab} - iqA_\mu\right)$ and e_a^μ and $\omega_\mu{}^{ab}$ being respectively the vielbein and the spin connection. Also, $a, b, \cdots = \{\underline{t}, \underline{x}, \underline{y}, \underline{r}\}$ denote the tangent space indices, $\Gamma^{\underline{t}}, \Gamma^{\underline{x}}, \Gamma^{\underline{y}}, \Gamma^{\underline{r}}$ are the Dirac matrices satisfying the Clifford algebra $\{\Gamma^a, \Gamma^b\} = 2\eta^{ab}$ and $\Gamma_{ab} = \frac{1}{2}[\Gamma_a, \Gamma_b]$. The overall negative sign in (5.28) ensures that the bulk action, once holographically renormalized, gives rise to a positive spectral density for the fermionic operator $\mathcal{O}_\psi$. In (5.28), $g_{\mu\nu}$ and A_μ are the background metric and the background gauge field whose expressions are given in (5.7) and (5.27), respectively.

In the probe limit that we are considering here the Dirac Lagrangian (5.28) is not capable of holographically realizing how the spectral function of the boundary theory fermionic operator $\mathcal{O}_\psi$ is affected in the presence the order parameter $\langle \mathcal{O}_{ij} \rangle$. To do so, one has to explicitly introduce bulk couplings between the spinor field ψ and the neutral massive spin-two field $\varphi_{\mu\nu}$. A similar problem arises in the context of holographic d-wave superconductivity [121, 150] although in that case one has to deal with coupling the bulk spinor to a charged massive spin-two field. Since our goal here is to capture the leading order effects on the retarded two-point function of the fermionic operator due to the presence of the order parameter, we consider those couplings in the bulk which are quadratic in the spinor field and have relatively low mass dimension. Furthermore, among the aforementioned couplings, we will only be interested in those which will potentially give rise to anisotropic features in the fermion spectral function. In other words, we ignore the terms which would just modify the mass of the spinor field. Leaving aside those terms which would vanish once evaluated on the background, we focus on the leading-order[3] non-trivial coupling (which can

[3]There is also a coupling of the form $\lambda_5\sqrt{-g}\,\varphi_{\mu\nu}\bar{\psi}\,\Gamma^5\Gamma^\mu D^\nu\psi$ that breaks parity in the boundary theory when the operator dual to $\varphi_{\mu\nu}$ condenses. We will not consider such a coupling in this Chapter as there is no clear indication that it gives rise to an anisotropy of the Fermi surface.

potentially contribute asymmetric features to the fermionic spectral function)

$$\mathcal{L}_{\rm int} = -i\lambda\sqrt{-g}\,\varphi_{\mu\nu}\bar{\psi}\,\Gamma^{\mu}D^{\nu}\psi, \tag{5.29}$$

with λ real. Thus, the bulk fermion Lagrangian that we study is $\mathcal{L}_{\psi} = \mathcal{L}_{\rm Dirac} + \mathcal{L}_{\rm int}$.

The Dirac equation following from $\mathcal{L}_{\psi}$ takes the form

$$(\not{D} - m + \lambda\varphi_{\mu\nu}\Gamma^{\mu}D^{\nu})\psi = 0. \tag{5.30}$$

To solve the above equation, we go to momentum space by Fourier transforming $\psi(r, x^{\mu}) \sim e^{ik.x}\psi(r, k^{\mu})$, where $k^{\mu} = (\omega, \vec{k})$. It is expedient to choose a basis for the Dirac matrices as follows

$$\begin{aligned}
\Gamma^{\underline{r}} &= \begin{pmatrix} -\sigma_3 & 0 \\ 0 & -\sigma_3 \end{pmatrix}, \quad \Gamma^{\underline{t}} = \begin{pmatrix} i\sigma_1 & 0 \\ 0 & i\sigma_1 \end{pmatrix}, \\
\Gamma^{\underline{x}} &= \begin{pmatrix} -\sigma_2 & 0 \\ 0 & \sigma_2 \end{pmatrix}, \quad \Gamma^{\underline{y}} = \begin{pmatrix} 0 & \sigma_2 \\ \sigma_2 & 0 \end{pmatrix}.
\end{aligned} \tag{5.31}$$

It is also convenient to remove the spin connection from the Dirac operator $\not{D}$ by rescaling ψ according to $\psi \to (-gg^{rr})^{-1/4}\psi$. Splitting the new (rescaled) spinor ψ according to $\psi^T = (\psi_1, \psi_2)$, where $\psi_1(r; \omega, \vec{k})$ and $\psi_2(r; \omega, \vec{k})$ are two-component spinors, and given the ansatz for the background form of $\varphi_{\mu\nu}$ where the only non-vanishing components are $\varphi_{xx} = -\varphi_{yy}$ and $\varphi_{xy} = \varphi_{yx}$, the equation (5.30) results in the following two coupled differential equations for ψ_1 and ψ_2

$$\left(\tilde{D}_r - i\sigma_2\sqrt{g^{xx}}\,\tilde{k}_x\right)\psi_1 + i\sigma_2\sqrt{g^{xx}}\,\tilde{k}_y\psi_2 = 0, \tag{5.32}$$

$$\left(\tilde{D}_r + i\sigma_2\sqrt{g^{xx}}\,\tilde{k}_x\right)\psi_2 + i\sigma_2\sqrt{g^{xx}}\,\tilde{k}_y\psi_1 = 0, \tag{5.33}$$

where we have defined

$$\tilde{D}_r = -\sigma_3\sqrt{g^{rr}}\,\partial_r + \sigma_1\sqrt{-g^{tt}}\,(\omega + qA_2) - m_{\psi}, \tag{5.34}$$

$$\tilde{k}_x = k_x\,(1 + \lambda g^{xx}\varphi_{xx}) + \lambda g^{xx}\varphi_{xy}k_y, \tag{5.35}$$

$$\tilde{k}_y = k_y\,(1 - \lambda g^{xx}\varphi_{xx}) + \lambda g^{xx}\varphi_{xy}k_x. \tag{5.36}$$

For $\lambda = 0$, or when $\varphi_{xx} = \varphi_{xy} = 0$, the Dirac equation (5.30) has been studied extensively in the literature

(although mainly on the Reissner-Nordström AdS_4 black hole background), following the work of [48, 60, 93, 94]. These studies show that in these cases there are symmetrical Fermi surfaces in the boundary theory whose underlying excitations can either be Fermi or non-Fermi liquid-like. On the other hand, when φ_{xx} develops a normalizable mode in the bulk, $\tilde{k}_x$ and $\tilde{k}_y$ will differ thereby giving rise to asymmetrical features in the fermionic correlators of the boundary theory. This can be shown explicitly.

To compute the retarded correlator of the boundary theory operator $\mathcal{O}_\psi$, one needs to solve the equations (5.32) and (5.33) with in-falling boundary condition at the horizon [109] and read off the source and the expectation value of $\mathcal{O}_\psi$ from the asymptotic expansion of ψ_α ($\alpha = 1, 2$) following the prescription of [110]. Indeed, choosing in-falling boundary conditions for ψ_α near the horizon, the leading-order asymptotic ($r \to \infty$) behavior of ψ_α takes the form $\psi_\alpha(r \to \infty) = (B_\alpha\, r^{-m_\psi}, A_\alpha r^{m_\psi})^T$, where the two-component spinor $A = (A_1, A_2)^T$ sources the boundary theory fermionic operator $\mathcal{O}_\psi$, while $B = (B_1, B_2)^T$ gives the vev of the operator. The spinor B is related to the spinor A through $B = \mathcal{S}A$ from which the retarded Green function of the operator $\mathcal{O}_\psi$ take the form [110]

$$G_R(\omega, \vec{k}) = -i\mathcal{S}\gamma^t. \tag{5.37}$$

Note that in our basis of gamma matrices $\gamma^t = i\sigma_1$. Up to a numerical constant, the spectral function of the operator $\mathcal{O}_\psi$ is given by $\rho(\omega, \vec{k}) = \mathrm{Tr}\,\mathrm{Im}G_R(\omega, \vec{k})$.

5.3.2 Fermi Surfaces and Low-Energy Excitations

To obtain the retarded Green function (5.37) of the fermionic operator $\mathcal{O}_\psi$, one should numerically solve the equations (5.32) and (5.33), or the flow equations obtained from them, with in-falling boundary condition at the horizon. We do this computation at finite temperature mainly because our background, in which there is a normalizable solution for the neutral massive spin-two field, is not, strictly speaking, valid at zero temperature. The Femi momentum $\vec{k}_\mathrm{F}$ appears as a pole in $\mathrm{Re}\,G_R(\omega, \vec{k})$, although at finite temperature such poles, instead of being the delta function, become broadened.

Carrying out the numerical computation, we find multiple Fermi surfaces for the parameters chosen. To demonstrate proof of concept, it is sufficient to focus on the first Fermi surface, where $|\vec{k}_\mathrm{F}|$ (measured compared to the effective chemical potential $q\mu$) has the smallest value. In generating the plots shown in this section, we first used the gauge (5.9) to set $\varphi_{xx} = \varphi_{xy}$ and then numerically solved the Dirac equations for a very small but non-zero frequency such that the delta functions at the Fermi surface are broadened.

First consider the case where the background value of $\varphi_{\mu\nu}(r)$ identically vanishes in the bulk. In other

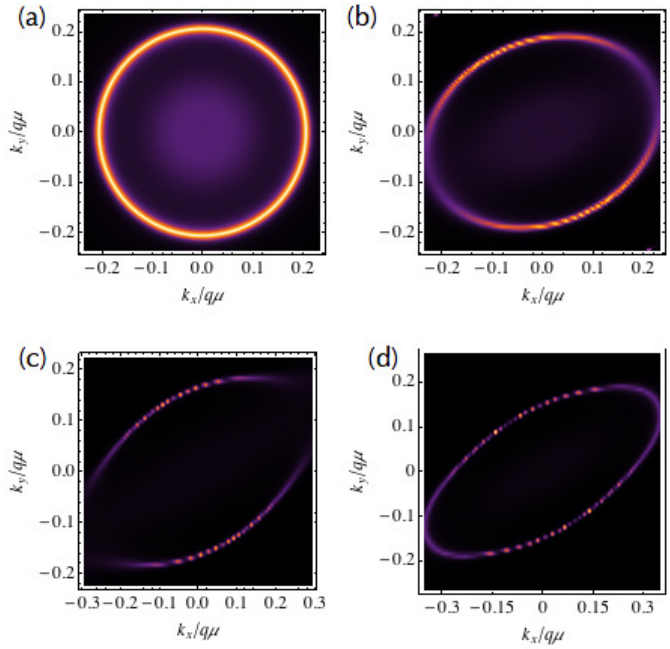

Figure 5.3: Density plots of the spectral function of the fermionic operator $\mathcal{O}_\psi$ in the boundary field theory. a) Spectral density when the boundary field theory is in the unbroken phase b) Spectral density in the broken phase showing an elliptic Fermi surface where we set $\lambda = -0.4$, c) spectral density in the broken phase where $\lambda = -0.95$ showing a suppression of the spectral weight and d) spectral density, also in the broken phase, when $\lambda = -1.4$.

words the boundary theory is in the symmetry-unbroken phase $\langle \mathcal{O}_{ij} \rangle = 0$. Not surprisingly, the Fermi surface obtained in this phase is isotropic, as is evident from Figure 5.3(a). To investigate the nature of the excitations, we computed the quasiparticle dispersion relation by focusing on the peak in the spectral function. In a Fermi liquid, $\omega(k) = k_\perp^z$ with $k_\perp = k - k_{\rm F}$ and $z = 1$. Figure 5.4 (see open circles) reveals that in the unbroken phase of the boundary theory where the Fermi surface is circular, the dynamical exponent $z = 0.64$ which indicates that the low-lying excitations form a non-Fermi liquid. Importantly then, any subsequent breaking of rotational symmetry of the Fermi surface will be from a non-Fermi liquid state, one of the key hurdles in describing the strong correlations in the experimental systems.

Focusing now on the interesting phase where the neutral symmetric traceless operator $\mathcal{O}_{ij}$ has spontaneously condensed, we find three significant features in the spectral function of the fermionic operator $\mathcal{O}_\psi$. First, the rotational symmetry of the Fermi surface is broken. As we alluded to earlier, such behavior is expected given the form of $\tilde{k}_x$ and $\tilde{k}_y$ at each r-slicing in the bulk. Second, the spectral weight is angularly dependent. For intermediate values of the coupling λ, a gap-like feature opens at the two end points of the major axis. This highly non-trivial behavior is not a generic feature of traditional treatments of the Pomeranchuk instability [161] but can be understood within the WentzelKramersBrillouin (WKB) approximation to the spectral function outlined in the next section. The diminished spectral density reappears once

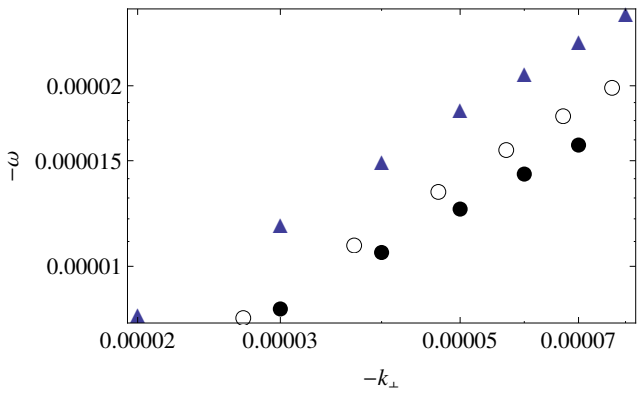

Figure 5.4: The dispersion relation, $\omega(k) \propto k_\perp^z$, of quasi-particles around k_F plotted on a log-log scale. The three cases correspond to a) open circles for the unbroken phase of the boundary theory with a circular Fermi surface where we find $z = 0.64$, b) solid circles for the dispersion relation (in the broken phase) along x-axis where we find $z = 0.74$ with $\lambda = -0.4$ and c) solid triangles for the dispersion relation along y-axis (in the broken phase) where $z = 0.84$ with $\lambda = -0.4$.

λ exceeds a critical value as shown in Figure 5.3(d). Finally, the excitations near the Fermi surface remain non-Fermi liquid-like. The solid circles and triangles in Figure 5.4 show that the dispersions along k_x and k_y deviate from linearity with exponents of $z = 0.74$ and $z = 0.84$, respectively. These values are, of course, parameter dependent.

5.4 WKB Analysis of Spectral Density

The WKB approach used recently[155] to analyze spectral functions in the electron star background can be used to uncloak the origin of the momentum-dependent spectral weight in Fig. (5.3). Setting $k_x = k\cos\theta$ and $k_y = k\sin\theta$, we define new momentum coordinates,

$$\begin{aligned}\tilde{k}'_x &= \sqrt{\tilde{k}_x^2 + \tilde{k}_y^2} \\ &= \sqrt{\left(k\cos\theta\left(1+\lambda g^{xx}\varphi_{xx}\right) + \lambda g^{xx}\varphi_{xy}k\sin\theta\right)^2 + \left(k\sin\theta\left(1-\lambda g^{xx}\varphi_{xx}\right) + \lambda g^{xx}\varphi_{xy}k\cos\theta\right)^2}\end{aligned} \tag{5.38}$$

and $\tilde{k}'_y = 0$ which are explicitly written in the "lab" frame. With these new coordinates and for a particular direction θ and k, the original Dirac equation is equivalent to two decoupled equations,

$$\left(\tilde{D}_r - i\sigma_2\sqrt{g^{xx}}\,\tilde{k}'_x\right)\psi_1 = 0, \tag{5.39}$$

$$\left(\tilde{D}_r + i\sigma_2\sqrt{g^{xx}}\,\tilde{k}'_x\right)\psi_2 = 0. \tag{5.40}$$

Any anisotropy that arises now in the spectral function must be tied to $\tilde{k}'_x$. To confirm this, we construct a contour plot of $\tilde{k}'_x$ at the horizon where the anisotropy is largest. Figs. (5.5) shows clearly that for a fixed

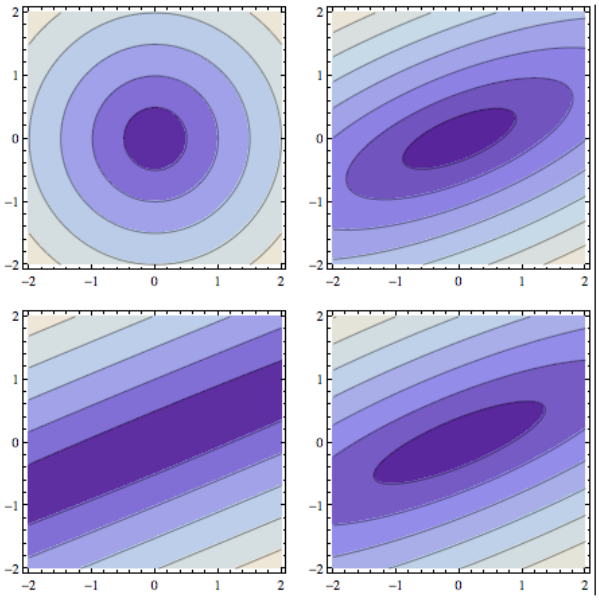

Figure 5.5: Contour plot of $\tilde{k}'_x$ for $\lambda = 0$, $\lambda = -0.4$, $\lambda = -0.95$ and $\lambda = -1.4$. (All of them have $m = 0$,$\omega = 0$ and $\mu q = 17$.)

value of k, $\tilde{k}'_x$ is minimum at $\theta = \pi/8$ and $9\pi/8$ which is consistent with the values of θ where the spectral density is a minimum.

Indeed, we can develop a better understanding on how $\tilde{k}'_x$ affects the spectral density by performing a WKB analysis on the Dirac equation. In the following, we will replace $\tilde{k}'_x$ by k for simplicity. In order to apply WKB approximation, we will take the limit where k, m, ω and q are large, but their ratio remains constant. To this end, it is convenient to rescale all of these quantities with the factor γ such that $k = \gamma\hat{k}$, $m_\psi = \gamma\hat{m}$, $q = \gamma\hat{q}$, and $\omega = \gamma\hat{\omega}$, where γ is the large parameter in WKB approximation. Central to the WKB approximation is the construction of a Schrödinger-like equation for each of the components of the two-component spinor,

$$\psi_1 = \begin{pmatrix} \Phi_1 \\ \Phi_2 \end{pmatrix}$$

The same treatment applies equally to ψ_2 with the replacement, $k \to -k$. To leading order in γ, the second-order differential equation for Φ_1 takes on the form,

$$\Phi_1'' = \gamma^2 g_{rr} \left(\hat{m}^2 + g^{tt} \left(\hat{\omega} + \mu\hat{q} \left(1 - \frac{r_0}{r} \right) \right)^2 + g^{xx} \hat{k}^2 \right) \Phi_1, \tag{5.41}$$

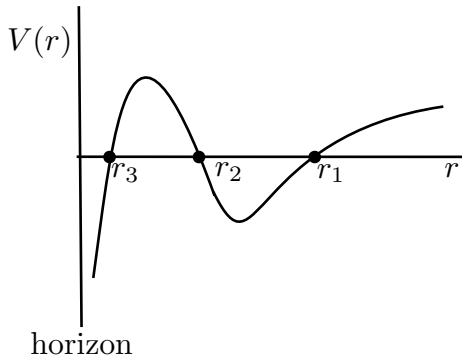

Figure 5.6: Potential as a function of r. The classical turning points as measured from the horizon are indicated explicitly by r_3, r_2, and r_1.

with

$$\Phi_2 = \frac{(-\sqrt{g^{rr}}\partial_r - m_\psi)\,\Phi_1}{-\sqrt{-g^{tt}}(\omega + qA_t) + \sqrt{g^{xx}}k} \tag{5.42}$$

In the context of a Schrödinger equation, the right-hand side of Eq. (5.41) can be regarded as the zero-energy potential

$$V = \gamma^2 g_{rr}\left(\hat{m}^2 + g^{tt}\left(\hat{\omega} + \mu\hat{q}\left(1 - \frac{r_0}{r}\right)\right)^2 + g^{ii}\hat{k}^2\right). \tag{5.43}$$

It is the turning points of this potential that govern the physics of the WKB approximation. In the near-horizon region, the potential is given by

$$V(r \to r_0) = \frac{L^2\gamma^2}{3r_0^3(r - r_0)}\left(L^2\hat{k}^2 + \hat{m}^2 r_0^2 - \hat{\omega}^2\frac{L^2 r_0}{3\,(r - r_0)}\right) + \cdots \tag{5.44}$$

If ω is non-zero, the near horizon potential is dominated by the term proportional to ω and is negative for real positive ω. Close to the boundary, the leading order term of the potential,

$$V(r \to \infty) = \frac{\gamma^2 L^2 \hat{m}^2}{r^2} + \cdots, \tag{5.45}$$

is always positive. Between these two extremes, there can be at most three turning points which we denote by r_1, r_2 and r_3, r_1 being the turning point closest to the boundary as indicated in Fig. (5.6). For the parameter range of interest here, all three turning points will enter the matching conditions.

What remains is a simple matching procedure to determine the form of Φ_1 in each of the regions that

bracket the turning points. This procedure, detailed previously[**?**], utilizes the functions,

$$X = \int_{r_3}^{r_2} dr\sqrt{V} + \log 2, \quad Y = \int_{r_2}^{r_1} dr\sqrt{-V} + \frac{\pi}{2} \tag{5.46}$$

which directly enter the retarded Green function

$$G^R(\omega, k) \propto \frac{i\mathcal{G}}{2} \lim_{r\to 0} r^{2mL} \exp\left(-2\int_{r_1}^{r} dr'\sqrt{V}\right) \tag{5.47}$$

where

$$\mathcal{G} = \frac{\cosh(X + iY) + \sinh(X - iY)}{\cosh(X - iY) - \sinh(X + iY)}. \tag{5.48}$$

The pole of the retarded Green function only comes from $\mathcal{G}$ and is given by $Y = \pi n - ie^{-2X} + \cdots$, where we have included the imaginary part up to leading order only. Since we are interested in the non-analytic dependence of the Green function on frequency and momentum, we will focus on the behavior in the vicinity of the pole where the Green function can be written as

$$\mathcal{G} = \sum_n \frac{i}{Y(\omega, k) - \pi n + ie^{-2X(\omega,k)}}. \tag{5.49}$$

Close to $\omega = 0$ and $k = k_F^{(n)}$, we can expand $Y(\omega, k)$ as $Y(0, k_F^{(n)}) + \omega\partial_\omega Y(0, k_F^{(n)}) + (k - k_F^{(n)})\partial_k Y(0, k_F^{(n)}) + \cdots$. [4] Hence, the retarded Green function is given by

$$G^R(\omega, k) \propto \sum_n \frac{-c_n e^{-2a_n}}{\omega + v_n(k - k_F^{(n)}) + ic_n e^{-2X(\omega,k)}} \tag{5.50}$$

$$\propto \sum_n \frac{-\left(\omega + v_n(k - k_F^{(n)})\right) c_n e^{-2a_n} + ic_n^2 e^{-2a_n} e^{-2X}}{\left(\omega + v_n(k - k_F^{(n)})\right)^2 + c_n^2 e^{-4X}} \tag{5.51}$$

where

$$v_n = \frac{\partial_k Y(0, k_F^{(n)})}{\partial_\omega Y(0, k_F^{(n)})}, \qquad c_n = \frac{1}{\partial_\omega Y(0, k_F^{(n)})},$$
$$a_n = \int_{r_1}^{\infty} \left(\sqrt{V(0, k_F^{(n)})}\right) dr \tag{5.52}$$

which is essentially Eq. (48) of [155].

[4] We have written the potential in $\hat{\omega}$, $\hat{k}$, however, in doing expansion of $Y(\omega, k)$, factors of γ cancel and we can drop the $\hat{}$ in ω and k.

Close to the Fermi surface, where the first term in the denominator of the second of Eqs. (5.50) can be dropped [5], the spectral function can be extracted from the imaginary part of the retarded Green function. Hence,

$$A(\omega, k) \propto e^{-2a_n+2X} \tag{5.53}$$

We can now understand the anisotropy of spectral weight from the dependence of a_n and X on the area enclosed by the potential integrated between the turning points r_2 and r_3[6] and between r_1 and ∞ which will determine a_n. In fact, for $m = 0$, $r_1 \to \infty$, a_n therefore vanishes and the angular dependence of the spectral weight will be dominated by X alone. Close to the horizon, the first turning point of the potential, r_3, is roughly given by

$$r_3 \approx r_0 + \frac{\omega^2 L^2 r_0}{3(m^2 r_0^2 + k(r_0)^2 L^2)} \tag{5.54}$$

From this we can see that in the limit $\omega \to 0$, that is, close to the Fermi surface, $r_3 \to r_0$.

In our analysis of the spectral function, we used $m = 0$, only X determines the spectral density. To illustrate the angular dependence, we plot the near-horizon effective WKB Schrodinger potential for $\lambda = -0.4$, $m = 0$ at first Fermi surface ($n = 0$) in Fig. (5.7)(corresponding to figure 3b in our Chapter). The dashed line corresponds to the potential along $\theta = \pi/8$, while the solid line corresponds to $\theta = 0$. It is now obvious that r_2 is larger for $\theta = 0$ than for $\theta = \pi/8$ and the potential is always larger for $\theta = 0$ than $\theta = \pi/8$ in the range of r shown. Hence X and spectral weight are larger along $\theta = 0$ than $\theta = \pi/8$, thereby explaining our key finding that the spectral weight is angularly dependent. In principle, the WKB approximate works only for large n, nevertheless, we see that the result qualitatively agrees with our numerical results even for small n.

5.5 Discussion

We have shown here how holography can be used to model a Pomeranchuk instability in a non-Fermi liquid through the condensation of a neutral symmetric traceless operator which is dual to a neutral massive spin-two field in the bulk. An open challenging problem remains: Is the condensation of the boundary theory operator $\mathcal{O}_{ij}$ possible starting from a bulk geometry which is not an Einstein manifold? In other

[5] We have assumed in the limit $\omega \to 0$, ω vanishes faster than $e^{-2X(\omega,k)}$, which is true in the range of parameters we are interested in.

[6] This will define X

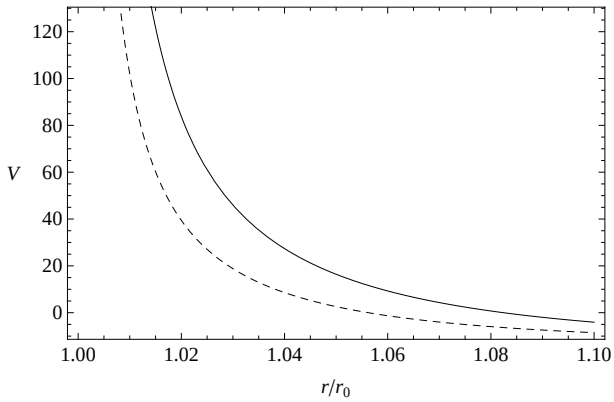

Figure 5.7: Effective WKB potential for $\lambda = -0.4$, $m = 0$ at the first Fermi surface. The solid line corresponds to $\theta = 0$ and the dashed line to $\theta = \pi/8$.

words, what is the backreacted background that allows for the ghost-free and causal propagation of a neutral massive spin-two field. These extensions are extremely desirable since they would enable an analysis at zero-temperature as well. In addition, is the angular dependent spectral weight a generic feature of holographic non-Fermi liquids with (partially) broken rotational symmetry? If so, then holography would have provided a key ingredient missing from most condensed matter analyses of the Pomeranchuk instability, namely a vanishing spectral weight for a finite range of momenta and hence a pseudogap as a function of frequency. Also, how does the resistivity tensor behave in the two different directions? In our probe analysis, where the backreaction of the massive spin-two field on the metric is ignored, the resistivity tensor is not sensitive to the anisotropy of the system when the boundary theory is in the broken phase. Nevertheless, one might be able to see the anisotropic contribution of the fermions to the resistivity through a fermion loop computation in the bulk similar to the analysis of [49].

References

[1] L. D. Landau, Zh. Eksp. Teor. Fiz., **30**, 1058 (1956).

[2] L. D. Landau, Zh. Eksp. Teor. Fiz., **32**, 59 (1957).

[3] R. Shankar, Rev. Mod. Phys., **66**, 129 (1994).

[4] S.-i. Tomonaga, Progress of Theoretical Physics, **5**, 544 (1950), http://ptp.oxfordjournals.org/content/5/4/544.full.pdf+html .

[5] J. M. Luttinger, Journal of Mathematical Physics, **4**, 1154 (1963).

[6] C. M. Varma, P. B. Littlewood, S. Schmitt-Rink, E. Abrahams, and A. E. Ruckenstein, Phys. Rev. Lett., **63**, 1996 (1989).

[7] K. B. Dave, P. W. Phillips, and C. L. Kane, Phys. Rev. Lett., **110**, 090403 (2013).

[8] C. T. Chen, F. Sette, Y. Ma, M. S. Hybertsen, E. B. Stechel, W. M. C. Foulkes, M. Schulter, S.-W. Cheong, A. S. Cooper, L. W. Rupp, B. Batlogg, Y. L. Soo, Z. H. Ming, A. Krol, and Y. H. Kao, Phys. Rev. Lett., **66**, 104 (1991).

[9] M. M. Qazilbash, K. S. Burch, D. Whisler, D. Shrekenhamer, B. G. Chae, H. T. Kim, and D. N. Basov, Phys. Rev. B, **74**, 205118 (2006).

[10] L. Baldassarre, A. Perucchi, D. Nicoletti, A. Toschi, G. Sangiovanni, K. Held, M. Capone, M. Ortolani, L. Malavasi, M. Marsi, P. Metcalf, P. Postorino, and S. Lupi, Phys. Rev. B, **77**, 113107 (2008).

[11] G. Möller, A. E. Ruckenstein, and S. Schmitt-Rink, Phys. Rev. B, **46**, 7427 (1992).

[12] A. B. Harris and R. V. Lange, Phys. Rev., **157**, 295 (1967).

[13] P. Phillips, Rev. Mod. Phys., **82**, 1719 (2010).

[14] E. C. Blomberg, M. A. Tanatar, A. Kreyssig, N. Ni, A. Thaler, R. Hu, S. L. Bud'ko, P. C. Canfield, A. I. Goldman, and R. Prozorov, Phys. Rev. B, **83**, 134505 (2011).

[15] R. M. Fernandes, E. Abrahams, and J. Schmalian, Phys. Rev. Lett., **107**, 217002 (2011).

[16] R. A. Borzi, S. A. Grigera, J. Farrell, R. S. Perry, S. J. S. Lister, S. L. Lee, D. A. Tennant, Y. Maeno, and A. P. Mackenzie, Science, **315**, 214 (2007), http://www.sciencemag.org/content/315/5809/214.full.pdf .

[17] M. B. Salamon and M. Jaime, Rev. Mod. Phys., **73**, 583 (2001).

[18] R. S. Perry, K. Kitagawa, S. A. Grigera, R. A. Borzi, A. P. Mackenzie, K. Ishida, and Y. Maeno, Phys. Rev. Lett., **92**, 166602 (2004).

[19] C. Stingl, R. S. Perry, Y. Maeno, and P. Gegenwart, Phys. Rev. Lett., **107**, 026404 (2011).

[20] V. Oganesyan, S. A. Kivelson, and E. Fradkin, Phys. Rev. B, **64**, 195109 (2001).

[21] I. K. Yanson, J. Exp. Theor. Phys., **39**, 506 (1974).

[22] W. K. Park, J. L. Sarrao, J. D. Thompson, and L. H. Greene, Phys. Rev. Lett., **100**, 177001 (2008).

[23] H. Z. Arham, C. R. Hunt, W. K. Park, J. Gillett, S. D. Das, S. E. Sebastian, Z. J. Xu, J. S. Wen, Z. W. Lin, Q. Li, G. Gu, A. Thaler, S. L. Budko, P. C. Canfield, and L. H. Greene, (2011), arXiv:1108.2749 [cond-mat] .

[24] H. Z. Arham, C. R. Hunt, W. K. Park, J. Gillett, S. D. Das, S. E. Sebastian, Z. J. Xu, J. S. Wen, Z. W. Lin, Q. Li, G. Gu, A. Thaler, S. Ran, S. L. Bud'ko, P. C. Canfield, D. Y. Chung, M. G. Kanatzidis, and L. H. Greene, Phys. Rev. B, **85**, 214515 (2012).

[25] W.-C. Lee and P. W. Phillips, Phys. Rev. B, **86**, 245113 (2012).

[26] W. A. Harrison, Phys. Rev., **123**, 85 (1961).

[27] M. J. Lawler, D. G. Barci, V. Fernández, E. Fradkin, and L. Oxman, Phys. Rev. B, **73**, 085101 (2006).

[28] M. Maple, C. Seaman, D. Gajewski, Y. Dalichaouch, V. Barbetta, M. Andrade, H. Mook, H. Lukefahr, O. Bernal, and D. MacLaughlin, Journal of Low Temperature Physics, **95**, 225 (1994), ISSN 0022-2291.

[29] C. L. Seaman, M. B. Maple, B. W. Lee, S. Ghamaty, M. S. Torikachvili, J.-S. Kang, L. Z. Liu, J. W. Allen, and D. L. Cox, Phys. Rev. Lett., **67**, 2882 (1991).

[30] R. Egger and A. Gogolin, The European Physical Journal B - Condensed Matter and Complex Systems, **3**, 281 (1998), ISSN 1434-6028.

[31] H. v. Löhneysen, T. Pietrus, G. Portisch, H. G. Schlager, A. Schröder, M. Sieck, and T. Trappmann, Phys. Rev. Lett., **72**, 3262 (1994).

[32] A. O. Gogolin, A. A. Nersesyan, and A. M. Tsvelik, *Bosonization and Strongly Correlated Systems* (Cambridge University Press, 2004).

[33] S. Tomonaga, **5**, 544 (1950).

[34] D. C. Mattis and E. H. Lieb, Journal of Mathematical Physics, **6**, 304 (1965).

[35] F. D. M. Haldane, Journal of Physics C: Solid State Physics, **14**, 2585 (1981).

[36] S. Sachdev, *Quantum Phase Transitions* (Cambridge University Press, 2011).

[37] A. H. Castro Neto and E. Fradkin, Phys. Rev. B, **49**, 10877 (1994).

[38] A. Houghton, H.-J. Kwon, and J. B. Marston, Advances in Physics, **49**, 141 (2000).

[39] A. Luther, Phys. Rev. B, **19**, 320 (1979).

[40] F. D. M. Haldane, in *Proceedings of International School of Physics*, Course 121, Varenna, 1992, edited by R. Schrieffer and R. A. Broglia (North-Holland, New York 1994).

[41] P. Kopietz, *Bosonization of Interacting Fermions in Arbitary Dimensions* (Springer, 1997).

[42] J. Maldacena, International Journal of Theoretical Physics, **38**, 1113 (1999), ISSN 0020-7748.

[43] G. Hooft, Nuclear Physics B, **72**, 461 (1974), ISSN 0550-3213.

[44] O. Aharony, (2002), arXiv:0212193 [hep-th] .

[45] O. Aharony, S. S. Gubser, J. Maldacena, H. Ooguri, and Y. Oz, Physics Reports, **323**, 183 (2000), ISSN 0370-1573.

[46] S. A. Hartnoll, C. P. Herzog, and G. T. Horowitz, Phys. Rev. Lett., **101**, 031601 (2008).

[47] S. A. Hartnoll, C. P. Herzog, and G. T. Horowitz, Journal of High Energy Physics, **2008**, 015 (2008).

[48] H. Liu, J. McGreevy, and D. Vegh, Phys. Rev. D, **83**, 065029 (2011).

[49] T. Faulkner, N. Iqbal, H. Liu, J. McGreevy, and D. Vegh, (2010), arXiv:1003.1728 [hep-th] .

[50] S. A. Hartnoll, (2011), arXiv:1106.4324 [hep-th] .

[51] S. Sachdev, Annual Review of Condensed Matter Physics, **3**, 9 (2012), http://www.annualreviews.org/doi/pdf/10.1146/annurev-conmatphys-020911-125141 .

[52] J. McGreevy, (2009), arXiv:0909.0518 [hep-th] .

[53] S. Kachru, X. Liu, and M. Mulligan, Phys. Rev. D, **78**, 106005 (2008).

[54] S. A. Hartnoll and A. Tavanfar, Phys. Rev. D, **83**, 046003 (2011).

[55] I. R. Klebanov and E. Witten, Nuclear Physics B, **556**, 89 (1999), ISSN 0550-3213.

[56] A. Zee, *Quantum Field Theory in a Nutshell* (Princeton University Press, 2010).

[57] P. Breitenlohner and D. Z. Freedman, Physics Letters B, **115**, 197 (1982), ISSN 0370-2693.

[58] N. Iqbal, H. Liu, M. Mezei, and Q. Si, Phys. Rev. D, **82**, 045002 (2010).

[59] S. S. Gubser, Classical and Quantum Gravity, **22**, 5121 (2005).

[60] T. Faulkner, H. Liu, J. McGreevy, and D. Vegh, Phys. Rev. D, **83**, 125002 (2011).

[61] I. Buchbinder, D. Gitman, and V. Pershin, Physics Letters B, **492**, 161 (2000), ISSN 0370-2693.

[62] A. P. Mackenzie, J. A. N. Bruin, R. A. Borzi, A. W. Rost, and S. A. Grigera, (2012), arXiv:1201.6639 [cond-mat] .

[63] A. W. Rost, S. A. Grigera, J. A. N. Bruin, R. S. Perry, D. Tian, S. Raghu, S. A. Kivelson, and A. P. Mackenzie, Proceedings of the National Academy of Sciences, **108**, 16549 (2011).

[64] S. Raghu, A. Paramekanti, E. A. Kim, R. A. Borzi, S. A. Grigera, A. P. Mackenzie, and S. A. Kivelson, Phys. Rev. B, **79**, 214402 (2009).

[65] W.-C. Lee and C. Wu, Phys. Rev. B, **80**, 104438 (2009).

[66] A. J. Millis, P. B. Littlewood, and B. I. Shraiman, Phys. Rev. Lett., **74**, 5144 (1995).

[67] W. Lv, J. Wu, and P. Phillips, Phys. Rev. B, **80**, 224506 (2009).

[68] W. Lv, F. Krüger, and P. Phillips, Phys. Rev. B, **82**, 045125 (2010).

[69] F. Krüger, S. Kumar, J. Zaanen, and J. van den Brink, Phys. Rev. B, **79**, 054504 (2009).

[70] C.-C. Lee, W.-G. Yin, and W. Ku, Phys. Rev. Lett., **103**, 267001 (2009).

[71] C.-C. Chen, J. Maciejko, A. P. Sorini, B. Moritz, R. R. P. Singh, and T. P. Devereaux, Phys. Rev. B, **82**, 100504 (2010).

[72] A. H. Nevidomskyy, (2011), arXiv:1104.1747 [cond-mat] .

[73] S. Graser, T. A. Maier, P. J. Hirschfeld, and D. J. Scalapino, New Journal of Physics, **11**, 025016 (2009).

[74] A. H. Castro Neto and E. Fradkin, Phys. Rev. Lett., **72**, 1393 (1994).

[75] A. Houghton and J. B. Marston, Phys. Rev. B, **48**, 7790 (1993).

[76] J. A. Hertz, Phys. Rev. B, **14**, 1165 (1976).

[77] A. J. Millis, Phys. Rev. B, **48**, 7183 (1993).

[78] W. Metzner, D. Rohe, and S. Andergassen, Phys. Rev. Lett., **91**, 066402 (2003).

[79] L. Dell'Anna and W. Metzner, Phys. Rev. B, **73**, 045127 (2006).

[80] V. P. Mineev and V. P. Michal, (2012), arXiv:1206.3468 [cond-mat] .

[81] S. Raghu, X.-L. Qi, C.-X. Liu, D. J. Scalapino, and S.-C. Zhang, Phys. Rev. B, **77**, 220503 (2008).

[82] S. Onari and H. Kontani, (2012), arXiv:1203.2874 [cond-mat] .

[83] X.-L. Qi, S. Raghu, C.-X. Liu, D. J. Scalapino, and S.-C. Zhang, (2008), arXiv:0804.4332 [cond-mat] .

[84] Y. Ohno, M. Tsuchiizu, S. Onari, and H. Kontani, (2012), arXiv:1209.3629 [cond-mat] .

[85] M. Tsuchiizu, S. Onari, and H. Kontani, (2012), arXiv:1209.3664 [cond-mat] .

[86] I. J. Pomeranchuk, Sov. Phys. JETP, **8**, 361 (1958).

[87] N. N. Bogoliubov and N. N. Bogoliubov jr, *An Introduction to Quantum Statistical Mechanics* (Gordon and Breach, New York 1992).

[88] C. J. Pethick and H. Smith, *Bose-Einstein Condensation in Dilute Gases* (Cambridge University Press, 2002).

[89] V. S. Shchesnovich, Physics Letters A, **349**, 398 (2006).

[90] S. A. Hartnoll, (2009), arXiv:0903.3246 [hep-th] .

[91] C. P. Herzog, Journal of Physics A: Mathematical and Theoretical, **42**, 343001 (2009).

[92] G. T. Horowitz, (2010), arXiv:1002.1722 [hep-th] .

[93] S.-S. Lee, Phys. Rev. D, **79**, 086006 (2009).

[94] M. Cubrović, J. Zaanen, and K. Schalm, Science, **325**, 439 (2009).

[95] T. Faulkner and J. Polchinski, Journal of High Energy Physics, **2011**, 1 (2011).

[96] J. P. Gauntlett, S. Kim, O. Varela, and D. Waldram, Journal of High Energy Physics, **2009**, 102 (2009).

[97] D. Cassani, G. DallÄôAgata, and A. Faedo, Journal of High Energy Physics, **2010**, 1 (2010).

[98] J. Gauntlett and O. Varela, Journal of High Energy Physics, **2010**, 1 (2010).

[99] J. T. Liu, P. Szepietowski, and Z. Zhao, Phys. Rev. D, **81**, 124028 (2010).

[100] F. Denef and S. A. Hartnoll, Phys. Rev. D, **79**, 126008 (2009).

[101] S. S. Gubser, C. P. Herzog, S. S. Pufu, and T. Tesileanu, Phys. Rev. Lett., **103**, 141601 (2009).

[102] J. P. Gauntlett, J. Sonner, and T. Wiseman, Phys. Rev. Lett., **103**, 151601 (2009).

[103] I. Bah, A. Faraggi, J. Jottar, R. Leigh, and L. Pando Zayas, Journal of High Energy Physics, **2011**, 1 (2011).

[104] I. Bah, A. Faraggi, J. Jottar, and R. Leigh, Journal of High Energy Physics, **2011**, 1 (2011).

[105] M. Edalati, R. G. Leigh, and P. W. Phillips, Phys. Rev. Lett., **106**, 091602 (2011).

[106] A. Zylbersztejn and N. F. Mott, Phys. Rev. B, **11**, 4383 (1975).

[107] M. Edalati, J. Jottar, and R. Leigh, Journal of High Energy Physics, **2010**, 1 (2010).

[108] N. Iqbal and H. Liu, Phys. Rev. D, **79**, 025023 (2009).

[109] D. T. Son and A. O. Starinets, Journal of High Energy Physics, **2002**, 042 (2002).

[110] N. Iqbal and H. Liu, Fortschritte der Physik, **57**, 367 (2009), ISSN 1521-3978.

[111] F. Denef, S. A. Hartnoll, and S. Sachdev, Phys. Rev. D, **80**, 126016 (2009).

[112] M. Edalati, J. Jottar, and R. Leigh, Journal of High Energy Physics, **2010**, 1 (2010).

[113] M. Edalati, J. Jottar, and R. Leigh, Journal of High Energy Physics, **2010**, 1 (2010).

[114] E. W. Leaver, Phys. Rev. D, **41**, 2986 (1990).

[115] M. M. Qazilbash, A. A. Schafgans, K. S. Burch, S. J. Yun, B. G. Chae, B. J. Kim, H. T. Kim, and D. N. Basov, Phys. Rev. B, **77**, 115121 (2008).

[116] G. T. Horowitz and M. M. Roberts, Journal of High Energy Physics, **2009**, 015 (2009).

[117] J.-W. Chen, Y.-J. Kao, and W.-Y. Wen, Phys. Rev. D, **82**, 026007 (2010).

[118] T. Faulkner, G. Horowitz, J. McGreevy, M. Roberts, and D. Vegh, Journal of High Energy Physics, **2010**, 1 (2010).

[119] S. Gubser, F. Rocha, and A. Yarom, Journal of High Energy Physics, **2010**, 1 (2010).

[120] M. Ammon, J. Erdmenger, M. Kaminski, and A. OÄôBannon, Journal of High Energy Physics, **2010**, 1 (2010).

[121] F. Benini, C. P. Herzog, and A. Yarom, Physics Letters B, **701**, 626 (2011), ISSN 0370-2693.

[122] D. Vegh, (2010), arXiv:1007.0246 [hep-th] .

[123] Q. Si and F. Steglich, Science, **329**, 1161 (2010), http://www.sciencemag.org/content/329/5996/1161.full.pdf .

[124] E. Fradkin, S. A. Kivelson, M. J. Lawler, J. P. Eisenstein, and A. P. Mackenzie, Annual Review of Condensed Matter Physics, **1**, 153 (2010), http://www.annualreviews.org/doi/pdf/10.1146/annurev-conmatphys-070909-103925 .

[125] J. A. Hertz, Phys. Rev. B, **14**, 1165 (1976).

[126] A. J. Millis, Phys. Rev. B, **48**, 7183 (1993).

[127] A. Abanov and A. Chubukov, Phys. Rev. Lett., **93**, 255702 (2004).

[128] S.-S. Lee, Phys. Rev. B, **80**, 165102 (2009).

[129] M. A. Metlitski and S. Sachdev, Phys. Rev. B, **82**, 075128 (2010).

[130] S. Kachru, X. Liu, and M. Mulligan, Phys. Rev. D, **78**, 106005 (2008).

[131] S. S. Gubser, Phys. Rev. D, **78**, 065034 (2008).

[132] T. Faulkner, G. T. Horowitz, and M. M. Roberts, Classical and Quantum Gravity, **27**, 205007 (2010).

[133] T. Faulkner, G. Horowitz, and M. Roberts, Journal of High Energy Physics, **2011**, 1 (2011).

[134] E. Witten, (2001), arXiv:[hep-th/0112258] .

[135] M. Berkooz, A. Sever, and A. Shomer, Journal of High Energy Physics, **2002**, 034 (2002).

[136] S. Hartnoll, J. Polchinski, E. Silverstein, and D. Tong, Journal of High Energy Physics, **2010**, 1 (2010).

[137] J. Boer, K. Papadodimas, and E. Verlinde, Journal of High Energy Physics, **2010**, 1 (2010).

[138] K. Goldstein, S. Kachru, S. Prakash, and S. Trivedi, Journal of High Energy Physics, **2010**, 1 (2010).

[139] V. Puletti, S. Nowling, L. Thorlacius, and T. Zingg, Journal of High Energy Physics, **2011**, 1 (2011).

[140] S. A. Hartnoll and P. Petrov, Phys. Rev. Lett., **106**, 121601 (2011).

[141] A. Sokol and D. Pines, Phys. Rev. Lett., **71**, 2813 (1993).

[142] S. Sachdev, A. V. Chubukov, and A. Sokol, Phys. Rev. B, **51**, 14874 (1995).

[143] K. Sun, B. M. Fregoso, M. J. Lawler, and E. Fradkin, Phys. Rev. B, **78**, 085124 (2008).

[144] K. Skenderis, Classical and Quantum Gravity, **19**, 5849 (2002).

[145] C. P. Herzog, P. K. Kovtun, and D. T. Son, Phys. Rev. D, **79**, 066002 (2009).

[146] D. B. Kaplan, J.-W. Lee, D. T. Son, and M. A. Stephanov, Phys. Rev. D, **80**, 125005 (2009).

[147] K. Jensen, A. Karch, D. T. Son, and E. G. Thompson, Phys. Rev. Lett., **105**, 041601 (2010).

[148] V. Efimov, Physics Letters B, **33**, 563 (1970), ISSN 0370-2693.

[149] J.-W. Chen, Y.-J. Kao, D. Maity, W.-Y. Wen, and C.-P. Yeh, Phys. Rev. D, **81**, 106008 (2010).

[150] F. Benini, C. Herzog, R. Rahman, and A. Yarom, Journal of High Energy Physics, **2010**, 1 (2010).

[151] P. Basu, J. He, A. Mukherjee, and H.-H. Shieh, Phys. Rev. D, **82**, 044036 (2010).

[152] S. Gubser, F. Rocha, and P. Talavera, Journal of High Energy Physics, **2010**, 1 (2010).

[153] M. Edalati, R. G. Leigh, K. W. Lo, and P. W. Phillips, Phys. Rev. D, **83**, 046012 (2011).

[154] D. Guarrera and J. McGreevy, (2011), arXiv:1102.3908 [hep-th] .

[155] S. Hartnoll, D. Hofman, and D. Vegh, Journal of High Energy Physics, **2011**, 1 (2011).

[156] M. R. Norman, D. Pines, and C. Kallin, Advances in Physics, **54**, 715 (2005), http://www.tandfonline.com/doi/pdf/10.1080/00018730500459906 .

[157] S. A. Grigera, P. Gegenwart, R. A. Borzi, F. Weickert, A. J. Schofield, R. S. Perry, T. Tayama, T. Sakakibara, Y. Maeno, A. G. Green, and A. P. Mackenzie, Science, **306**, 1154 (2004), http://www.sciencemag.org/content/306/5699/1154.full.pdf .

[158] X. F. Sun, S. Ono, Y. Abe, S. Komiya, K. Segawa, and Y. Ando, Phys. Rev. Lett., **96**, 017008 (2006).

[159] J. J. Ying, X. F. Wang, T. Wu, Z. J. Xiang, R. H. Liu, Y. J. Yan, A. F. Wang, M. Zhang, G. J. Ye, P. Cheng, J. P. Hu, and X. H. Chen, Phys. Rev. Lett., **107**, 067001 (2011).

[160] J.-H. Chu, J. G. Analytis, K. De Greve, P. L. McMahon, Z. Islam, Y. Yamamoto, and I. R. Fisher, Science, **329**, 824 (2010), http://www.sciencemag.org/content/329/5993/824.full.pdf .

[161] E. Fradkin, (2010), arXiv:1004.1104 [cond-mat] .

[162] C. J. Halboth and W. Metzner, Phys. Rev. Lett., **85**, 5162 (2000).

[163] B. Valenzuela and M. A. H. Vozmediano, Phys. Rev. B, **63**, 153103 (2001).

[164] N. Iqbal, H. Liu, and M. Mezei, (2011), arXiv:1110.3814 [cond-mat] .

[165] M. Fierz and W. Pauli, Proceedings of the Royal Society of London. Series A. Mathematical and Physical Sciences, **173**, 211 (1939), http://rspa.royalsocietypublishing.org/content/173/953/211.full.pdf+html .

[166] C. Aragone and S. Deser, Il Nuovo Cimento A, **3**, 709 (1971), ISSN 0369-3546.

[167] S. Deser and R. I. Nepomechie, Annals of Physics, **154**, 396 (1984), ISSN 0003-4916.

[168] S. Deser and A. Waldron, Nuclear Physics B, **607**, 577 (2001), ISSN 0550-3213.

[169] S. Deser and A. Waldron, Physics Letters B, **508**, 347 (2001), ISSN 0370-2693.